MACQUARIE University
SYDNEY·AUSTRALIA

Exploring the chemical space around austdiol by semi-synthesis

Stefan Valter

School of Natural Sciences

Macquarie University

Date of Submission: 7 September 2022

Declaration

I hereby declare that this thesis entitled ‘Exploring the chemical space around austdiol by semi-synthesis’ represents my own work entirely and has not previously been submitted for a degree or diploma to any other university or tertiary institution. In addition, I certify that all information sources and literature used are clearly indicated in the thesis.

_____ 07/09/2022

Stefan Valter Date

Acknowledgements

I would like to thank my supervisor, A/Prof Andrew Piggott, for all the support and help given to me during my MRes studies amidst the COVID-19 pandemic. His advice and helpful critiques during the year has helped challenge me and achieve better. Thanks also to my associate supervisor, A/Prof. Joanne Jamie, for her feedback during early presentations of the project that helped shape.

Many thanks to Dr Ernest Lacey, my supervisor at Microbial Screening Technologies (MST), for his continuous support and providing access to the equipment and resources at MST. I would also like to thank the other lab members, especially Andrew Crombie and Daniel Vuong for their help around the lab that made it enjoyable to work at MST.

I would also like to thank the members of the Piggott Group, Dr Paul Malek Mirzayans and Dr John Kalaitzis for affording their expertise in the realms of synthesis and NMR spectroscopy.

Finally, I would like to thank my parents, Vlad and Viorica, for all their support throughout the year.

Abstract

Natural products provide structurally diverse chemical scaffolds with applications in pharmaceuticals and agrichemicals. However, many natural products do not possess PK/PD properties suitable for direct application as chemotherapeutic agent. When isolated material is sufficient, semi-synthetic modification of a natural product scaffolds is a useful technique for exploring chemical space around a pharmacophore to improve bioactivity and druggability. In this thesis, chemical derivatisation was used to expand the chemical space around austdiol, a toxic azaphilone first isolated in 1973 from the fungus *Aspergillus ustus*. A small semi-synthetic library of fourteen austdiol analogues was synthesised, focusing primarily on degradation, reduction, oxidation and amination reactions. Their structures were determined by HRESIMS and spectroscopic methods, including NMR and UV-vis. These derivatives were screened for antibacterial, antifungal, and cell cytotoxic activities. Finally, a 2,4-dinitrophenylhydrazone derivative of austdiol was explored as a chiral derivatisation agent to assist in the resolution of L and D enantiomers of amino acids commonly found in natural products, by UV-vis detection in reversed-phase liquid chromatography.

Table of Contents

1. Introduction

1.1. Antibiotics, Anticancer Drugs, and Drug Resistance

The introduction of antibiotics has transformed the treatment of infectious diseases and enabled advances in modern medical care. However, their widespread use and misuse has led to increased antimicrobial resistance (AMR), with many common bacterial infections becoming untreatable.[1] Globally, at least 700 000 people die each year from AMR infections, with more than 35 000, 33 000 and 290 deaths in the U.S., Europe, and Australia, respectively.[2-4] If ignored, AMR will become the leading cause of death by 2050 with an estimated annual rate of 10 million deaths, surpassing 8.2 million deaths due to cancer.[5]

Type text here

Inappropriate prescriptions and self-medications have escalated during the COVID-19 pandemic, where an estimated 72% of COVID-19 patients have used antibiotics despite only 7% having bacterial co-infections.[6] In addition, the overuse of antibiotics in husbandry and aquaculture at sub-therapeutic levels has resulted in the selection of pathogenic bacteria resistant to multiple drugs, namely "superbugs".[7] Innate or acquired resistance mechanisms allow multidrug-resistant (MDR) bacteria to maintain an evolutionary advantage over current drug therapy. Innate resistance arises from mutation and evolutionary selective pressure, whereas acquired "resistance genes" are obtained by horizontal gene transfer.[8] Resistance mechanisms include drug inactivation, altering drug targets protein, upregulating degradation enzymes, upregulating efflux pumps and downregulating influx proteins.[8]

ESKAPE pathogens are a collection of six multidrug resistant bacteria responsible for most life-threatening nosocomial infections.[9] The World Health Organization (WHO) deemed four of these (*Klebsiella pneumoniae, Acinetobacter baumannii, Pseudomonas aeruginosa,* and *Enterobacter* sp.) as a critical priority, while vancomycin-resistant strains of the other two (*Enterococcus faecium* and *Staphylococcus aureus*) as a high priority.[10] In a 2020 article by the Australian Government Department of Health, around 5% of MDR tuberculosis (MDR-TB) cases since 1999–2018 had no treatment success (**Figure 1.1**). However small these numbers may seem, the cases of several MDR pathogens are only increasing and therefore new antimicrobial drug classes are required to treat these infections.[11]

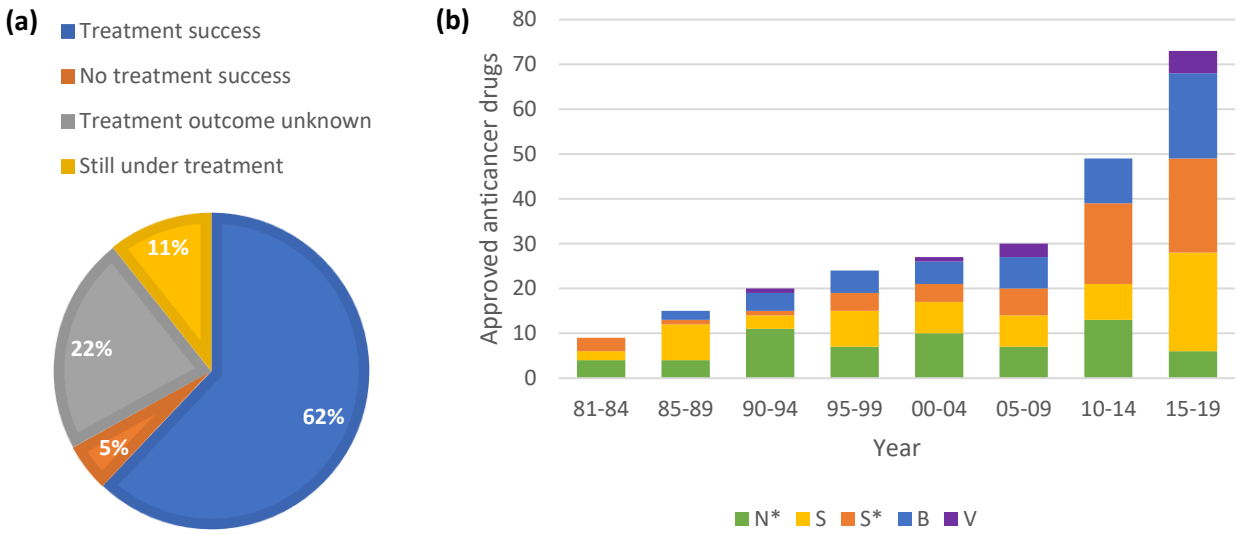

Figure 1.1. a. Multidrug-resistant tuberculosis case notifications in Australia (1999–2018) as of May 2019, n = 375. Adapted from Communicable Diseases Intelligence - Department of Health 2020 - Volume 44.[11] **b.** All FDA-approved anticancer agents 1981–2019, n = 247, with categories: N* = natural, botanical and natural derivatives, S = synthetic, S* = natural-inspired synthetic, B = biological macromolecule, and V = vaccine. Adapted from Newman, 2020.[14]

In addition to AMR, anticancer drug resistance has been shown to result in treatment failure in different types of cancers and is responsible for up to 90% of cancer-related deaths.[12] Human cancer cells with high proliferation rates are genetically unstable and evolve resistance mechanisms, such as altered drug metabolism and upregulated drug efflux, that reduce treatment effectiveness. Anticancer drug resistance mechanisms arise due to individual genetic factors such as cell death inhibition, DNA repair, gene amplification and epigenetic altering of cancer cells, which only heighten the complexity.[13] While anticancer drug resistance is a serious concern, the development of new chemotherapeutic agents is increasing to match this demand (**Figure 1.1**).[14]

1.2. Microbial Natural Products in Drug Discovery

Nature has been a major source for antimicrobial and anticancer drugs since the discovery of penicillin in 1928.[15] Around 35% of medicines originated from Nature, with 53% of small-molecule drugs approved by the FDA in the past decade being inspired or derived from natural products.[14,16] Successful clinical trials of penicillin ushered in the "Golden-age of antibiotics" (1940s–1950s), during which new antibiotic classes were found with ease from low-throughput cultivation and phenotypic screening. Popularised by Selman Waksman, following the discovery of streptomycin, the Waksman Platform involved screening a variety of soil-derived actinomycetes for bioactivity

using zone inhibition on a plate.[15,17] However, the increasing difficulty in identifying new compounds and scaling up productions were many of the reasons new approaches needed to be considered.[18] In the following decades, synthetic modifications were made to existing scaffolds to improve bioactivity which ushered in the Medicinal Chemistry era (1960s–1990s).[19] This accelerated the growth of natural product drug discovery through increased collaboration with other disciplines such as biochemistry, synthetic chemistry, and cell biology.

Emergence of high-tech drug discovery techniques (1990s–2010s), such as combinatorial chemistry, promised to make millions of "hit or lead" compounds.[19] By the late 1990s, many large pharmaceutical companies had scaled back research and development of natural product programs due to the soaring costs associated with drug development and running clinical trials.[15] It is estimated that upwards of US $2–3 billion is required to put a single drug in the market and thus companies focused on easier, revenue-generating "blockbuster" drugs that provided greater than US $1 billion in annual sales.[21] However, new technology failed to meet expectations with only three approved drugs (sorafenib, ataluren and vemurafenib) being *de novo* combinatorial discoveries. This led to a drug discovery vacuum and subsequent "drying up" of the drug pipeline.[14]

There is now greater appreciation for natural products as they possess high levels of three-dimensional sophistication as a consequence of highly-specific biosynthetic enzymes.[20] Synthetic chemists are competing with these enzymes to develop new drug scaffolds which may seem as a fruitless endeavour. However, Nature has provided the building blocks to generate novelty, from which combinatorial chemistry has potential to streamline optimisation rather than discovery to elaborate natural product leads and improve druggability.[20] These new synthetic techniques are required to discover new, and improve existing drug classes to combat the problem of antimicrobial and anticancer resistance.

1.2.1. Semi-Synthesis of Natural Products

Semi-synthetic modification has long been used to modify natural product drug leads to generate compounds with improved pharmacological properties. The antibiotic class of β-lactams have notable semi-synthetic examples that have broader spectrum (e.g. amoxicillin), greater resistance to penicillinase (e.g. methicillin), and expanded spectrum (e.g. azlocillin) (**Figure 1.2**).[22] The biological active principle of this class is the β-lactam ring, with reactivity and selectivity towards biological substrates influenced by substituents or fused rings.

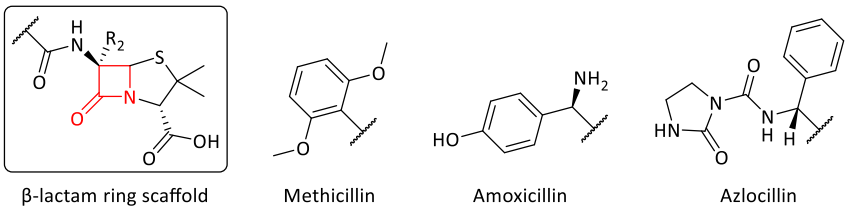

Figure 1.2. Structures of semi-synthetic derivatives of penicillin

The discovery of the fungal natural products compactin and lovastatin in the 1970s introduced the statins as a drug class. Statins are HMG-CoA reductase inhibitors and are effective for treating high blood cholesterol and lowering the risk of cardiovascular disease. A series of statins was also obtained by chemical modification of the C-8 side chain in the lovastatin scaffold, followed by a systematic evaluation of the structure-activity relationship (SAR).[23] One of the semi-synthetic derivatives, simvastatin, was found to be twice as potent as lovastatin (**Figure 1.3**).[24]

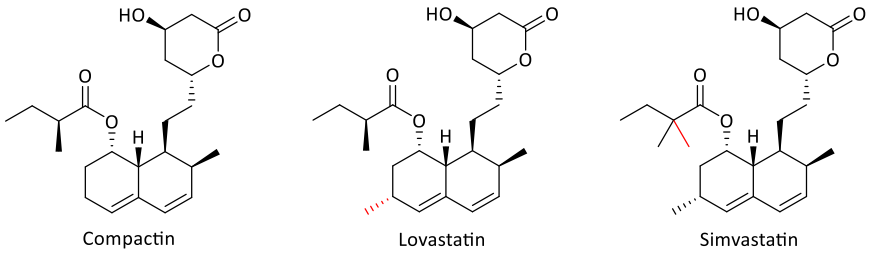

Figure 1.3. Structures of naturally occurring compactin, lovastatin and semi-synthetic derivative, simvastatin.

Sesquiterpene lactones (SLs) are a family of plant-derived compounds that have shown biological activities against inflammation and cancer.[25] Guaianolides are a subclass of SLs that consist of a tricyclic 5,7,5-ring system, from which the prominent member arglabin and its derivaties have shown to demonstrate promising cytotoxicity against varying tumour cell lines.[26,27] Arglabin is isolated from the plant *Artemisia glabella* in very low yields (0.27%), therefore a semi-synthetic method has been developed from parthenolide, extracted in high yield (3.1–8.0%) from root bark of *Magnolia delavayi*.[28] Retrosynthetic analysis indicated the main possible routes, which included cyclisation, epoxidation, and elimination. Initial cyclisation yielded micheliolide, which then underwent epoxidation and dehydrative elimination (**Scheme 1.1**). Argablin was shown to inhibit farnesyl transferase, which leads to RAS proto-oncogene activation, playing a role in 20–30% of all human tumours.[29] Arglabin has been later modified through addition of a dimethylamino group to the C-13 to yield arglabin-DMA with increased solubility in water and bioavailability when compared to parthenolide.[27]

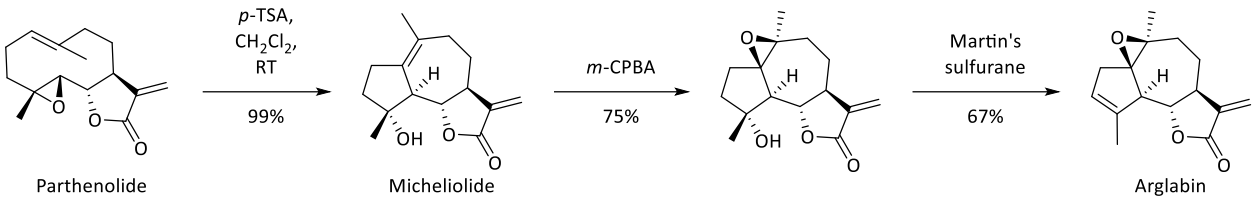

Scheme 1.1. Semisynthesis of arglabin from parathenolide

Recently, the semi-synthetic modification of the atypical tetracycline amidochelocardin (CDCHD), obtained via genetic engineering of the chelocardin (CHD) producer strain *Amycolatopsis sulphurea*, generated derivatives with broad-spectrum antibiotic potential.[30] A 2–4-fold increase in antibacterial activity of CDCHD (*P. aeruginosa*: MIC_{50} = 8 µg mL^{-1}) compared to CHD prompted investigation of the CDCHD scaffold.[31] Functionalisation was inspired by similar synthetic procedures available for tetracyclines and focused at the most tractable positions, namely the C-4 amino group, electron-rich C-7 position, and the C-10/C-11 positions. Modifications included methylation, acylation, electrophilic substitution, and oxidative C-C coupling reactions to create 22 compounds (**Figure 1.4**).

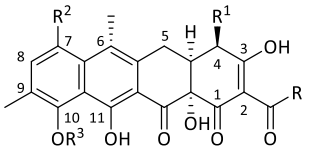

R = CH_3, Chelocardin (CHD)
R = NH_2, Amidochelocardin (CDCHD)
and compounds 3, 13 and 21

Compound	R^1	R^2	R^3	E	S	P
CHD	NH_2	H	H	8	8	64^b; 4^c
CDCHD	NH_2	H	H	4	8	16^b; 0.5c
3	NHCBz	H	H	0.25	> 64	> 64^b
13	NH_2	F	H	-	4	8^b; 4^c
21	NH_2	H	Ac	16	-	> 64^c

Figure 1.4. MIC_{50} (ug mL^{-1}) values of semi-synthetic amidochelocardin (CDCHD) derivatives against bacterial pathogens. E = *E. faecium* DSM-20477, S = *S. aureus* DSM-11822, P = ^{b}*P. aeruginosa* PA14, ^{c}*P. aeruginosa* PA14ΔmexAB. Table adapted from Grandclaudon *et al.*, 2020.[29]

Replacement of the C-4 free amine by a dimethylamino group was detrimental to activity of CDCHD against Gram-negative bacteria. Furthermore, small substitutions at the C-7 position were tolerated, with a fluorine substitution being particularly favourable against both Gram-positive and Gram-negative pathogens. The difference between the CDCHD and tetracycline SAR demonstrate the different modes of action, which can pave the way for a promising new class.

1.2.2 Total Synthesis of Natural Products

Natural products are an important source of new drug leads but are available in extremely small quantities from natural sources.[32] Due to this, access and supply presents a "bottleneck" in translating their biological activities to practical applications. Throughout the years, natural product total synthesis has evolved with many new discoveries, strategies, and technologies that have allowed chemists to explore biologically important molecules of the natural landscape from simple, commercially-available precursors, which separate it from semi-synthesis and biosynthesis. This field can be traced back to the simple, one-step synthesis of urea by Friedrich Wohler in 1828 by treating silver cyanate with ammonium chloride.[33] This foundational milestone contributed to the "demystification of Nature" from which challenges and major accomplishments have sharpened the synthetic tools and pushed the general field of organic synthesis forward.

Chemistry played a central role moving into the 20th century, with incredible scientific advancements in pharmaceuticals, cosmetics, and pesticides. R.B. Woodward was a prominent figure in elevating total synthesis as a powerful tool, conquering some of the most complex chemical architectures of the time. A few of his major synthetic achievements include the synthesis of antimalarial quinine (1944),[34] β-lactam antibiotic cephalosporin C (1966),[35] and macrolide antibiotic erythromycin A (1981).[36] The avalanche of new natural products due to improving analytical techniques during this period demanded a new systematic approach and strategy design. E.J. Corey's synthesis of longifolene in 1961 introduced the "logic" of chemical synthesis, which marked the official introduction of retrosynthetic analysis and raised organic synthesis to the next level of sophistication.[37] Retrosynthesis is the technique of deconstructing complex target molecules into simpler intermediates and employing synthetic schemes for their reconstruction and has become a mainframe in organic synthesis planning.

Recently, the synthesis of polyketides (+)- and (−)-tetrapetalones A and C was achieved, motivated by the synthetic challenge of a highly functionalised compact structure.[38] Tetrapetalone A is a novel soybean lipoxygenase inhibitor (IC_{50} = 190 μM) isolated from *Streptomyces* sp. USF-4727 in 2003, with later studies leading to the discovery of tetrapetalones B–D.[39,40] The synthetic strategy involved assembly of *N*-aryl masked tetramic acid followed by a highly selective intramolecular Friedel-Crafts acylation to produce the azepine intermediate. Recently developed C-H activation and following Heck cyclisation achieved the aglycone framework in 12 steps. Stereospecific glycosylation with enantiopure glycosyl donor and separation led to either (+)- or (−)-tetrapetalones A and C (**Scheme 1.2**).

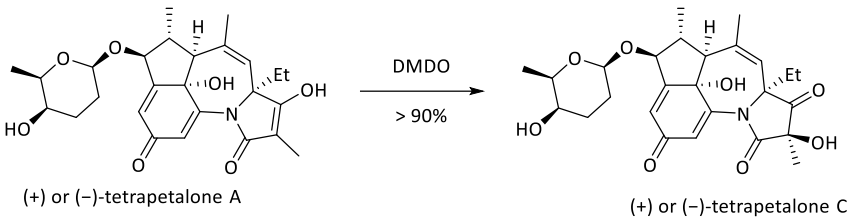

Scheme 1.2. Conversion of tetrapetalone A into tetrapetalone C with dimethyldioxirane (DMDO).

The interesting, highly-functionalised and unique hydradindane skeleton of botyranes, a group of sesquiterpene antibiotics isolated from the fungus *Bortrytis cinera*, have attracted interest from chemists due to their promising pharmacological properties.[41] For example the metabolite botrydial produced by *Botrytis cinerrea* is a hypersensitive response inducer and showed significant antibiotic activity against *Bacillus subtilis* and cytoxicity against human cancer cell lines.[42] The total synthesis of a collection of botyranes, including (±)-hypocrolide, has been reported via an unusual intramolecular Diels-Alder reaction promoted by *p*-toluenesulfonic acid as the protic acid.[43] Sustained interest in natural product total synthesis has led to the evolution of organic synthesis such that it may be possible to create any natural product from commercially-available precursors, which can help further biological research.

1.3. Austdiol, the Cytotoxic Azaphilone Possessing a Unique Bicyclic Skeleton

Azaphilones are a class of fungal polyketide pigments that share a highly oxygenated pyrone-quinone bicyclic core and a chiral quaternary centre.[44] As their name suggests, azaphilones have high affinity for amines and will react with primary amines to yield vinylogous γ-pyridones via an enamine intermediate.[45] There is emerging interest in azaphilones, with 252 (40% of naturally discovered azaphilones) natural azaphilones reported over the past seven years.[45,46] A major part of this revival is due to the application of fungal polyketides as natural food colourants.[47] *Monascus purpureus* is known to produce azaphilone pigments and has been primarily used in East Asia for hundreds of years for making red rice wine and Anka (red rice).[48] However, its use remains limited due to the co-production of the mycotoxin, citrinin.[49] Currently, food supplements based on red yeast *Monascus* have a maximum citrinin limit of 200 ng/g in Japan and 2 mg/kg in the European Union.[50,51]

Azaphilones are also known to exhibit a wide range of biological activities such as enzyme inhibition,[46] antimicrobial,[52] cytotoxicity,[53] antitumour,[54] and anti-inflammatory[55] activities and so have potential applications as therapeutic agents. Many of these may be attributed to reactions with amine-containing compounds such as amino acids, proteins, and nucleic acids.[44] Recently, a

variety of azaphilones with novel structures and promising bioactivities have been reported. Marine-derived penicilones B-D from *Penicillium janthinellum* HK1-6 showed potent anti-methicillin-resistant *Staphylococcus aureus* (MRSA) activities (MIC = 3.13–6.25 μg mL^{-1}) (**Figure 1.5**).[56] Isolation of the azaphilone derivative, penicilazaphilone C from marine fungus strain *Penicillium sclerotiorum* M-22, showed selective cytotoxicity against melanoma cells (IC_{50} = 0.065 mM) and induced apoptosis in human gastric cancer cells (IC_{50} = 0.720 mM) by blocking the notch signal pathway.[57,58] The unprecedented bis-azaphilones, hybridorubrins A–D, isolated from *Hypoxylon fragiforme*, composed of mitorubrin and fragirubrin-type moieties exhibited strong inhibitory activity against biofilm formation by *S. aureus*.

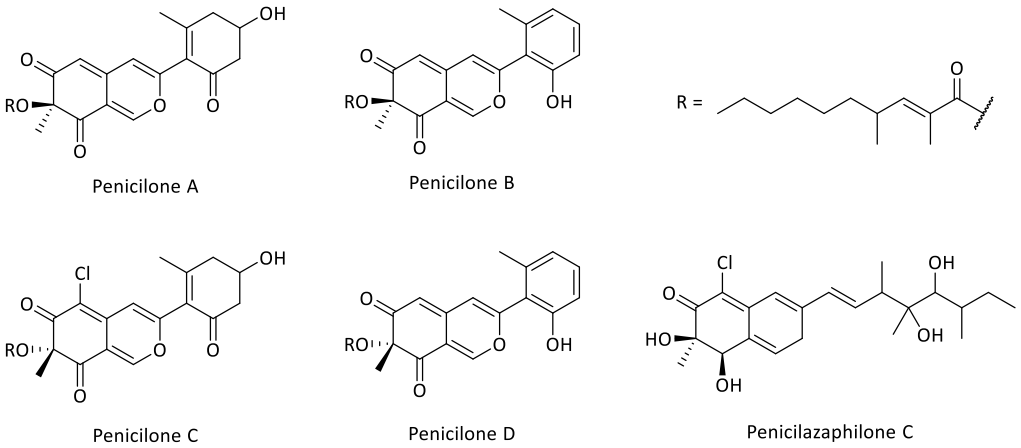

Figure 1.5. Structures of penicoliones A–D and penicilazaphilone C.

Austdiol (**1**) is a gastrointestinal mycotoxin first isolated in 1973 from mouldy maize meal cultures of *Aspergillus ustus*.[59] The maize meal cultures were found to cause acute toxicoses in day-old ducklings, which led to the isolation of five related diketopiperazines and the major toxin, austdiol.[59,60] The chemical structure of **1** was identified by NMR spectroscopy. Horeaus's partial resolution corresponded closely to mitrorubrin except for a deshielded H-4 which was proposed to be from a nearby aldehyde. The presence of the C-5 aldehyde was then confirmed by formation of dark red 2,4-dinitrophenylhydrazone. The conformation and absolute configuration of **1** were later confirmed with X-ray crystallography of the bromo-derivative to establish the *trans*-*vic*-diol and 7*R*,8*S* configuration (**Figure 1.6**).[60,61] Unlike other azaphilones, treatment of **1** with ammonia led to extensive decomposition and attempts to oxidise the C-8 hydroxy group were futile. Later, the metabolite dihydrodeoxy-8-*epi*-austdiol was isolated from the same source and possessed a *cis*-*vic*-diol with 7R,8R configuration, which allowed C-8 oxidation and even cyclic acetal formation.[60]

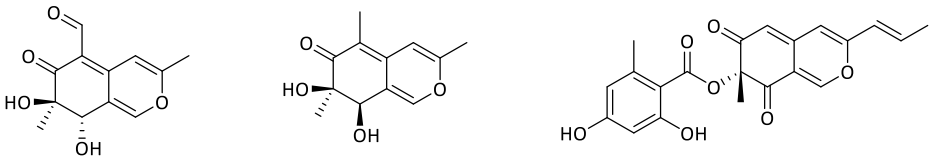

Figure 1.6. Structures of austdiol, dihydrodeoxy-8-*epi*-austdiol and mitorubrin.

Along with 16 other mycotoxins screened for mutagenetic activity against *Salmonella typhimurium*, **1** was found to be mutagenic with and without metabolic activation.[62] In Chinese hamster ovary (CHO-K1) cells, austdiol exhibited cytotoxicity via DNA damage which increased the frequency of micronuclei and nucleoplasmic bridges in binucleated cells.[63]

In the following years, **1** and a variety of austdiol derivatives were isolated from different fungal sources. The Kittakoop group in 2012 isolated the novel metabolite dothideomycetide A from *Dothideomycete* sp., which is the first polyketide containing a tricyclic 6,6,6 ring system and was proposed to be biosynthetically derived from austdiol (**Figure 1.7**).[64] Dothideomycetide A exhibited cytotoxic activity (MOLT-3 cells: IC_{50} = 15 µg mL^{-1}) and antibacterial activity (*S. aureus*/MRSA: MIC = 128/256 µg mL^{-1}).

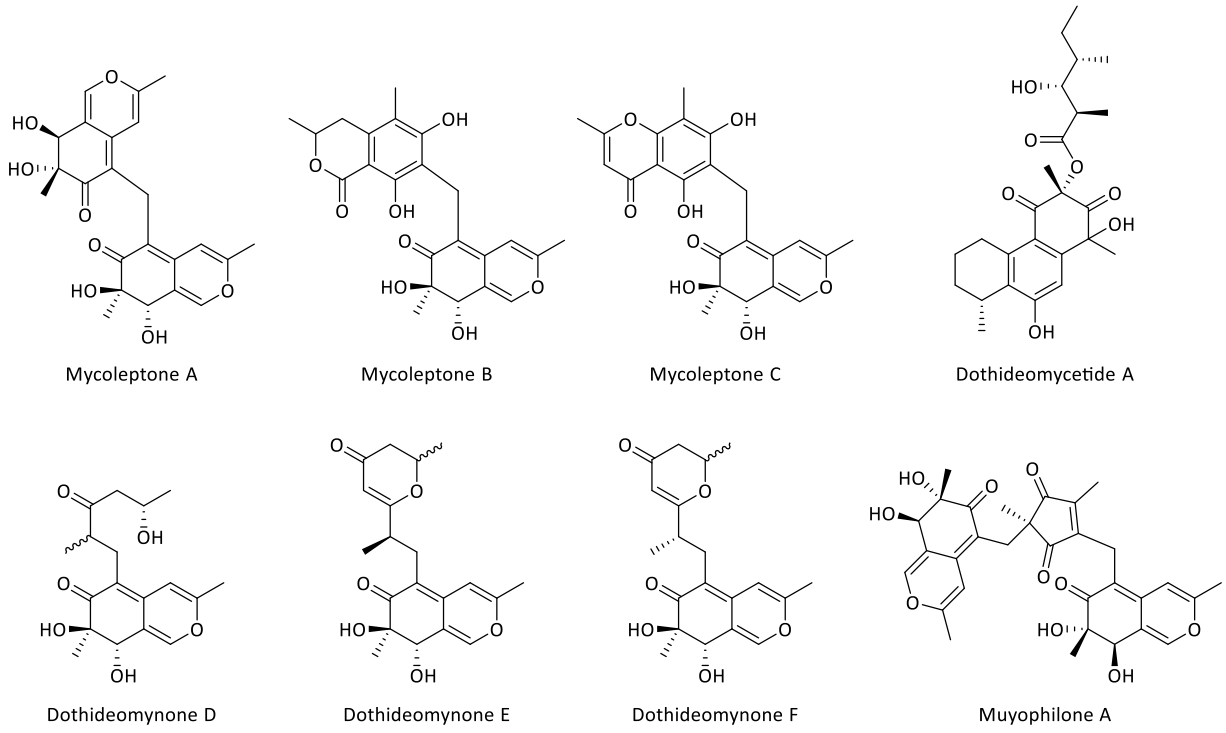

Figure 1.7. Structures of mycoleptones A–C, dothideomycetide A, dothideomynones D–F, and muyophilone A as co-metabolites of austdiol.

In 2014, the novel compounds mycoleptone A-C were isolated from *Mycoleptodiscus indicus*, and found to contain an uncommon methylene bridge between two austdiol monomers, which few azaphilone dimers possess.[46,65] Biosynthesis of mycoleptone A was proposed by condensation of two austdiol units, one unit decarbonylated while the other aldehyde was reduced to a reactive carbocation, which then reacted by Friedel-Crafts alkylation. Mycoleptone B was found to be the most cytotoxic (PC3 cells: IC_{50} = 7.1 ± 3.8 μM), which was still less potent than the reference compound, doxorubicin (PC3 cells: IC_{50} = 0.41 ± 0.05 μM).

The success of employing the one-strain-many-compounds (OSMAC) method to produce new azaphilones from *Dothidoeomycete* sp.[66] and biohalogenated depsidones with halogen-containing media, inspired the Kittakoop group. This resulted in the production of nine new polyketides and five known compounds including **1**, in high yield.[67] Interestingly, the novel metabolites dothideomynone D–F, closely resembled **1** except for substitution of the C-5 aldehyde, which can provide insight into the biosynthesis of these polyketides. The austdiol derivatives did not possess any cytotoxic or antibacterial activity, however, supporting the hypothesis that the C-5 aldehyde is partly responsible for the toxicity of austdiol. Austdiol was also reported to possess bacteriostatic activity against *Xanthomonas axonopodis* pv. *passiflorae*, a bacterium which causes bacterial blight in passionfruit, in 2019.[68] This recent application of azaphilones can change the perspectives of polyketides primarily sought for human therapy and demonstrates the importance of wide biological screening. Recently, the novel heterotrimer muyophilone A was isolated from the endophytic fungus, *Muyocopron laterale*, which represents the first example within the azaphilone heterotrimers class.[69] The heterotrimeric derivative is composed of two austdiol units connected through a five-membered carbon bridge possibly originating from 4,6-dimethylcurvulinic acid, which were also both isolated. No antibacterial or antifungal activity was observed for muyophilone A. However, expanding the structural diversity of azaphilone trimers and exploring this unique biosynthetic pathway is worth further investigation.

Isotopic labelling studies were performed by Colombo *et al.* and was determined by ^{13}C-NMR analysis of [1,2-$^{13}C_2$] acetate- and [Me-^{13}C] methionine-derived austdiol as the starting materials.[70] The austdiol skeleton is derived from a single pentaketide chain, composed of head-to-tail acetate units, and two C_1 units introduced by *S*-adenosyl-methionine (SAM) to give C-5 aldehyde and C-7 methyl groups. Cultivation was carried out in an ^{18}O-enriched atmosphere followed by ^{13}C-NMR to distinguish between ^{13}C-^{16}O and ^{13}C-^{18}O peak shifts. This revealed a mechanism involving addition of an activated oxygen molecule to the C-7–C-8 double bond of quinone-methide or dialdehyde,

mediated by a mono-oxygenase.[71] Subsequent reduction of the C-8 carbonyl group would yield the *trans*-vicinal diol system (**Figure 1.8**).

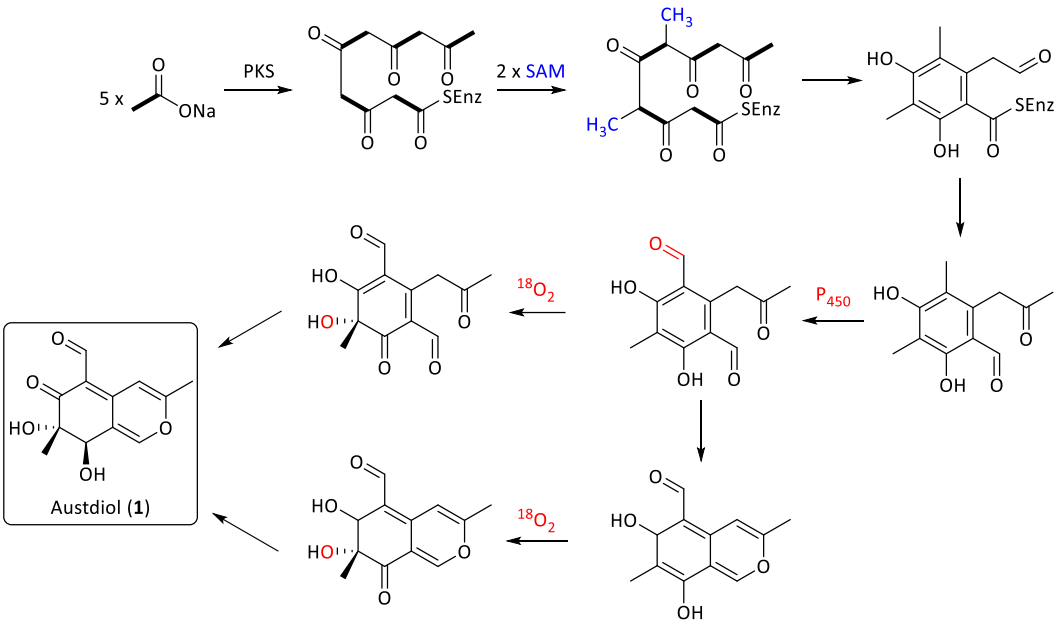

Figure 1.8. Proposed biosynthetic pathway to austdiol which was carried out in $^{18}O_2$-enriched environment to confirm the site of oxidation by NMR peak shifts. Adapted from Colombo *et al*.[70,71]

Bulgarialactones and deflectins contain a linear γ-lactone ring on an azaphilone nucleus at C-6/7 and C-7/8 respectively and were found to be a new class of heat shock protein Hsp90 inhibitors.[72] It was also observed that an *N*-benzyl moiety exerted enhanced Hsp90 binding. However, the deflectins possessed an angular structure reducing the effect of Hsp90 binding and antiproliferative properties. A SAR study of the novel compound 5-bromoochrephilone, indicated that a 5-halogen atom, an 8-H, and a conjugated diene moiety in the C-3 side chain are important for inhibiting gp120-CD4 binding, required for human immunodeficiency virus (HIV) cell entry and consequent progressive destruction of CD4 white blood cells.[73] SAR studies indicate that the presence of electrophilic ketone(s) and/or enone(s) at both C-6 and C-8 are essential for cholesteryl ester transfer protein (CETP) inhibition.[74] Preliminary SAR studies also showed that the presence of a halogen atom at C-5 and a phenyl group at C-3 improved activity, that introducing a methyl group at C-1 led to reduction in activity, and that a free hydroxy group at C-7 plays an important role in antimicrobial activity.[75]

1.4. Aims and Scope of Study

In this study, austdiol derivatives were generated to investigate their biological properties, explore SAR, and expand the chemical space of the azaphilone family. While austdiol has been identified throughout the literature, little has been done to explore the reactivity of this known precursor. In this thesis, the stability of austdiol will be investigated under different reaction conditions to explain its prevalence in Nature. A small semi-synthetic library of austdiol derivatives will also be generated to understand the key reactivity sites of the austdiol scaffold which can provide insight into the azaphilones. A known high-producing austdiol strain, *Mycoleptodiscus* sp. MST-FP2931, generated sufficient austdiol supply for use in semisynthesis. These derivatives were screened for antibacterial, antifungal, and cell cytotoxic activities to identify structure-activity relationships. Finally, a 2,4-dinitrophenylhydrazone derivative of austdiol was explored as a chiral derivatisation agent to assist in the resolution of L and D stereoisomers of amino acids commonly found in natural products, by UV-vis detection in reversed-phase liquid chromatography.

2. Stability of Austdiol

2.1. Introduction

In their 1974 paper, Vleggaar *et al*. noted that austdiol (**1**) appeared to be unaffected by the addition of a base, while prolonged exposure led to extensive decomposition.[59] The authors did not further investigate the base degradation products or explore the stability of austdiol under acidic conditions. Before attempting to perform semi-synthetic modifications to the austdiol scaffold, the stability of the compound was explored in various solvents at different temperatures and pHs.[59]

2.2. Degradation of Austdiol

A solution of **1** in DMSO-d_6 was observed to change colour from yellow to green over 30 minutes, albeit with no apparent change in ^{1}H-NMR spectrum. Over 18 hours, the colour of the solution changed to dark green, then to brown over 3 days (**Figure 2.1**) again with no apparent change in its ^{1}H-NMR spectrum. This can be due to trace degradation of **1** that would cause changes in the conjugated pi electrons of the molecule which would affect the light that is absorbed and generate highly coloured trace compounds. Austdiol was also shown to be stable up to 80 °C in methanol.

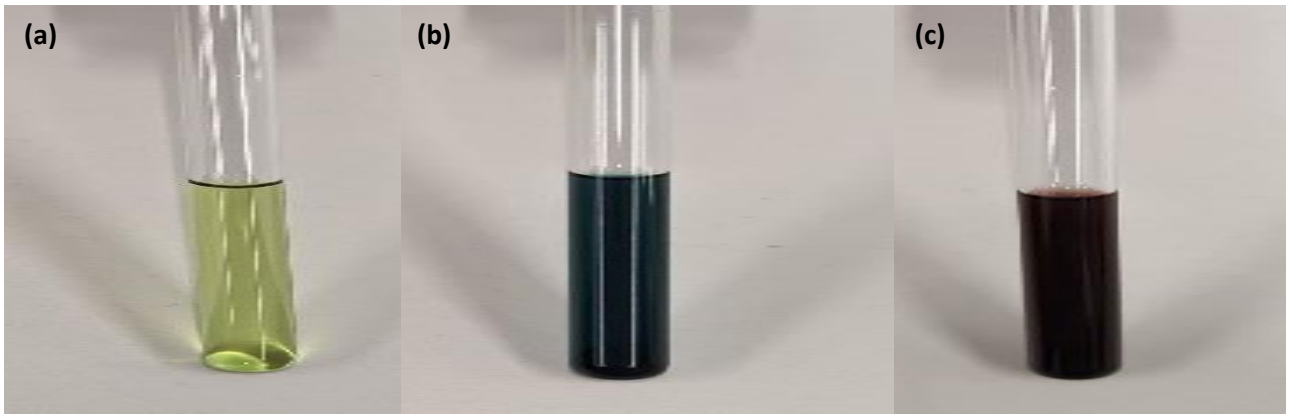

Figure 2.1. Colour change of a solution of **1** in DMSO-d_6 at (**a**) 30 min, (**b**) 18 h, and (**c**) 3 d.

Reaction of **1** with 1% aqueous 1 M sodium hydroxide (0.5 eq.) in methanol produced a major product (**2**) confirmed by HPLC (**Scheme 2.1**). It was revealed that **1** underwent ~50% conversion into **2** which was observed as a later-eluting peak by HPLC and is possibly due to the sub-stoichiometric concentration of sodium hydroxide used (**Figure 2.2**).

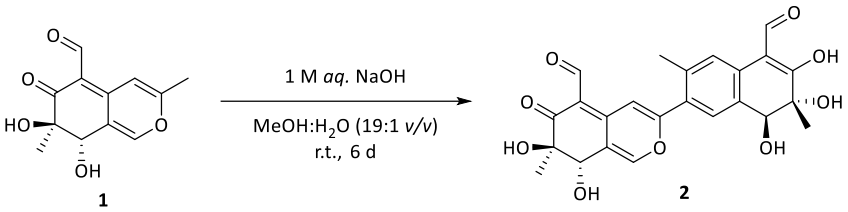

Scheme 2.1. Base-catalysed dimerisation of austdiol (**1**) into austdiol-dimer (**2**)

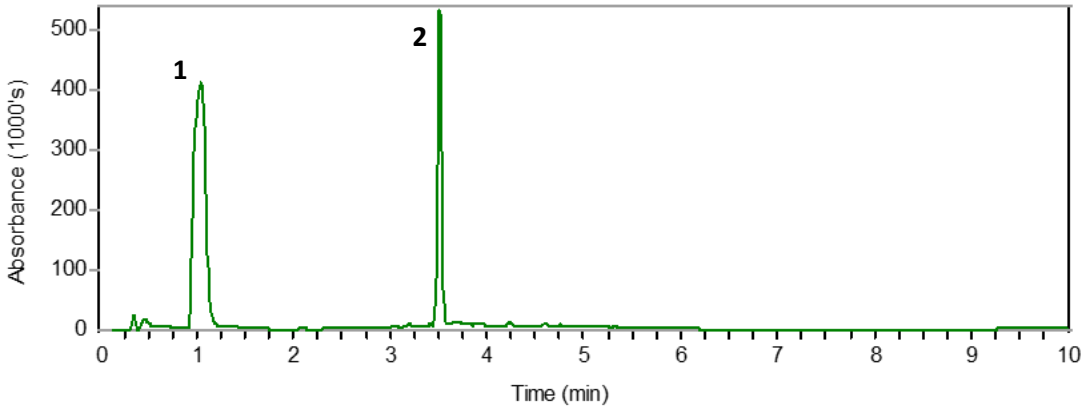

Figure 2.2. HPLC trace of reaction mixture of austdiol in 1% aqueous 1 M sodium hydroxide in methanol after 6 days.

LCMS analysis of the reaction mixture revealed **2** to be 18 u less than double the molecular weight of **1** ([M + H] $^{+}$ *m/z* 455.1 for **2** vs. **1** *m/z* 237.1) suggesting dimerisation with concomitant dehydration. The significant difference in molecular weight between **1** and **2** and good solubility in methanol prompted purification on Sephadex LH-20, resulting in the red solid, austdiol-dimer (**2**). HR-ESI(+)-MS analysis revealed a protonated molecule ([M + H]$^{+}$ *m/z* 455.1340) indicative of a molecular formula $C_{24}H_{22}O_9$ requiring 14 double bond equivalents (DBEs), which fits with 10 double bonds and 4 rings and is twelve carbons, ten hydrogens, and 4 oxygens more compared to **1** ($C_{12}H_{12}O_5$). The UV spectrum of **2** has similarities with **1** (λ_{max} 206 and 260 nm), with a bathochromic shift from 381 to 406 nm (20 nm) suggesting an extension in conjugation equivalent to one additional double bond (**Figure 2.3**).

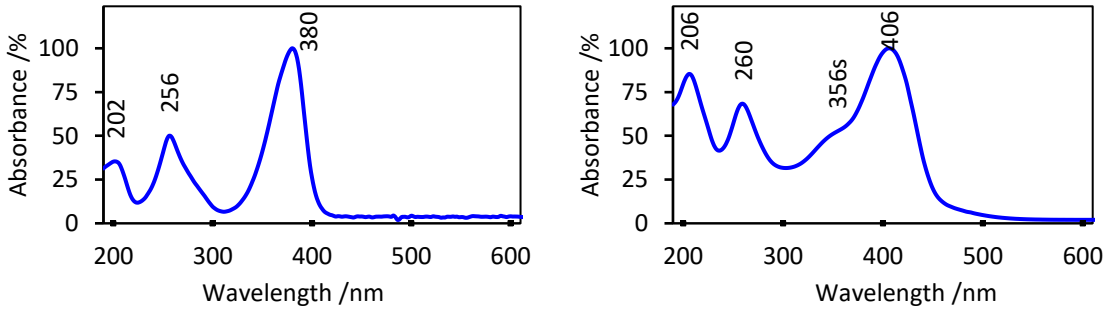

Figure 2.3. UV-vis spectra of **1** (left) in methanol and **2** (right) in acetonitrile.

The ^{1}H-NMR spectrum of **2** revealed pairs of peaks with similar chemical shifts to those observed in **1**, suggesting the presence of two austdiol monomers. The initially proposed mechanism involved deprotonation of the C-9 methyl group of one austdiol monomer, which then attacks the C-10 carbonyl of a second austdiol monomer via an aldol-like condensation. This was followed by an E1cB elimination of water to form the double bond bridge between two austdiol monomers. However, the ^{1}H-NMR data for **2** revealed two aldehyde protons (δ_H 10.04 and 9.78 ppm), which, does not support this proposed mechanism. Due to retention of 7-OH and 8-OH between the two monomers, it was predicted that elimination of water contained a pyran oxygen and thus required a ring opening mechanism. As previously thought, the C-9 of one austdiol monomer was deprotonated but now instead attacks the C-1 position of the other austdiol monomer via a Michael-type addition which is stabilised by the multiple resonance forms of the conjugated system. This causes the ring opening step to form a ketone. The C-9 is deprotonated again which forms the nucleophilic double bond that attacks the carbonyl ketone for ring closure. Subsequent elimination of water and conversion from C-6′ keto to the enol form helps restore aromaticity aiding in stability of **2**.

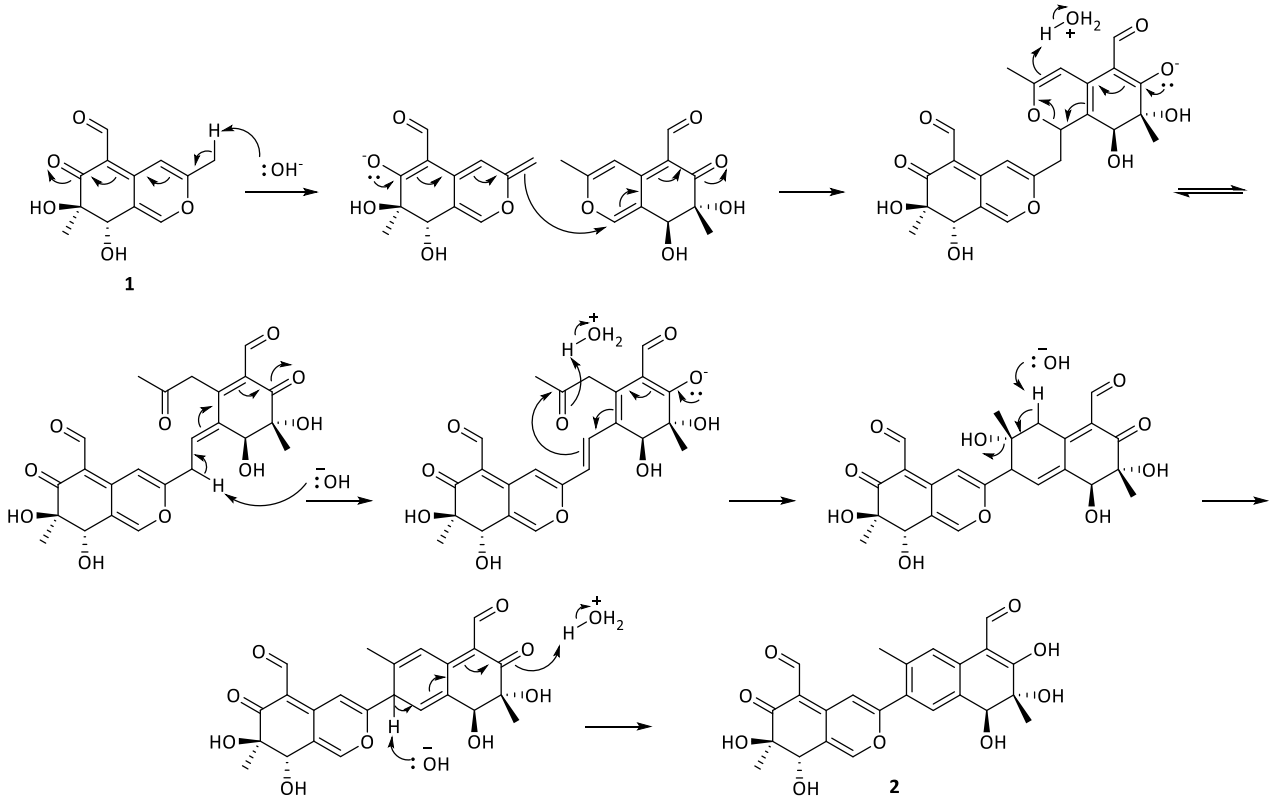

Scheme 2.2. Proposed mechanistic pathway for the base-catalysed dimerisation of austdiol (**1**) to form austdiol-dimer (**2**).

The HMBC correlations of **2** showed pairs of peaks that were similar to **1**, which indicated the presence of two austdiol monomers. Differences in HMBC correlations arose around C-3, C-4, C-1', C-2', C-3' and C-9' which indicated a bridge between the two monomers. HMBC correlations between H-4 and C-2' and, H-4 and C-2' as well as between H-1 and C-3 and, H-1' and C-3 revealed the bridge to connect C-9 of one austdiol monomer to the C-1' and C-3' of the other monomer. ROESY correlations between H-9' and H-4, and H-4' and H-1' provide further evidence for this structure. A peak corresponding to 6'-OH was not observed in the ^{1}H NMR spectrum. Therefore, analysis of 2D NMR spectra led to the assignment of all protons and carbons in **3** and secured the structure (**Figure 2.4** and **Table 10.1.1**).

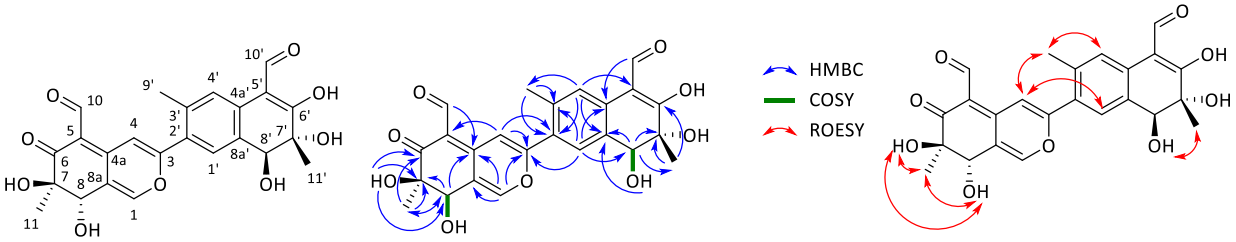

Figure 2.4. Key 2D NMR correlations observed in austdiol-dimer (**2**).

Reaction of **1** with 1% or 5% aqueous 1 M hydrochloric acid in methanol formed a major and minor product, as confirmed by TLC and HPLC (**Scheme 2.3**). The rate of reaction increased with higher concentration of acid and higher temperature (20 °C and 60 °C), with prolonged exposure leading to extensive degradation. The reaction mixture was purified by flash chromatography with MeOH/CH_2Cl_2/AcOH (8:91:1 *v/v/v*) mobile phase yielding 5-deformylaustdiol (**3**) as the major product.

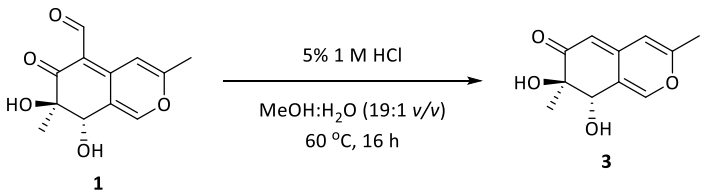

Scheme 2.3. Reaction of austdiol (**1**) with 1 M hydrochloric acid to yield 5-deformylaustidol (**3**)

HR-ESI(+)-MS analysis of **3** revealed a protonated molecule ($[M + H]^+$ *m/z* 209.0820) indicative of a molecular formula $C_{11}H_{12}O_4$ requiring 6 DBEs, which fits with 4 double bonds and 2 rings, and is one carbon and one oxygen fewer than for **1** ($C_{12}H_{12}O_5$). The UV spectrum of **3** is similar to that of **1**, with a hypsochromic shift of λ_{max} (20 nm) indicative of a reduction in conjugation equivalent to one double bond. The ^{1}H and ^{13}C NMR spectra of **3** were very similar to those for **1** with the absence of

resonances associated with the aldehyde (δ_H 10.00; δ_C 189.4 ppm) and the presence of a new peak in ^{1}H-NMR spectrum (δ_H 5.18 ppm) indicative of a 5-deformyl analogue of **1**. An HMBC correlation from H-5 to C-7 indicates protonation at C-5. A ROESY correlation from H-4 to H-5 suggested decarbonylation at C-5 Therefore, analysis of 2D NMR spectra led to the assignment of all protons and carbons in **3** and secured the structure (**Figure 2.5** and **Table 10.1.2**).

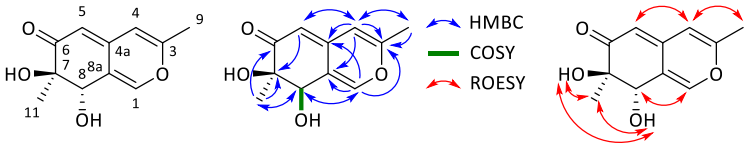

Figure 2.5. Key 2D NMR correlations observed in 5-deformylaustdiol (**3**).

Vleggaar *et al.* synthesised **3** by firstly brominating C-5 followed by reduction with hydrogen over platinum dioxide (Adams' catalyst), which demonstrates the reactivity of the aldehyde under acidic conditions and a possible decarboxylation mechanism.[59] Andrioli *et al.* proposed a mechanistic pathway for the biosynthesis of the austdiol dimer, mycoleptone A, which was formed via a Friedel-Crafts reaction of a C-10 decarbonylated, and C-10 reduced austdiol suggesting a possible decarbonylation mechanism.[65] Finally, Senadeera *et al.* proposed the biosynthesis of the novel tricyclic polyketide, dothideomycetone A, from austdiol by initial oxidation of the C-5 aldehyde, followed by protonation of C-5 and finally C-10 decarboxylation (**Scheme 2.4**).[64]

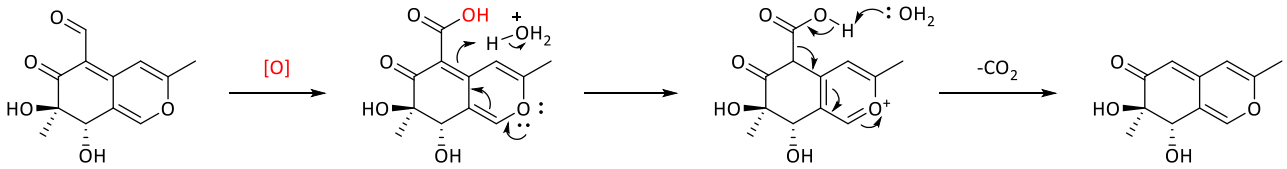

Scheme 2.4. Proposed mechanism for the deformylation of **1** to yield **3**.

2.3. Summary

Austdiol was shown to undergo a base-catalysed dimerisation, which was supported by NMR comparison with austdiol that showed a change at C-9 and the condensation of two austdiol monomers. An acid-catalysed decarboxylation was also witnessed with no changes to the ketone indicating that the aldehyde is labile under acidic conditions. Therefore, for future semi-synthetic procedures, reactions that are pH-dependent, a weak acid or base should be employed to minimise side-products.

3. Semi-synthetic Derivatives of Austdiol

3.1. Introduction

Vleggaar *et al*. synthesised several austdiol derivatives to elucidate the structure and stereochemical configuration of **1**.[59] As no other publications are known to expand upon this seminal work, further semi-synthetic modifications of **1** were performed to explore the chemical space around this unique metabolite. Reduction and oxidation of austdiol was undertaken due to interest in understanding the reactivity of the highly conjugated scaffold. Austdiol is an azaphilone, which reacts with primary amines to form vinylogous γ-pyridones.[46] The synthesised austdiol-amine derivatives were explored to test the effect of different primary amines containing different R-groups for biological activity. Austdiol also has a C-5 aldehyde, rarely seen in azaphilones, which was exploited to generate a small library of novel semi-synthetic imine derivatives with the possibility of further reduction.

3.2. Oxidation of Austdiol

Vleggaar *et al.* attempted to oxidise 8-OH with a variety of oxidising agents to obtain an extended conjugated azaphilone structure but were unsuccessful. No further details of the specific oxidising agents used, nor the products formed, were mentioned, which prompted the investigation of both the oxidation and reduction of austdiol (**1**). Oxidation of **1** was attempted with the strong oxidant, Jones reagent (chromic acid) in methanol and was analysed with HPLC (**Scheme 3.1**).

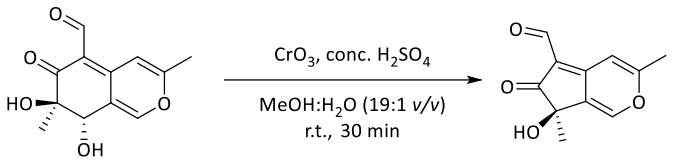

1 **4**

Scheme 3.1. Oxidation of austdiol (**1**) with Jones reagent (CrO_3/H_2SO_4) to yield decarbonyl[4.3.0]austdiol (**4**).

The major product was separated by preparative HPLC to give a light-brown solid, 8-decarbonyl[4.3.0]austdiol (**4**). HR-ESI(+)-MS analysis of **4** revealed a protonated molecule ($[M + H]^+$ *m/z* 207.0656) indicative of a molecular formula of $C_{11}H_{10}O_4$ requiring 7 DBEs, which fits with 5 double bonds and 2 rings and is one carbon, two hydrogens and one oxygen fewer than **1** ($C_{12}H_{12}O_5$).

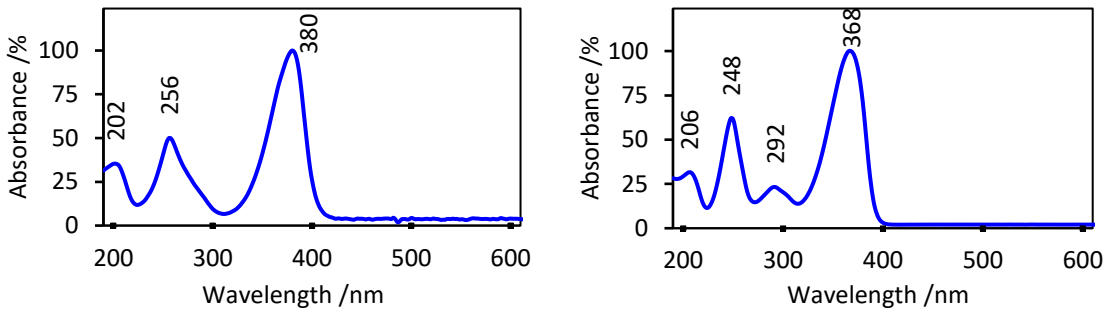

Figure 3.1. UV-vis spectra of austdiol (**1**) (left) in methanol and 8- decarbonyl[4.3.0]austdiol (**4**) (right) in acetonitrile.

It was initially proposed that oxidation of both the C-8 hydroxy and C-5 aldehyde groups had occurred followed by decarboxylation of the C-5 carboxylic acid. This proposal was also supported by minor peaks on LCMS matching with the proposed intermediates of the aldehyde oxidation ($[M + H]^+$ *m/z* 253) and di-oxidation ($[M + H]^+$ *m/z* 251). However, the NMR data suggested that an aldehyde group was still present (δ_H, 9.72 ppm; δ_C 185.5 ppm). Similarly to **1**, the HMBC correlations from H-11 to C-6, C-7, and C-8 were seen, and an additional correlation was present from H-1 to C-7 that was not observed in **1**. This new correlation suggested elimination of C-8 and bond formation between C-7 and C-8a to form a 5-membered ring.

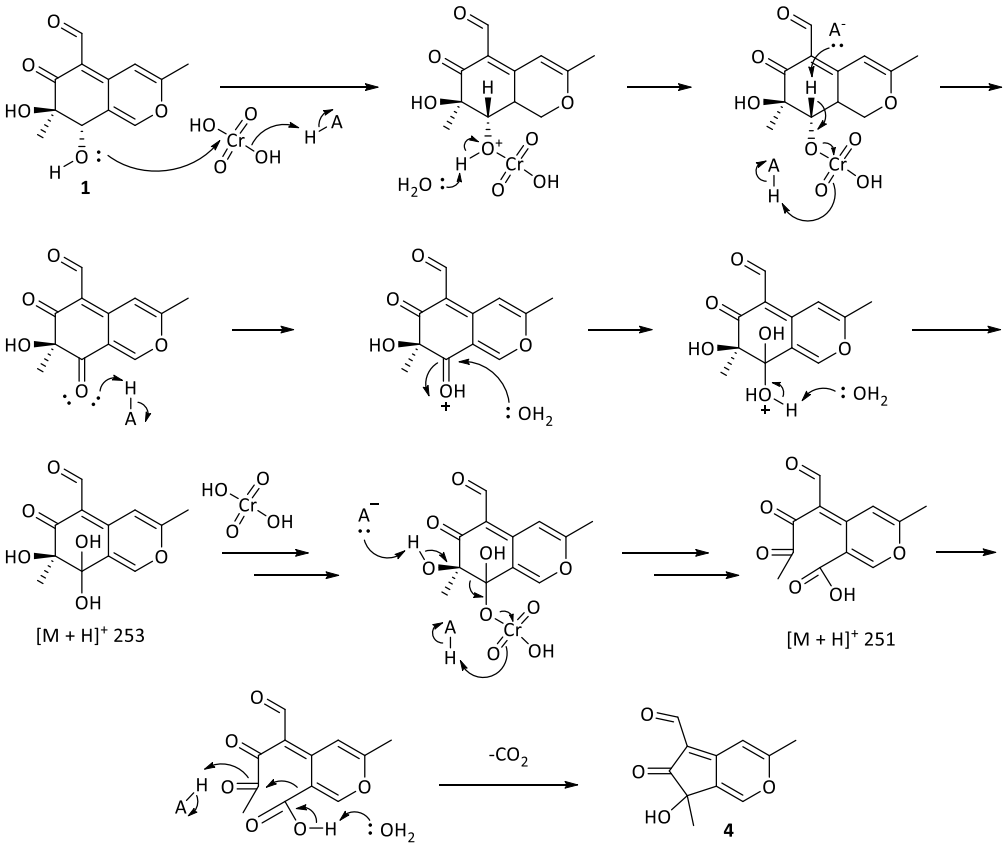

Scheme 3.2. Proposed mechanism for the formation of decarbonyl[4.3.0]austdiol (**4**) from austdiol (**1**).

The proposed mechanism involves oxidation of C-8 followed by nucleophilic attack on the carbonyl carbon by water to form a *gem*-diol, which was observed as a minor compound by LCMS ($[M + H]^+$ *m/z* 253). The 8-OH attacks another chromic acid by cleavage of the C-7/8 bond forming the C-7 ketone and C-8 carboxylic acid which was also observed by LCMS ($[M + H]^+$ *m/z* 251). Finally, decarboxylation and bond migration to form the C-6/8a occurs, yielding 8-decarbonyl[4.3.0]austdiol (**4**) (**Scheme 3.2**). Therefore, analysis of 2D NMR spectra led to the assignment of all protons and carbons in **4** and secured the planar structure (**Figure 3.2.** and **Table 10.1.3**). The proposed mechanism would likely result in loss of chirality at C-7 (as it transitions through a ketone) but, electronic circular dichroism (ECD) spectra showed that the molecule still has chirality (**Figure 10.2**). Density-functional theory (DFT) calculations may be useful to resolve configuration and possibly revise the mechanism.

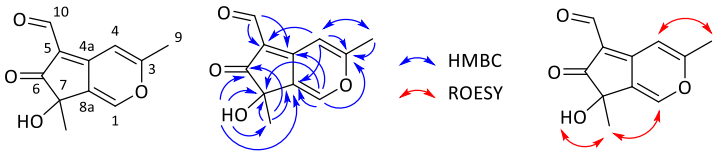

Figure 3.2. Key 2D NMR correlations observed in 8-deformyl[4.3.0]austdiol (**4**).

3.3. Reduction of Austdiol

Reduction of **1** with sodium borohydride in methanol produced a mixture of products, as shown by HPLC. The major compound was separated by preparative HPLC, yielding 10,10*O*-dihydroaustdiol (**5**) as a pale-yellow solid (**Scheme 3.3**). HR-ESI(+)-MS analysis of **5** revealed a protonated molecule ($[M + H]^+$ *m/z* 239.1635) indicative of a molecular formula of $C_{12}H_{14}O_5$, requiring 6 DBEs, which fits with 4 double bonds and 2 rings and is two hydrogens more than **1** ($C_{12}H_{12}O_5$). The UV spectrum λ_{max} of **5** demonstrated a hypsochromic shift from 384 nm to 365 nm (20 nm), which is indicative of a reduction in conjugation equivalent to one double bond (**Figure 3.3**).

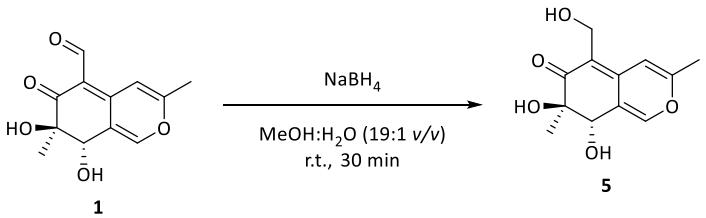

Scheme 3.3. Reduction of austdiol (**1**) with sodium borohydride to yield 10,10*O*-dihydroaustdiol (**5**).

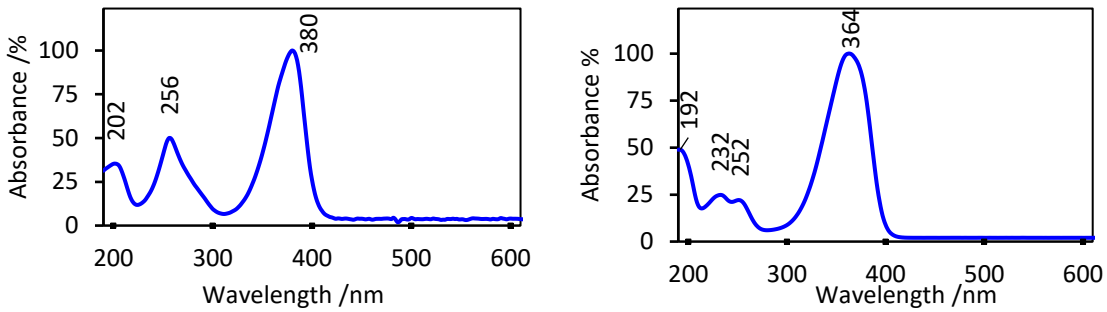

Figure 3.3. UV spectra of austdiol (left) in methanol and 10,10*O*-dihydroaustdiol (**5**) (right) in acetonitrile.

The ^{1}H and ^{13}C NMR data for **5** also indicated the absence of signals corresponding to the aldehyde (δ_H 10.00, δ_C 189.3 ppm). The presence of signals attributable to a new methylene group with an unusually shielded carbon nucleus (δ_H 3.28, δ_C 18.7 ppm) showing HMBC correlation to C-6 ketone and non-substituted C-4a suggested the aldehyde group of **1** had been reduced to a primary alcohol. The C-6 ketone remained unchanged (δ_C 198.0 ppm). Similarly, to the other exchangeable protons, 7-OH and 8-OH, that show no HMBC correlation, 10-OH shows no HMBC correlation to C-10. Therefore, analysis of 2D NMR spectra led to the assignment of all protons and carbons in **5** and secured the structure (**Figure 3.4** and **Table 10.1.4**).

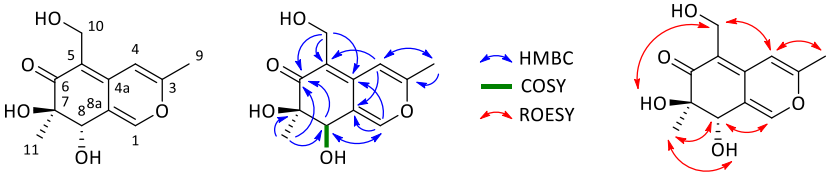

Figure 3.4. Key 2D NMR correlations observed in 10,10*O*-dihydroaustdiol (**5**).

3.4. Amination of Austdiol

Azaphilones are known to react with primary amines via an exchange reaction by substitution of the oxygen in the 4*H*-pyran ring to form the vinylogous γ-pyridone with the elimination of water.[46] The nitrogen is proposed to first attack the C-1 or C-3 position to form the carbinolamine, which is stabilised by the conjugated system. This is followed by a ring opening and proton transfer to form the enol, which tautomerises into either the ketone (C-1 attack) or aldehyde (C-3 attack). The 6-membered ring recyclises via nucleophilic addition of the terminal nitrogen with the electrophilic carbonyl to form the carbinolamine. Aromaticity is then regenerated by the elimination of water to yield the vinylogous γ-pyridone (**Scheme 3.4**).

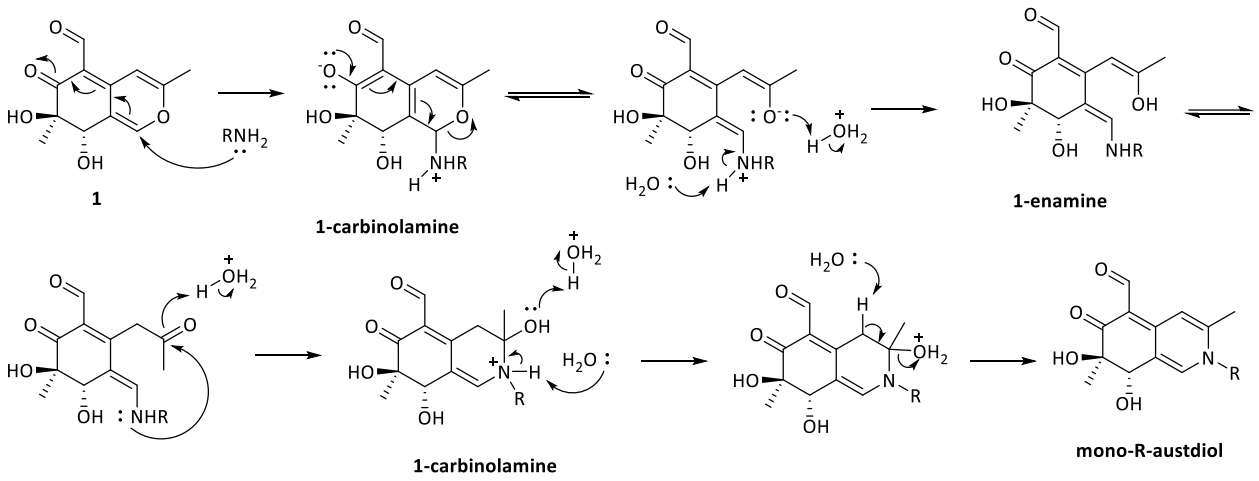

Scheme 3.4. Proposed mechanism for reaction of austdiol (**1**) with primary amines.

Vleggaar *et al.* treated austdiol with ammonia, which led to extensive decomposition products.[59] However, unlike other azaphilones, the presence of an aldehyde group at C-5 provides the opportunity for austdiol to also react with amines to form an imine via a pH-dependent equilibrium, with the optimum pH known to be at slightly acidic conditions (pH 4–6).[76] At high pH, there is insufficient acid to activate the system by protonation of the carbonyl oxygen and at too low pH, the amine will be protonated, which will hinder its ability for nucleophilic attack at the carbonyl carbon.

3.4.1. Austdiol-ethanolamine

Ethanolamine was added to a solution of austdiol in methanol/water (95:5 *v/v*), which resulted in two major products as shown by HPLC. The two products were separated by C_{18} preparative-HPLC to yield austdiol-mono-ethanolamine (**6**) as a red solid and austdiol-di-ethanolamine (**7**) as a yellow solid (**Scheme 3.5**).

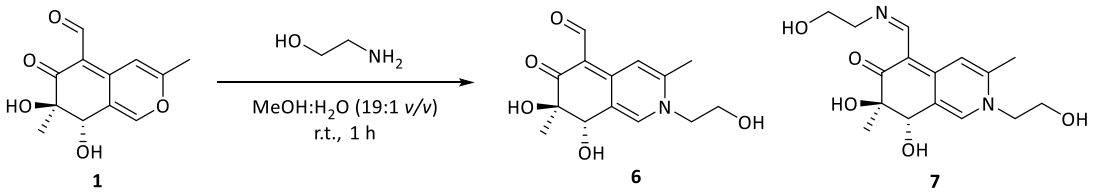

Scheme 3.5. Reaction of austdiol (**1**) with ethanolamine to yield austdiol-mono-ethanolamine (**6**) and austdiol-di-ethanolamine (**7**)

Even with excess ethanolamine (8 eq.), the major product was **6**. This may be due to ethanolamine being basic and thus excess would result in a high pH in aqueous conditions, which would inhibit imine formation, as explained earlier. ESI(+)-MS analysis of **6** revealed a protonated molecule ($[M + H]^+$ *m/z* 280.1185) indicative of a molecular formula of $C_{14}H_{17}NO_5$ requiring 7 DBEs, which fits with 5 double bonds and 2 rings and is two carbons, five hydrogens and one nitrogen more than **1** ($C_{12}H_{12}O_5$). The mass of **6** is 43 u heavier than austdiol, suggesting the addition of ethanolamine and elimination of water. An additional HMBC correlation from H-1 to C-1′ (δ_H 5.30 ppm) indicates the exchange of nitrogen for the pyran oxygen with COSY correlation revealing 2′-CH_2 (δ_H 3.75 ppm) and 2′-OH (δ_H 5.12 ppm). ROESY correlations were also seen between 1′-H and 1-H, and between and 2′-H and 9-H. Further evidence of the retention of ketone (δ_C 196.2 ppm) and aldehyde (δ_H 9.86; δ_C 185.3 ppm) indicated no imine formation at these sites. Therefore, analysis of 2D NMR spectra, as well as the data correlation with those of **1** led to the assignment of protons and carbons in **6** and secured the structure (**Figure 3.5** and **Table 10.1.5**).

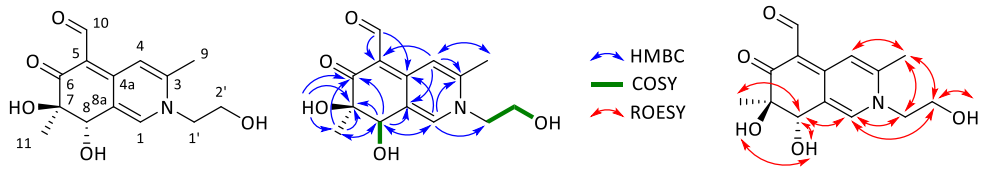

Figure 3.5. Key 2D NMR correlations observed in austdiol-mono-ethanolamine (**6**).

The minor product, **7**, with ESI(+)-MS analysis revealed a protonated molecule ($[M + H]^+$ *m/z* 323.1645) indicative of a molecular formula of $C_{16}H_{22}N_2O_5$ requiring 7 DBEs, which fits with 5 double bonds and 2 rings and is four carbons, ten hydrogens and two nitrogens more than **1** ($C_{12}H_{12}O_5$). The mass of **7** is 86 u more than austdiol indicating condensation of two ethanolamine molecules. Similarly, to **6**, an HMBC correlation between H-1 (δ_H 8.32 ppm) and C-1′ (δ_C 57.0 ppm) was detected, along with COSY correlations from H_2-1′ through to 2′-OH. NMR signals associated with the C-5 aldehyde were not observed, while the presence of new upfield signal (δ_H 8.38; δ_C 157.7 ppm) were indicative of the formation of an imine at C-10. An HMBC correlation from H-10 to C-1′′ and COSY correlation from H_2-1′′ through to 2′′-OH provided further evidence of the presence of a second ethanolamine moeity. Therefore, analysis of 2D NMR spectra, as well as the data correlation with those of austdiol led to the assignment of protons and carbons in **7** and secured the structure (**Figure 3.6** and **Table 10.1.6**).

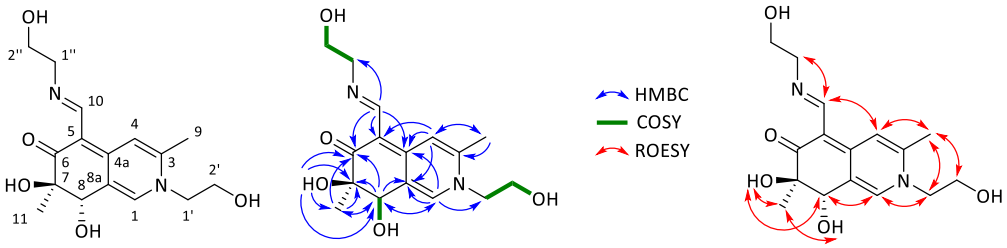

Figure 3.6. Key 2D NMR correlations observed in austdiol-di-ethanolamine (**7**).

The UV spectrum of austdiol-mono-ethanolamine is similar to austdiol but with λ_{max} 250 nm showing a hypsochromic shift from λ_{max} 385 nm to 355 nm (20 nm), which is indicative of a reduction in conjugation equivalent of one double bond (**Figure 3.7.**).

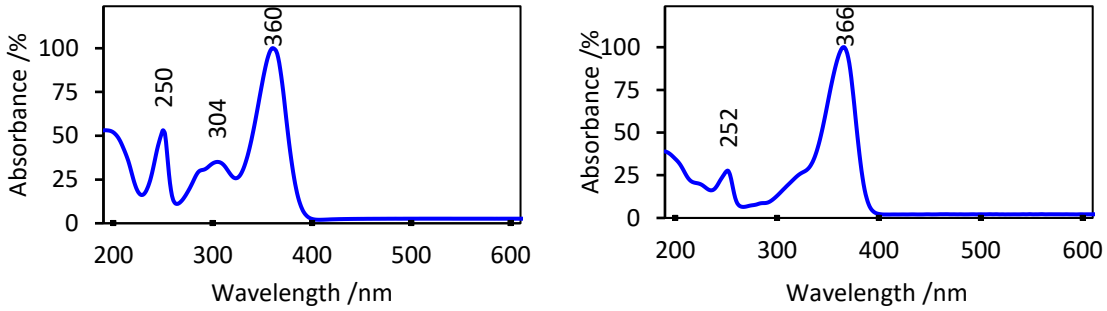

Figure 3.7. UV spectra of austdiol-mono-ethanolamine (**6**) (left) and austdiol-di-ethanolamine (**7**) (right) in acetonitrile.

3.4.2. Austdiol-Val-OMe

Valine methyl ester hydrochloride was converted to the free base with triethylamine and then added to a solution of **1** in methanol/water (95:5 *v/v*) (**Scheme 3.6**). Analytical HPLC trace showed the formation of two major products and two minor products. LCMS analysis of the major ion peaks ($[M + H]^+$ *m/z* 349.4) suggested the condensation of one valine methyl ester moiety, while the minor ion peaks ($[M + H]^+$ *m/z* 462.5) suggested the condensation of two valine methyl ester moieties. Purification of the reaction mixture by preparative HPLC yielded austdiol-mono-L-Val-OMe (**8**) and austdiol-mono-D-Val-OMe (**9**) as purple solids. Comparison to the analytical HPLC trace of the reaction mixture when using enantiomerically pure L-Val-OMe was used to assign **8** as the L form and **9** as the D form.

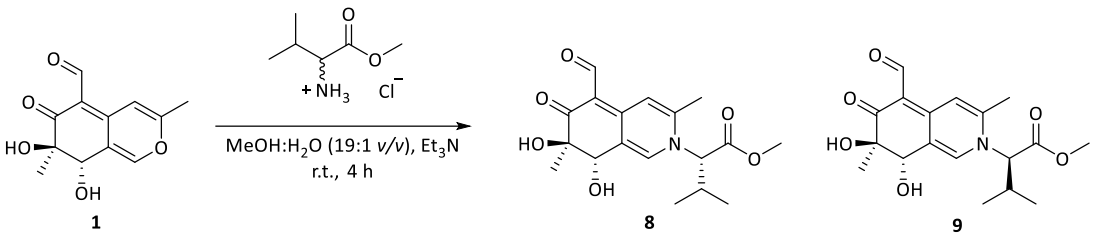

Scheme 3.6. Reaction of austdiol (**1**) with D/L-valine methyl ester to yield austdiol-mono-L-Val-OMe (**8**) and austdiol-mono-D-Val-OMe (**9**).

HR-ESI(+)-MS analysis of **8** and **9** revealed ions ($[M + H]^+$ *m/z* 350.1607 and 350.1609 respectively) indicative of a molecular formula of $C_{18}H_{23}NO_6$ requiring 8 DBEs, which fits with 6 double bonds and 2 rings and is six carbons, eleven hydrogens, one nitrogen, and one oxygen more than **1** ($C_{12}H_{12}O_5$). The UV spectra of **8** and **9** share similar λ_{max} with **7** indicating condensation of a single Val-OMe moiety seen as the broad peak λ_{max} 280–300 nm. ECD spectra of the two compounds revealed different enantiomeric products with chirality of the amino acid giving rise to the Cotton effect at around 220 nm.

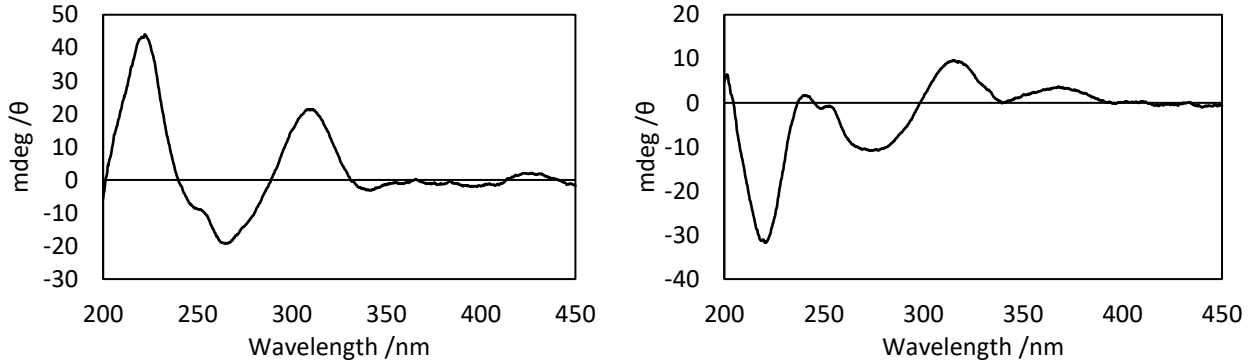

Figure 3.8. ECD spectra of austdiol-mono-L-Val-OMe (**8**) (left) and austdiol-mono-D-Val-OMe (**9**) (right) in acetonitrile.

A comparison of the ^1H and ^{13}C NMR spectra of **8** and **9** revealed slight differences in chemical shifts around C-1, C-8, C-9, C-6', and C-7' indicating the ability of austdiol to induce differences between derivatised L and D enantiomers of Val-OMe. Therefore, analysis of 2D NMR spectra, as well as the data correlation with those of austdiol led to the assignment of protons and carbons in **8** and **9** and secured the structures (**Figure 3.9** and **Table 10.1.7**; **Figure 3.10** and **Figure 10.1.8**).

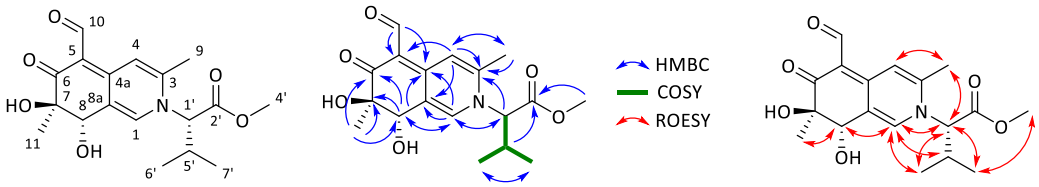

Figure 3.9. Key 2D NMR correlations observed in austdiol-mono-L-Val-OMe (**8**).

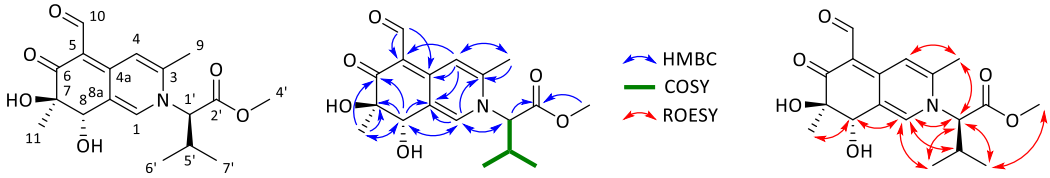

Figure 3.10. Key 2D NMR correlations observed in austdiol-mono-D-Val-OMe (**9**).

3.4.3. Synthesis of Austdiol-hydrazones

Hydrazines react with carbonyl compounds to form hydrazones via a condensation reaction and are widely used to help identify carbonyl functionality of unknown compounds, a well-known hydrazine being 2,4-dinitrophenylhydrazine (Brady's reagent).[77] Due to the ability of **1** to react with amines at two locations (C-5 aldehyde and O-2), two hydrazines were employed as aldehyde protecting groups to simplify the reaction mixture and form only the mono-amino-austdiol products. This has potential to be used as a characterisation tool by NMR spectroscopy by identifying the known peaks of the hydrazone.

3.4.4. Austdiol-2′,4′-dinitrophenylhydrazone (Austdiol-DNP)

A solution of 2,4-dinitrophenylhydrazine and concentrated H_2SO_4 (7 eq.) in methanol was added to a solution of austdiol in methanol/water (95:5 *v/v*) to produce a precipitate (**Scheme 3.7**). Filtration to obtain the precipitate yielded austdiol-2′,4′-dinitrophenylhydrazone (**10**) as a red solid.

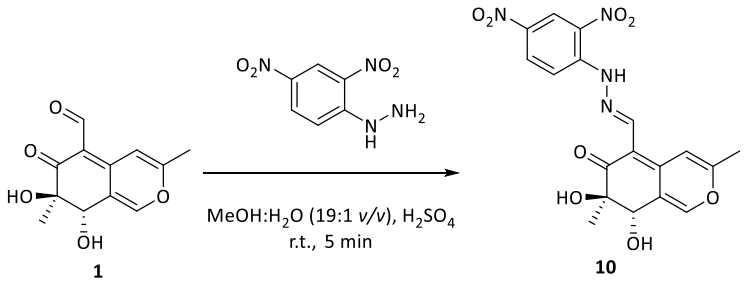

Scheme 3.7. Reaction of austdiol (**1**) with 2,4-dinitrophenylhydrazine to yield austdiol-2′,4′-dinitrophenylhydrazone (**10**).

HR-ESI(+)-MS analysis of **10** revealed a protonated molecule ($[M + H]^+$ *m/z* 417.1044) indicative of a molecular formula of $C_{18}H_{16}N_4O_8$ requiring 13 DBEs, which fits with 10 double bonds and 3 rings and is six carbons, four hydrogens, four nitrogens, and three oxygens more than **1** ($C_{12}H_{12}O_5$). The UV-vis spectrum of **10** revealed similar peaks to austdiol, λ_{max} 380 nm and 260 nm, with no peak shift. However, two new peaks are revealed at λ_{max} 300 nm and 464 nm demonstrating a new conjugated system separate from austdiol which is attributable to the 2'-4'-dinitrophenyl moiety (**Figure 3.11**).

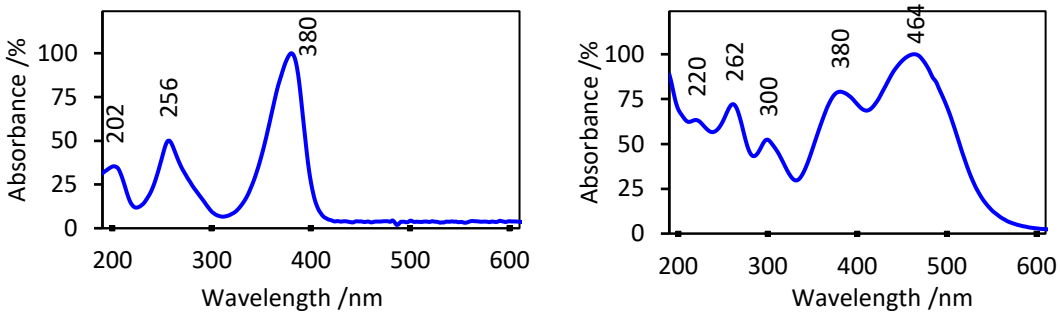

Figure 3.11. UV-vis spectra of austdiol (**1**) (left) in methanol and austdiol-DNP (**10**) (right) in acetonitrile.

The ^1H and ^{13}C NMR data for **10** and **1** were similar except for shifts around C-10. Austdiol-DNP showed new signals corresponding to three aromatic protons, C-3' (δ_H 8.85; δ_C 123.2 ppm), C-5' (δ_H 8.42; δ_C 130.0 ppm), and C-6' (δ_H 7.77; δ_C 116.2 ppm). These were supported by COSY correlation between H-5' and H-6' and the splitting pattern of H-3' showing meta coupling as a doublet (J = 2.6 Hz), C-5' showing ortho-meta coupling as a doublet-doublet (J = 9.6, 2.6 Hz) and C-6' showing ortho coupling as a doublet (J = 9.6 Hz). Absence of the aldehyde signal (δ_H 10.00; δ_C 198.0 ppm) and the appearance of a new signal for 1'-NH (δ_H 11.53 ppm) with HMBC correlation to the C-10 imine (δ_C 148.1 ppm), and the C-6 ketone (δ_C 197.1 ppm) provided evidence for the condensation of one 2,4-dinitrophenylhydrazine unit onto the C-5 aldehyde. Further analysis of 2D NMR spectra led to the assignment of all protons and carbons in **10** and secured the structure (**Figure 3.12** and **Table 10.1.9**).

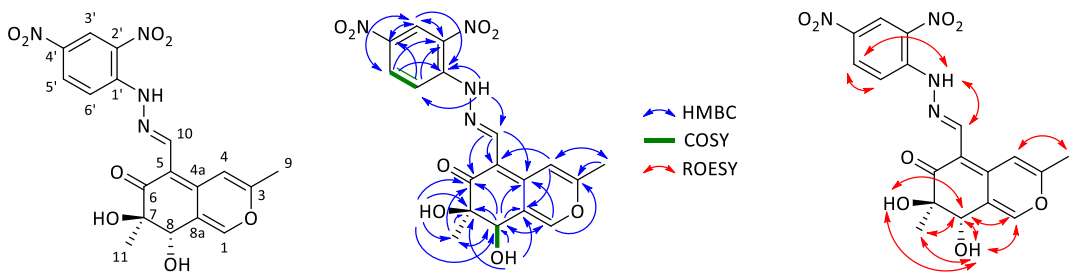

Figure 3.12. Key 2D NMR correlations observed in austdiol-2',4'-dinitrophenylhydrazone (**10**).

A solution of semicarbazide hydrochloride and sodium acetate trihydrate in methanol was added to a solution of austdiol in methanol to afford austdiol-semicarbazone (**11**) (**Scheme 3.8**). After purification by preparative HPLC, austdiol-semicarbazone (**11**) was obtained as a yellow solid.

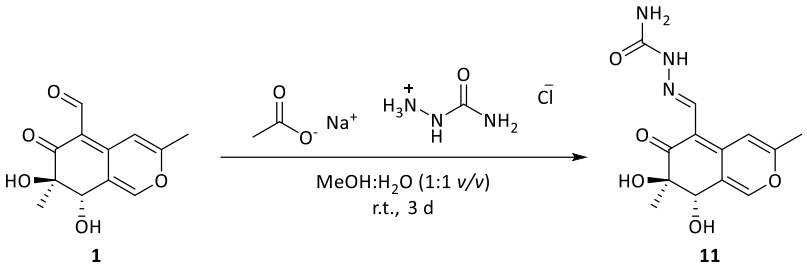

Scheme 3.8. Reaction of austdiol (**1**) with semicarbazide to yield austdiol-semicarbazone (**11**).

HR-ESI(+)-MS analysis of **11** revealed a protonated molecule ($[M + H]^+$ *m/z* 295.0936) indicative of a molecular formula of $C_{13}H_{15}N_3O_5$ requiring 8 DBEs, which fits with 6 double bonds and 2 rings and is one carbon, three hydrogens and three nitrogens more than **1** ($C_{12}H_{12}O_5$). The UV-vis spectrum of **11** is similar to austdiol but with λ_{max} 385 nm showing a bathochromic shift from λ_{max} 385 nm to 404 nm (20 nm) which is indicative of an addition in conjugation equivalent to one double bond (**Figure 3.13**).

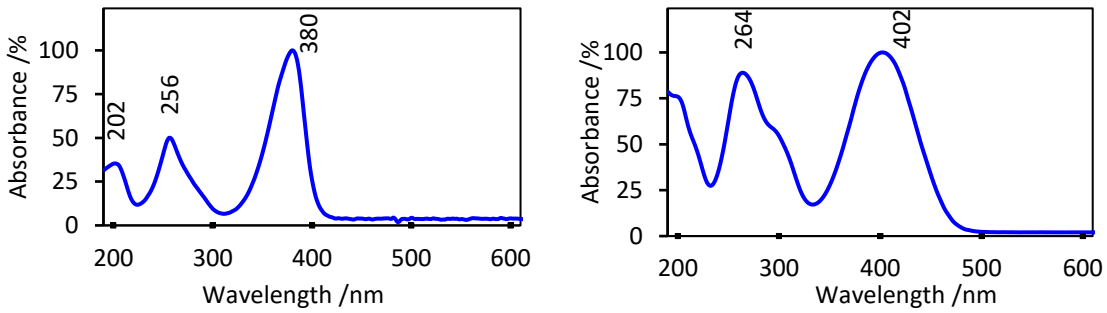

Figure 3.13. UV-vis spectra of austdiol (**1**) (left) in methanol and austdiol-semicarbazone (**11**) (right) in water.

The ^1H and ^{13}C NMR data for **11** and austdiol were similar except for shifts around C-10. Absence of the aldehyde signal (δ_H 10.00; δ_C 198.0 ppm) and presence of the hydrazone was supported by HMBC correlation from 1'-NH (δ_H 9.91 ppm) to C-1' (δ_C 156.6 ppm) and C-10 imine (δ_H 8.02; δ_C 138.6 ppm). H-10 also shows HMBC correlation to the austdiol scaffold of C-4a (δ_C 141.3 ppm), C-5 (δ_C 106.4 ppm), and C-6 ketone (δ_C 197.4 ppm). Further analysis of 2D NMR spectra permitted the assignment of all protons and carbons in **11** and secured the structure (**Figure 3.14** and **Table 10.1.10**).

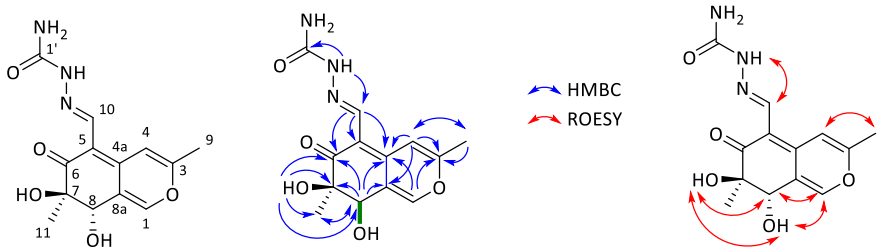

Figure 3.14. Key 2D NMR correlations observed in austdiol-semicarbazone (**11**).

3.5. Reduction of Austdiol-imine Derivatives

Reduction of the synthesised imines were attempted with sodium cyanoborohydride, sodium triacetoxyborohydride, and sodium borohydride under slightly acidic conditions but proved to be unsuccessful as evidenced by the absence of peaks with *m/z* +2 on LCMS.

3.6. Summary

This chapter described the semi-synthesis of nine austdiol analogues used to explore the reactivity of the austdiol scaffold. The assigned structures of the derivatives were supported by 2D NMR spectroscopy and HR-MS. Reaction with sodium borohydride led to reduction of the aldehyde, while oxidation with Jones reagent resulted in the unprecedented bicyclo[4.3.0] system. Reactions with amines in basic conditions predominantly formed the mono-product with acidic conditions favouring the formation of the imine. This strategy would be suitable for constructing a small semi-synthetic library of austdiol analogues, which could then be screened for biological activity to elucidate key structure-activity relationships (SARs).

4. The Biological Activity of Austdiol and Related Analogues

4.1. Introduction

This chapter describes *in vitro* assaying the biological activity of austdiol (**1**) and semi-synthetic derivatives against bacterial, fungal, cancer, and non-cancer cell lines. Antibacterial activity was tested against the fast-growing and best-studied Gram-positive organism, *Bacillus subtilis*, and Gram-positive, *Staphylococcus aureus*, as treatments remain a challenge for multi-drug resistant strains such as MRSA. Antifungal activity was tested against the best-studied, unicellular eukaryote, *Saccharomyces cerevisiae,* due to its simplicity, and fungal pathogen, *Candida albicans*, the most common cause of serious fungal infections. Cell cytotoxicity was assessed against mouse NS-1 myeloma cells, due to genetic and physiological similarities to humans, and against human neonatal foreskin fibroblast (NFF) cells as they are robust, have short doubling time and their viability can be easily measured by staining. Herbicidal activity was tested against *Eragrostis tef*, a fast-germinating grass. The compounds tested were austdiol (**1**), 8-deformyl[4.3.0]austdiol (**4**), 10,10*O*-dihydroaustdiol (**5**), austdiol-mono-ethanolamine (**6**), austdiol-mono-L-Val-OMe (**8**), austdiol-2',4'-dinitrophenylhydrazone (**10**), austdiol-semicarbazone (**11**). Testing of austdiol-DNP derivatives was not performed due to their poor solubility in aqueous media.

4.2. Antibacterial activity of austdiol and analogues

Antibacterial activity was assessed against *Bacillus subtilis,* and *Staphylococcus aureus,* and all compounds were inactive up to 100 μg mL^{-1}.

4.3. Antifungal activity of austdiol and analogues

Antifungal activity was assessed against *Saccharomyces cerevisiae* and *Candida albicans* and all compounds were inactive up to 100 μg mL^{-1}.

4.4. Cytotoxicity of austdiol and analogues

Austdiol (**1**), 8-decarbonyl[4.3.0]austdiol (**4**), 10,10*O*-dihydroaustdiol (**5**), austdiol-mono-ethanolamine (**6**), austdiol-mono-L-Val-OMe (**8**), austdiol-2',4'-dinitrophenylhydrazone (**10**), austdiol-semicarbazone (**11**) were tested against mouse NS-1 myeloma cells and against neonatal foreskin fibroblast (NFF) cells for cytotoxicity against myeloma and mammalian cells respectively. All compounds except for austdiol-mono-ethanolamine exhibited weak activity with **4** exhibiting the highest activity. Interestingly, no activity was observed for all compounds for NFF cells (**Table 4.1** and **Table 10.3**). This demonstrated that austdiol and derivatives could be selective to cancer cell lines compared to non-cancer mammalian cell lines. This is similar to the results previously obtained

by Andrioli *et al.*, which showed increased activity against 5 cancer cell lines (HCT.8, HL-60, MDA-MB435, SF-295) and no activity against human lymphocytes (not specified).[65] They also tested austdiol-diacetate similarly and reported moderate activity against two parasite strains (*L. major* and *L. donovani*). Wehner *et al.* also showed austdiol to have mutagenetic activity in *Salmonella typhimurium* strains TA98, TA100, TA1535, and TA1537 with and without metabolic activation.[62] When compared to **1**, reduction of the aldehyde as shown by **4** reduced activity against NS-1. Decreased polarity of the hydrazone appears to also increase activity. A comparison of **6** and **8** reveals that the amine has a considerable effect on the activity against NS-1. The ethanolamine derivative appeared to decrease inhibition at low concentrations, while the inhibitory effect of **1**, **4**, and **5** was reduced at the increased concentrations of 100, 100, and 25 μg mL^{-1}respectively.

Table 4.1. IC_{50} of austdiol and derivatives against NS-1 and NFF cell lines.

Compound	NS-1 (IC_{50}, μM)	NFF (IC_{50}, μM)
Austdiol (**1**)	60	> 340
8-deformyl[4.3.0]austdiol (**4**)	18	> 340
10,10*O*-dihydroaustdiol (**5**)	156	> 340
Austdiol-mono-ethanolamine (**6**)	> 340	> 340
austdiol-mono-L-Val-OMe (**8**)	154	> 340
Austdiol-2',4'-dinitrophenylhydrazone (**10**)	23	> 340
Austdiol-semicarbazone (**11**)	> 340	> 340

4.5. Herbicidal activity of austdiol and analogues

Herbicidal activity was assessed against *Eragrostis tef* and all compounds were inactive up to 100 μg mL^{-1}.

4.6. Summary

This chapter described bioassay profile of austdiol and semi-synthetic derivatives. From the bioassay results it was revealed that austdiol derivatives were active against mouse NS-1 myeloma. Among all isolated new compounds, **4** was found to be the most potent exhibiting cytotoxic activity. Due to this, and the low activity against human NFF non-cancer cell lines, the unique structure **4** may be a suitable scaffold for further development. Finally, this chapter described SAR of austdiol pharmacophore, which suggested different activities based on the primary amine used and the importance of the C-5 aldehyde position for activity against mouse NS-1 myeloma.

5. Austdiol-DNP as an Amine Derivatising Agent

5.1. Introduction

Naturally-derived amines, also known as alkaloids, have had a large impact on drug discovery, often revealing unique chemical scaffolds that have widespread pharmacological properties.[78] In 2020, the *Journal of Natural Products* reported 316 new alkaloids with 124 metabolites displaying 25 different biological activities.[79] Austdiol-hydrazone derivatives can be added to natural crude extracts which can react with primary amines. Their products can then be detected by HPLC from a change in UV spectra, retention time, or ion mass increase in LCMS due to condensation of the hydrazine. This method has the potential to increase the rate of discovery of potential drug leads by quickly identifying amine-containing compounds from the HPLC trace of a crude extract. More focus can be used to isolate these compounds of interest by separative methods such as preparative HPLC which can save time.

5.2. Evaluation of Austdiol-hydrazones

During the original investigation of austdiol by Vleggaar *et al.*, the formation of austdiol 2',4'-dinitrophenylhydrazone (**10**) was used to elucidate the position of the aldehyde which was supported by ^{1}H NMR in pyridine-d_5.[59] NMR showed the loss of aldehyde [τ −0.67 (CHO)], formation of the hydrazone [τ 1.00 (CH=N)] and three new signals corresponding to the aromatic protons. In this thesis, austdiol (**1**), austdiol-2',4'-dinitrophenylhydrazone (**10**) and the new austdiol-semicarbazone (**11**) were compared for their potential as primary amine derivatising agents. Important factors that were considered are solubility in solvents commonly used for crude extractions (water, methanol, etc.), HPLC retention time using gradient elution and C_{18} column since RP-HPLC is mostly used in natural products chemistry, and finally a change in UV-vis spectra which occurs in the visible region. Austdiol is soluble in methanol, however, amination reactions of austdiol will form a mixture of the mono- and di- products that will increase the complexity of the HPLC trace. Austdiol is also very polar and elutes close to the solvent front which is undesirable as reactions with polar amines can cause the product to elute even earlier which may be undetectable in the solvent front. Austdiol-semicarbazone is soluble in water and will only form the mono-derivatised product. However, like austdiol, the compound is very polar and elutes close to the solvent front (**Figure 5.1**). The polarity issue can be overcome by using a longer gradient or a different column, but this will limit the use in high-throughput screening of crude extracts which is an aim of this method.

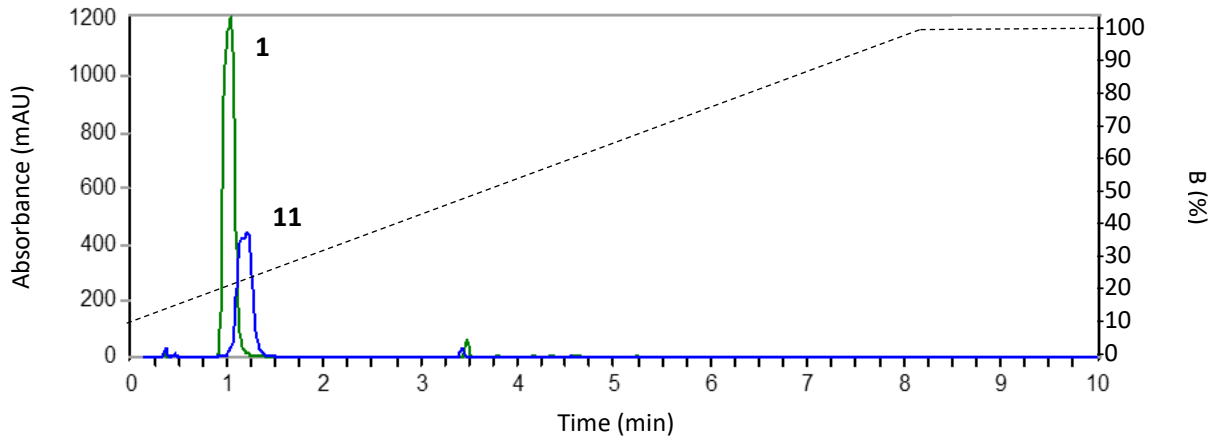

Figure 5.1. HPLC trace of austdiol (**1**) (t_R = 1.0 min) and austdiol-semicarbazone (**11**) (t_R = 1.1 min) with B representing the concentration of acetonitrile in water with 0.01% TFA as a dotted line.

Austdiol-DNP has low solubility in methanol and water, which may limit its use in biological studies. However, it was hoped this could lead to products that are amenable to purification by recrystallisation. Unfortunately, the DNP-products did not form crystals and could not be crystallised for purification. Yet, its low solubility favoured washing with minimal solvent to purify austdiol-DNP derivatives. Similarly to **11**, austdiol-DNP will only form the mono-derivatised product, but the introduction of the non-polar dinitrophenyl moiety decreased the polarity. This resulted in the compound being eluted closer to the middle of a gradient elution which is highly favourable to be applicable for polar and non-polar amines (**Figure 5.2**). The UV λ_{max} of austdiol-DNP is also shifted towards longer wavelengths, providing visual indication after amine coupling.

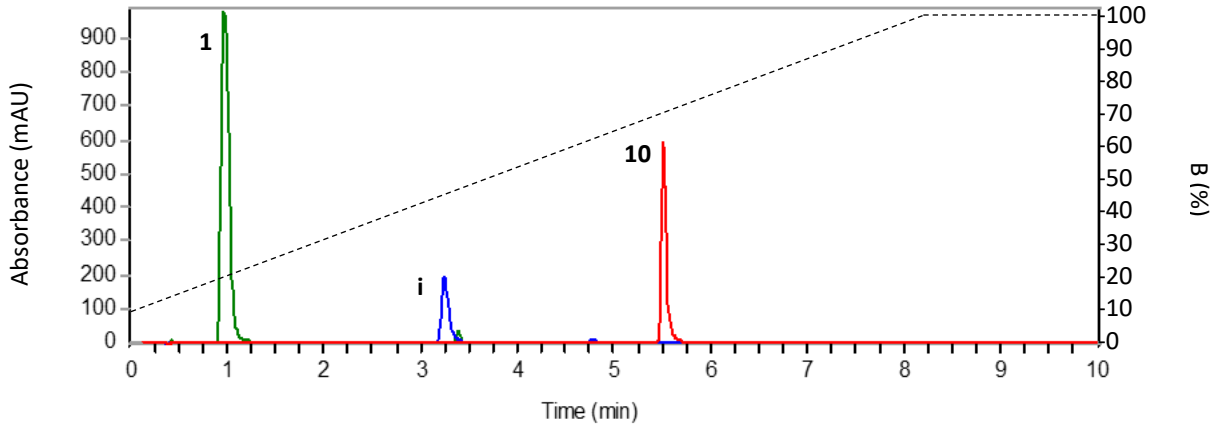

Figure 5.2. HPLC trace of austdiol (**1**) (t_R = 1.0 min), 2,4-dinitrophenylhydrazine (**i**) (t_R = 3.2 min), and austdiol-DNP (**10**) (t_R = 5.4 min) with B representing the concentration of acetonitrile in water with 0.01% TFA as a dotted line.

5.3. Optimisation of Austdiol-DNP Reaction Conditions

In Chapter 3, austdiol reactions were conducted in methanol due to greater solubility compared to other common organic solvents (acetonitrile, dichloromethane, etc.). However, the reaction between Austdiol-DNP and ethanolamine in methanol revealed a mixture of 4 compounds by HPLC. The compounds were numbered **I**–**IV** according to elution rank, with LCMS analysis revealing protonated molecules *m/z* $[M + H]^+$ 459, 416, 459, and 416, respectively. Compound **IV** was identified austdiol-DNP from previously attained retention time and UV spectrum. Compound **III** is the proposed product, which showed a mass equivalent of the condensation of one ethanolamine moiety to austdiol-DNP and UV spectrum showing a highly conjugated system. Compounds **I** and **II** are the proposed enol tautomers for compounds **III** and **IV** respectively (**Figure 5.3**). This is further supported by the lack of conjugation of both enol forms seen in the UV spectra of **I** and **II** and loss of colour on addition of acid (**Figure 5.4**). Antipova *et al.* also witnessed the NH- and OH-tautomers of the azaphilone, *cis*-cavernamine, observing a change in colour depending on the pH of the methanol solution.[80]

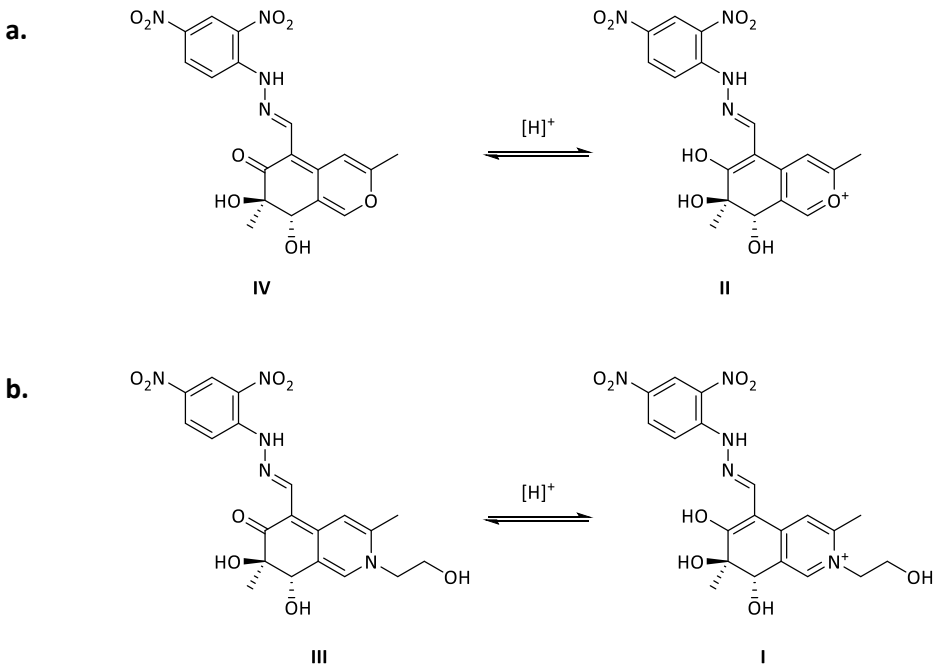

Figure 5.3. a. Proposed keto-enol tautomerism of austdiol-DNP (**10**) (**IV**/**II**) and **b.** austdiol-DNP-ethanolamine (**12**) (**III**/**I**).

The addition of base (triethylamine) and higher temperatures (40 °C) increased the formation of **III** with minimal reduction of the intermediate peaks. It was later discovered that 60 °C was required for the reaction to proceed for zwitterionic species such as amino acids. The most dramatic difference was the use of acetonitrile as the solvent with nearly 100% conversion of **IV** to **III**. The

use of a polar protic solvent appears to contribute to the stabilisation of the enol-form which is less reactive to amines. Increased pH also increased the reaction rate possibly by shifting the keto-enol equilibrium towards the reactive keto-form and facilitating the removal of water when restoring conjugation in the final mechanistic step, as described previously in Chapter 3.2.3 (**Figure 5.4**). The UV spectrum of **III** is characteristic of austdiol-DNP-amine coupling showing the highest absorbance peak around λ_{max} 380 nm and three shoulder peaks around 250, 330, and 460 nm.

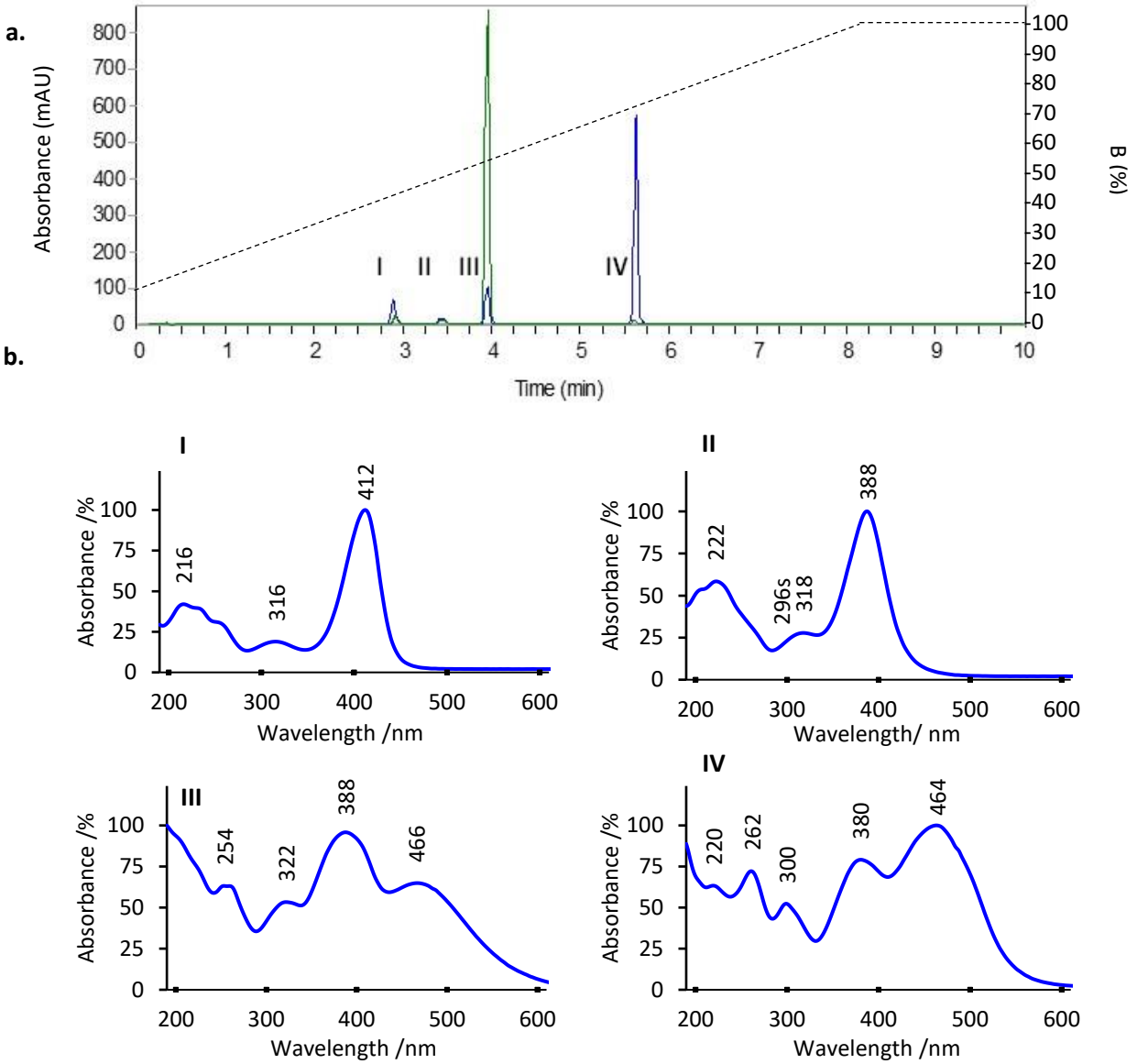

Figure 5.4. a.HPLC traces of austdiol-DNP (**10**) in methanol at 20 °C [t_R (mAU) = 2.8 min (100), 3.4 min (25), 3.9 min (100), 5.6 min (600)] and in acetonitrile with 3 eq. triethylamine at 40 °C [t_R (mAU) 3.9 min (900)] after incubation for 30 min with B representing the concentration of acetonitrile in water with 0.01% TFA as a dotted line. **b.** UV-vis spectra of enol-austdiol-DNP-ethanolamine (**I**), enol-austdiol-DNP (**II**), keto-austdiol-DNP-ethanolamine (**III**) and keto-austdiol-DNP (**IV**). B: acetonitrile-0.01% TFA.

Austdiol-DNP showed only slightly better solubility in acetonitrile than methanol, which prompted test reactions in other aprotic solvents such as DMSO, DMF, and pyridine. Austdiol-DNP has good solubility in DMSO and DMF however, DMSO was the preferred solvent as DMF can decompose to dimethylamine, which could interfere with other amines. Pyridine was also tested with no added triethylamine. However, the reaction did not proceed until triethylamine was later added suggesting the requirement for a stronger base. The solubilities of other solvents were also tested by dropwise addition of solvent to a vial containing 5 mg of austdiol-DNP followed by shaking. The solubilities were then calculated from the volumes required for **10** to fully dissolve in each solvent (**Table 5.1**).

Table 5.1. Solubility of austdiol-DNP in a variety of solvents.

Solvent	MeOH	H_2O	MeCN	DMSO	DMF	Pyridine	THF	Acetone	CH_2Cl_2
Solubility /mg mL^{-1}	< 1	< 1	< 1	12	10	10	9	2	< 1

5.4. Amination of Austdiol-DNP

To test the ability of austdiol-DNP to couple with different amines a variety of substrates were used. These included ethanolamine, aminoglycosides, piperazine, and representative amino acids.

5.4.1. Austdiol-DNP-ethanolamine

Ethanolamine was added to a solution of austdiol-DNP in MeCN: H_2O (19:1 *v/v*) with triethylamine (3 eq.) and stirred at 40 ˚C. The solid was washed with acid to remove triethylamine salts and then again with acetonitrile which yielded austdiol-DNP-ethanolamine (**12**) as a pure dark brown solid. HR-ESI(+)-MS analysis of austdiol-DNP-ethanolamine revealed a protonated molecule ($[M + H]^+$ *m/z* 460.1472) indicative of a molecular formula of $C_{20}H_{21}N_5O_8$ requiring 13 DBEs which fits with 10 double bonds and 3 rings which is six carbons, four hydrogens, four nitrogens, and three oxygens more than **10** ($C_{18}H_{16}N_4O_8$). The UV spectrum of **12** revealed similar peaks to **10** (λ_{max} 254, 388, and 466 nm) however, with a hyperchromic shift of λ_{max} 388 nm to become the new tallest peak. A bathochromic peak shift from λ_{max} 300 nm to 322 nm (20 nm) was observed, which is indicative of an addition in conjugation equivalent to one double bond (**Figure 5.5**).

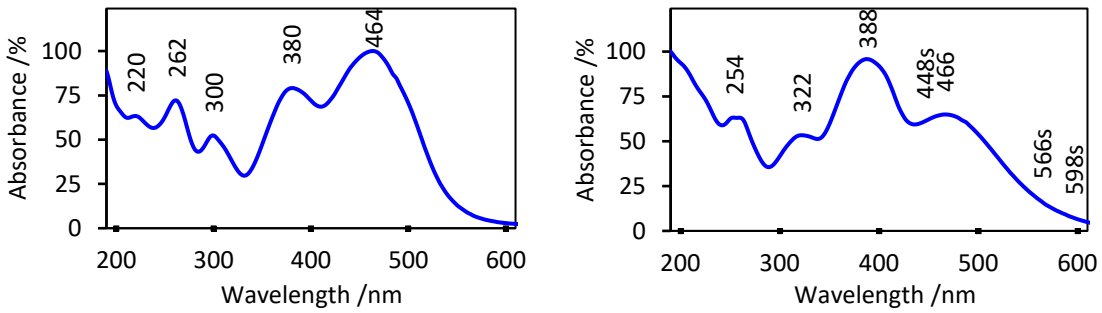

Figure 5.5. UV spectra of austdiol-DNP (**10**) (left) and austdiol-DNP-ethanolamine (**12**) (right) in acetonitrile.

The ^{1}H and ^{13}C NMR data for **12** and **10** were similar except for shifts around C-1 and C-3 indicating the exchange of ethanolamine at the O-2 position with HMBC correlation between H-1 and C-1'. COSY correlations between H-1' and H-2', and H-2' and 2'-OH, supported the presence of one ethanolamine moiety. Further analysis of 2D NMR spectra led to the assignment of all protons and carbons in **10** and secured the structure (**Figure 5.6** and **Table 10.1.11**).

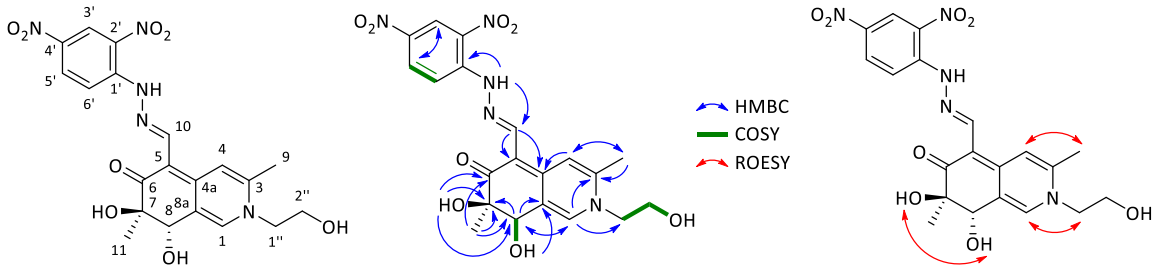

Figure 5.6. Key 2D NMR correlations observed in austdiol-DNP-ethanolamine (**12**).

5.4.2. Aminoglycosides and Piperazine

Aminoglycosides are a class of broad-spectrum antibiotics isolated from *Streptomyces* and have played a major part in drug discovery with the first-in-class drug discovered in 1944, streptomycin. Due to the importance of this class, quick identification of aminoglycosides in crude extracts may lead to increased isolation rates. Unfortunately, reactions with D-glucosamine, kasugamycin and hygromycin B yielded no clear identification of DNP-aminoglycosides. LCMS traces revealed peaks displaying the characteristic UV spectra of austdiol-DNP-amine. However, their masses did not match with their expected products. Only trace amounts of $[M + H]^+$ *m/z* 578 were identified, which could be austdiol-DNP-glucosamine product. It is possible that the aminoglycosides decompose in basic conditions at high temperatures and their decomposition products react with austdiol-DNP. The secondary diamine piperazine was also tested to form the mono- and bis-austdiol-DNP-piperazine products that would contain nitrogen with a formal positive charge. Early LCMS traces revealed an ion peak $[M]^+$ *m/z* 485 which fits with [Austdiol-DNP-piperazine]$^+$ but this compound

later decomposed. A formal positive charge on the nitrogen, results in the nitrogen lone pair being unavailable to contribute to the conjugated system, thus explaining the change in UV spectra.

5.4.3. Amino acids

5.4.3.1. Austdiol-DNP-L-Val

L-valine was added to a solution of austdiol-DNP in DMSO: H_2O (9:1 *v/v*) with triethylamine (3 eq.) and stirred at 60 °C for 16 h. The product was recovered from DMSO by C_{18} solid phase extraction (SPE) and was washed with 0.1 M hydrochloric acid to remove triethylamine salts, then washed again with minimal acetonitrile which yielded austdiol-DNP-L-Val (**13**) as a dark brown solid. HR-ESI(+)-MS analysis of austdiol-DNP-L-Val revealed a protonated molecule ($[M + H]^+$ *m/z* 516.1730) indicative of a molecular formula of $C_{23}H_{25}N_5O_9$, requiring 14 DBEs which fits with 11 double bonds and 3 rings and is five carbons, nine hydrogens, one nitrogen, and one oxygen more than **10** ($C_{18}H_{16}N_4O_8$). The ^1H and ^{13}C NMR data for **10** and **13** were similar except for major shifts around C-1, C-3 and C-4. An additional HMBC correlation from H-1 to C-1'' indicates the exchange of the valine amino-group for the pyran oxygen with COSY correlation revealing H-3'' (δ_H 2.49 ppm), H-4'' (δ_H 1.15 ppm) and H-5'' (δ_H 0.81 ppm). ROESY correlations were also seen between H-1'' and H-1 and, H-1'' and H-9. HMBC correlation between H-1'' and downfield C-2'' along with a broad and deshielded peak (δ_H 13.83 ppm) shown by ^1H-NMR supported the presence of the carboxylic acid. Further analysis of 2D NMR spectra permitted the assignment of all protons and carbons in **13** and secured the structure (**Figure 5.7** and **Table 10.1.12**).

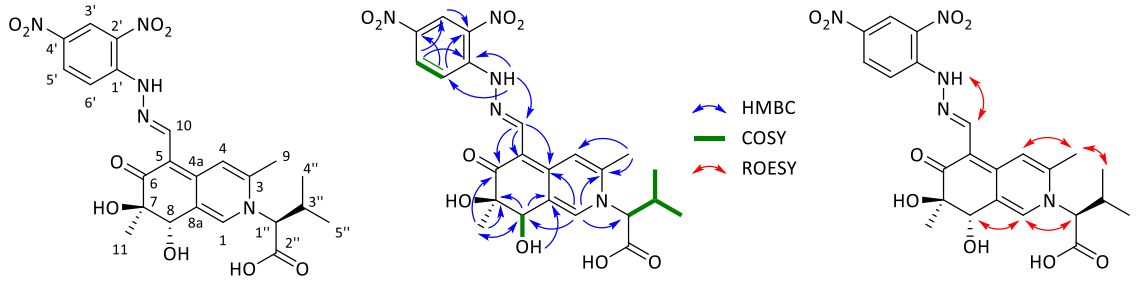

Figure 5.7. Key 2D NMR correlations observed in austdiol-DNP-L-Val (**13**).

5.4.3.2. Austdiol-DNP-D-Val

D-valine was added to a solution of austdiol-DNP in DMSO: H_2O (9:1 *v/v*) with triethylamine (3 eq.) and stirred at 60 ˚C for 16 h. The product was recovered by C_{18} SPE and washed with 0.1 M hydrochloric acid then minimal acetonitrile which yielded austdiol-DNP-D-Val (**14**) as a dark brown solid. HR-ESI(+)-MS analysis of **14** revealed a protonated molecule ($[M + H]^+$ *m/z* 516.1730) indicative of a molecular formula of $C_{23}H_{24}N_6O_{10}$, requiring 14 DBEs, which fits with 12 double bonds and 3

rings and is five carbons, nine hydrogens, one nitrogen, and one oxygen more than **10** ($C_{18}H_{16}N_4O_8$). The ^{1}H and ^{13}C NMR data for **13** and **14** were nearly identical except for very slight shifts possibly indicating L- and D- isomer derivatives. Further analysis of 2D NMR spectra permitted the assignment of all protons and carbons in **14** and secured the structure (**Figure 5.8** and **Table 10.1.13**).

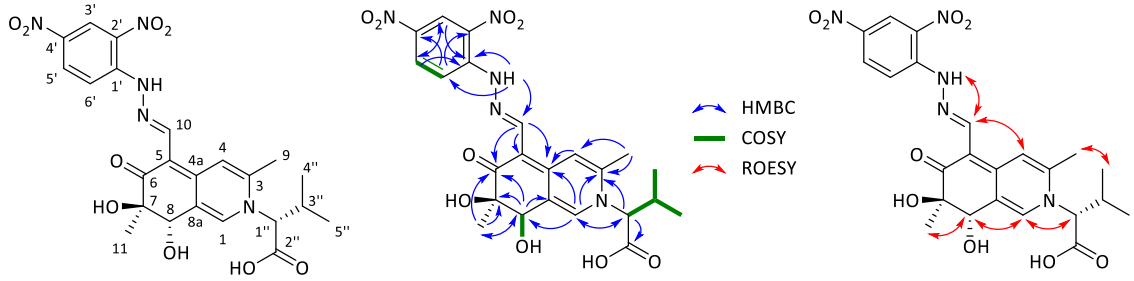

Figure 5.8. Key 2D NMR correlations observed in austdiol-DNP-D-Val (**14**).

5.4.3.3. Austdiol-DNP-L-Gln

L-glutamine was added to a solution of austdiol-DNP in DMSO:H_2O (9:1 *v/v*) with triethylamine (3 eq.) and stirred at 60 °C for 16 h. The product was recovered from DMSO by C_{18} SPE and washed with 0.1 M hydrochloric acid then acetonitrile which yielded austdiol-DNP-α-L-Gln (**15**) as a dark brown solid. HR-ESI(+)-MS analysis of **15** revealed a protonated molecule ($[M + H]^+$ *m/z* 545.1629) indicative of a molecular formula of $C_{23}H_{24}N_6O_{10}$, requiring 14 DBEs, which fits with 12 double bonds and 3 rings and is five carbons, eight hydrogens, two nitrogens, and two oxygens more than **10** ($C_{18}H_{16}N_4O_8$). The ε-NH_2 of L-glutamine could also react with austdiol-DNP to form austdiol-DNP-δ-L-Gln which was seen as a minor peak in LCMS and shared an equal mass. However, this compound is present in trace amounts and could not be isolated for characterisation. COSY correlations were observed between H-1'', H-3'' and between H-3'' and H-4'', with the two protons on C-3'' shown to experience different chemical environments. HMBC correlations from H-1'' to C-2'' and from H-4'' to C-5'', and ROESY correlation between H-4'' and H-5'', supported the presence of a carboxylic acid at C-2'' and an amide at C-5''. Further analysis of 2D NMR spectra permitted the assignment of all protons and carbons in **15** and secured the structure (**Figure 5.7** and **Table 10.1.14**).

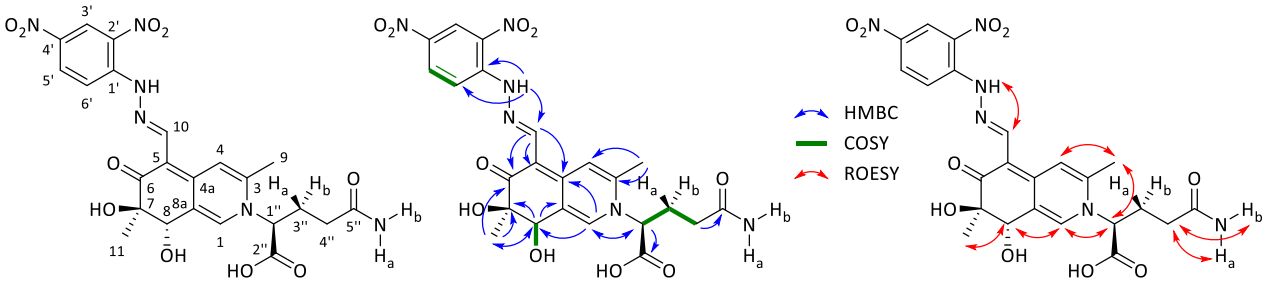

Figure 5.7. Key 2D NMR correlations observed in austdiol-DNP-L-Gln (**15**).

5.4.3.4. Austdiol-DNP-L-Glu

L-glutamic acid was added to a solution of austdiol-DNP in DMSO:H_2O (9:1 *v/v*) with triethylamine (3 eq.) and stirred at 60 °C for 16 h. The product was recovered from DMSO by C_{18} SPE and washed with 0.1 M hydrochloric acid then acetonitrile which yielded austdiol-DNP-L-Glu (**16**) as a dark brown solid. HR-ESI(+)-MS analysis of **16** revealed a protonated molecule ($[M + H]^+$ *m/z* 546.1469) indicative of a molecular formula of $C_{23}H_{23}N_5O_{11}$ requiring 14 DBEs and fits with 12 double bonds and 3 rings and is five carbons, seven hydrogens, one nitrogen, and three oxygens more than **10** ($C_{18}H_{16}N_4O_8$). The ^1H and ^{13}C NMR data for **10** and **16** were similar with new correlations that were different from **13** or **14**, arising due to the difference of amino acid side chain. COSY correlations were observed between H-1'' and H-3'', and between H-3'' and H-4'', with the two protons on C-3'' shown to experience different chemical environments. An HMBC correlation from H-4'' to C-5'' further confirmed the presence of two carboxylic acids that were seen as two broad, downfield signals. Further analysis of 2D NMR spectra permitted the assignment of all protons and carbons in **16** and secured the structure (**Figure 5.8** and **Table 10.1.15**).

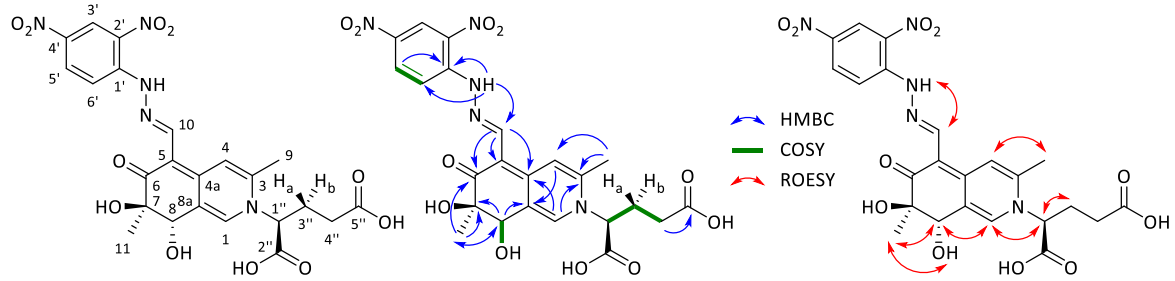

Figure 5.8. Key 2D NMR correlations observed in austdiol-DNP-L-Glu (**16**).

5.5. Summary

In this chapter, austdiol-DNP was tested as primary amine derivatisation agent against a variety of amines commonly found in nature such as aminoglycosides and amino acids. The reaction of these compounds showed a characteristic UV spectrum and a retention shift on HPLC which can be used to identify primary amines. Measurable differences in retention time between L-Val and D-Val derivatives on HPLC prompted the investigation of austdiol-DNP as a chiral derivatising agent for resolving L- and D- amino acids.

6. Austdiol-DNP as a Chiral Derivatising Agent

6.1. Introduction

Natural compounds that contain proteinogenic amino acids can often contain D- and *allo*-configuration amino acid isomers, which are generally indistinguishable by NMR or achiral HPLC. Indirect separation uses an optically pure chiral derivatising agent that reacts with enantiomers to form diastereomers that can be separated by chromatography in an achiral environment.[82]

A measurable difference in retention time when running analytical HPLC between austdiol-DNP-L-Val and austdiol-DNP-D-Val prompted an investigation into the potential application of austdiol-DNP as a chiral derivatising agent similar to Marfey's reagent (1-fluoro-2-4-dinitrophenyl-5-L-alanine amide; FDAA) (**Figure 6.1**).[81] Synthesis of austdiol-DNP from austdiol is a quick 1-step conversion requiring little workup and is obtained in high yield and purity. Austdiol-DNP can also selectivity react with primary amine nucleophiles.

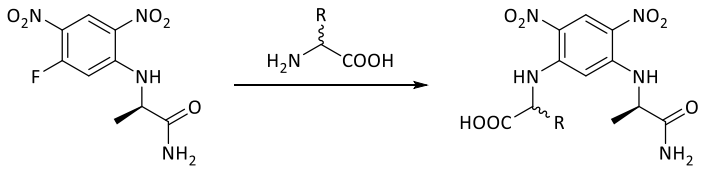

Figure 6.1. Derivatisation of amino acids with Marfey's reagent.

6.2. Optimisation of Reaction Conditions

A typical procedure for the derivatisation of amino acids with Marfey's reagent follows the addition of a 1% acetone solution of FDAA to aqueous solutions of amino acids followed by the addition of base and heating at 30–40 °C for 1 h. It has also been recognised that DMSO and triethylamine increases the reaction rate of derivatisation for Marfey's reagent.[83] In this work, different equivalents of triethylamine and amino acids were reacted with L- and D-valine to give the highest yield for an overnight reaction at 60 °C. It was determined that 3 equivalents of triethylamine and 5 equivalents of amino acid resulted in maximum conversion of austdiol-DNP into austdiol-DNP amino acid derivatives.

The 19 standard proteinogenic amino acids (excluding glycine) plus alloisoleucine were selected for a total of 20 amino acids. Aqueous solutions of L and D stereoisomers of amino acids (50 µL, 12 µmol, 5 eq.) were placed in separate 2 mL vials. To each was added 1 mL of a solution of austdiol-DNP (1 mg, 2.4 µmol, 1 eq.) in DMSO, followed by triethylamine (0.14 mM, 50 µL, 7.2 µmol, 3 eq.). The contents were mixed and heated over a hot plate at 60 °C for 16 h to give 40 reactions. Afterwards,

aliquots (50 µL) of the L- and D-derivative of each amino acid were pooled together (LD mix) for coinjection on HPLC. Coinjection of L- and D-derivatives was used to minimise the effects of retention time variation from separate injections without the use of an internal standard.

6.3. Optimisation of HPLC Method

To optimise baseline separation of derivatised isomers, a variety of pH, gradients, and columns were tested with 4 representative amino acids that were derivatised with austdiol-DNP. The amino acids used were selected to represent negatively charged (glutamic acid), uncharged (glutamine), positively charged (lysine), and hydrophobic (phenylalanine) molecules. The mobile phase consisted of MeCN/H_2O with and without 0.01% trifluoroacetic acid (TFA) modifier. The addition of acid markedly improved the peak shape and thus, separation. An initial gradient of 10–100% MeCN/H_2O with 0.01% TFA over 30 min was tested with C_{18}, C_8, Phenyl, and CN columns (Zorbax, SB-C_{18}/C_8/Phenyl/CN, 4.6 × 150 mm, 5 µm) with a flow rate of 1 mL/min. The CN column gave the best average separation, mainly due to the limited resolution of the glutamic acid isomers on the C_{18}, C_8, and Phenyl columns. The ranking of best to the poorest average separation for this gradient was CN > C_{18} > C_8 > Phenyl. Due to the increased polarity of the products, the gradient was reduced to 10-50% and then again to 5–50% over 1 h to further increase separation. Interestingly, when the initial condition was 5% MeCN, the C_{18} column performed the best giving sharper peaks and better separation compared to CN, even for the glutamic acid derivative. Thus, the optimised HPLC method used was 5–50% MeCN/H_2O with 0.01% TFA modifier achieved by 95–50% channel A (H_2O), 0–45% channel B (MeCN), and 5% isocratic channel D (MeCN - 0.2% TFA) over 60 min with 1 mL/min flow rate on a Zorbax SB-C_{18} (4.6 × 150 mm, 5 µm) column with UV detection at 365 nm.

6.4. Evaluation of Austdiol-DNP as an Amino Acid Derivatising Agent

Cysteine and proline derivatives formed multiple compounds and hence further optimisation would be required to derivatise these two amino acids. For the reactions with aspartic acid and glutamic acid, some austdiol-DNP remained unreacted, which could be due to neutralisation of the triethylamine, by the acidic side chains. The retention times of the separate L and D runs were used to determine the elution rank in the LD mix, from which the final difference in isomer retention time was calculated (**Table 10.4**).

The L- and D-derivatives of lysine revealed two product peaks with similar UV-vis spectra. The products can be attributed to the presence of the α and ε amines that can react with austdiol-DNP to give the two products observed. The L-derivatives for arginine, aspartic acid, glutamic acid,

isoleucine, alloisoleucine, leucine, methionine, phenylalanine, threonine, tryptophan, and valine were observed to elute earlier than their D-derivatives. The most hydrophobic amino acid derivative of this series was austdiol-DNP-D-alloisoleucine, with a retention time of 48.845 min, while the most hydrophilic was austdiol-DNP-D-histidine, with a retention time of 22.824 min. Eleven of the twenty amino acids gave good baseline separation ($|\Delta t_R| > 0.5$ min), with a majority of those containing hydrophobic sidechains (**Table 10.4**). It is possible to use a CN column, previously investigated in method optimisation, to give better average separation for amino acid derivatives containing a charged sidechain.

Due to their structural similarity, alloisoleucine, isoleucine and leucine are widely known to be difficult to separate, with many protocols requiring tedious sample preparations or long chromatographic separations.[84] Many published methods that use reversed-phase HPLC to resolve amino acid enantiomers report having poor selectivity between these three isomers which has even led companies to create specific columns for their resolution.[85] In this work, separation between the L- and D-derivatives for alloisoleucine, isoleucine and leucine was achieved (e.g. L-Leu and D-Leu) However, separation was not achieved between amino acid derivatives with matching L or D configuration (e.g. L-Alle, L -Ile and L -Leu).

6.5. Summary

Austdiol-DNP was tested as a chiral derivatising agent and was found to be effective in separating L- and D-isomers of amino acids with hydrophobic side groups. Minimal or no separation was achieved with amino acid containing polar groups and future efforts should be made to test a polar reverse-phase column. Amino acid derivatisation is also long (16 h), requires high temperatures (60 °C), and basic conditions, which can cause decomposition products resulting in complex chromatograms. Yet, austdiol-DNP poses advantages over Marfey's reagent, requiring a longer synthesis, presents austdiol-DNP as a promising chiral-derivatising candidate with further optimisation.

7. Concluding Remarks

Drug resistance is a growing threat to humans worldwide, regardless of location or socioeconomic status. New drugs with novel mechanisms of actions are required to combat infections caused by drug-resistant bacteria and fungi. Recently, the COVID-19 pandemic has alerted the public to this growing trend and efforts in rediscovering forgotten pharmacologically active natural products is a promising route in the discovery of drug leads.

In this study, the chemical space around the austdiol scaffold was investigated to assess its potential as a next-generation anticancer lead or as a chiral derivatising agent. A small library of austdiol analogues was generated by semi-synthesis to explore these applications. It was found that austdiol undergoes a base-catalysed dimerisation and an acid-catalysed deformylation under standard conditions. Oxidation of austdiol followed by decarboxylation yielded an unprecedented [4.3.0]-bicyclo derivative, which displayed increased cytotoxic activity when compared to austdiol. Reduction of the aldehyde of austdiol was also demonstrated. Reactions of austdiol with primary amines greatly favoured γ-pyridone formation with secondary imine formation only shown to be favourable under slightly acidic conditions. The C-6 ketone remained stable throughout all experiments, which may be attributed to the extensive conjugated system of austdiol. Keto-enol tautomerisation of austdiol and amine derivatives was determined by a loss in colour after addition of acid. The keto and enol forms were identified by differences in retention times and UV-vis spectra with the enol form shown to have reduced reactivity with amines. No semi-synthetic derivative had significant antimicrobial or herbicidal activities. The investigated compounds may have other applications, rather than drug candidates, such as chemical tags in mechanistic studies or assisting biological studies which can be explored in the future.

Exploration of the 2,4-dinitrophenylhydrazone analogue of austdiol as a potential indirect derivatisation agent was undertaken to resolve chiral compounds by C_{18} HPLC. This was prompted by a difference in retention time of L and D-valine derivatives. It was demonstrated that austdiol-DNP was able to resolve ten of twenty amino acids (19 chiral proteinogenic and allo-isoleucine), with increased resolution for derivatives with hydrophobic amino acids. This was performed on a C_{18} HPLC with a gradient of 5–50% MeCN: H_2O with 0.01% TFA modifier over 1 h.

Future experiments will be conducted to explore the chemical space around the oxidation product, 8-decarbonyl[4.3.0]austdiol to further increase its potency against cancer cell lines.

8. Experimental

8.1. Materials and Equipment

All chemicals and reagents unless otherwise stated were purchased from Sigma-Aldrich (St. Louis, U.S.A) and used without further purification. TLC was performed with Merck Kieselgel 60 F_{254} plates with viewing under ultraviolet light (254 nm and 365 nm).

^{1}H NMR and ^{13}C NMR spectra were recorded in 5 mm Pyrex tubes (Wilmad, USA) on either a Bruker AVIIIHD 400 MHz, Bruker AVIIIHD 500 MHz, or Bruker AVII 600 MHz NMR spectrometer. All spectra were obtained at 25 °C, processed using Bruker Topspin 4.1 software and referenced to residual solvent signals (DMSO-d_6 δ_H 2.50/δ_C 39.5 ppm). The following abbreviations are used to describe the NMR data – singlet (s), doublet (d), triplet (t), quartet (q), doublet of doublets (dd), multiplet (m), and broad (br). High resolution electrospray ionisation mass spectra (HRESIMS) were obtained on an Agilent 1260 Infinity II Q-TOF LC/MS mass spectrometer by direct infusion. Electrospray ionisation mass spectra (ESIMS) were acquired on an Agilent 1260 LC/MS coupled to an Agilent 6120B single quadrupole mass detector. Analytical HPLC was performed on a gradient Agilent 1260 Infinity quaternary HPLC system consisting of a G4212B diode array detector, G1311B quaternary pump, and G7167A multisampler. The column was an Agilent Poroshell 120 SB-C_{18} (4.6 × 50 mm, 2.7 µm) eluted with a 1 mL/min gradient of 10–100% acetonitrile/water (0.01% TFA) over 8.33 min. Preparative HPLC was performed on a gradient Shimadzu HPLC system comprising two LC-8A preparative liquid pumps with static mixer, SPD-M10AVP diode array detector and SCL-10AVP system controller with standard Rheodyne injection port. The column was an Agilent Zorbax SB-C_{18} (50 × 150 mm, 5 µm) eluted isocratically with acetonitrile at 20 mL/min. UV-vis spectroscopy was performed on a JASCO V-760 UV-Visible Spectrophotometer measured between 640 and 190 nm with a 200 nm/min scan rate in a 1 cm quartz cuvette. Polarimetry was performed on a JASCO P-2000 Polarimeter with a sodium D-line filter (589 nm) and 3 mm x 10 mm cell. Circular dichroism was performed on a JASCO J-1500 between 450 and 200 nm and a 200 nm/min scan rate in a 1 cm quartz cuvette.

8.2. Chemical Synthesis

8.2.1. Semi-synthetic Analogues of Austdiol

*8.2.1.1. Austdiol-dimer (**2**)*

To a solution of austdiol (**1**; 99.9 mg, 0.428 mmol) in methanol:water (19:1 *v/v*; 20 mL), aqeuous sodium hydroxide (1 M; 200 µL, 0.214 mmol) was added. The reaction mixture changed colour from pale yellow to red. The reaction was stirred at 20 °C for 18 h. The reaction mixture was neutralised with 1 M HCl and evaporated to dryness under nitrogen then diluted with MeOH (1 mL) before purifying by Sephadex LH-20 with methanol to yield austdiol dimer (**2**) as a red solid. (7.1 mg, 7.4%). $[\alpha]_D^{20}$ +40 (*c* 0.1, MeCN). UV (MeCN) λ_{max} (log ε) 399 (3.34), 254 (3.31) nm. ECD (*c* = 110 µM, l = 1 cm, T = 20 °C, MeCN) λ_{max} (Δε) 436 (−1.12), 407 (0), 378 (+3.24), 351 (0), 338 (−1.04), 322 (0), 316 (+0.12), 312 (0), 294 (−1.08), 268 (0), 254 (+1.97), 248 (+1.70), 243 (+2.06), 233 (0), 223 (−3.00) nm. HR-ESI(+)-MS *m/z* $[M + H]^+$ 455.1340 (calculated for $C_{24}H_{23}O_9^+$ 455.1331). ^1H and ^{13}C NMR, see **Table 10.1.1**.

*8.2.1.2. 5-deformylaustdiol (**3**)*

To a solution of austdiol (**1**; 97.4 mg, 0.413 mmol) in methanol/water (19:1 *v/v*; 20 mL), was added hydrochloric acid (1 M; 200 µL, 0.1 mmol). The reaction was allowed to stir at 20 °C for 30 min. The reaction mixture, which instantly turned lighter in colour and was stirred at 60 °C for 12 h (monitored by HPLC). The reaction mixture was evaporated to 1 mL under nitrogen then purified by normal-phase flash chromatography using methanol/dichloromethane/acetic acid (5:95:1 *v/v/v*) as eluant to yield 5-deformylaustdiol (**3**) as a pale-yellow solid. (R_f = 0.27; 9.2 mg, 11%). $[\alpha]_D^{20}$ +200 (*c* 0.1, MeCN). UV (MeCN) λ_{max} (log ε) 230 (3.69) nm. ECD (c = 24.0 µM, l = 1 cm, T = 20 °C, MeCN) λ_{max} (Δε) 395.8 (0), 368.6 (−4), 351.4 (0), 320.6 (29.96), 278.2 (4.58), 273.6 (5.54), 262.8 (0), 244.8 (−26.39), 228 (−3.72), 216.2 (−5.71), 202 (+0.37) nm. HR-ESI(+)-MS *m/z* $[M + H]^+$ 209.0816 (calculated for $C_{11}H_{13}O_4^+$ 209.0803). ^1H and ^{13}C NMR, see **Table 10.1.2**.

*8.2.1.3. 8-decarbonyl[4.3.0]austdiol (**4**)*

To a solution of austdiol (**1**; 99.7 mg, 0.422 mmol) in methanol/water (19:1 *v/v*; 20 mL), Jones reagent (1 M; 500 µL, 0.506 mmol) was added. The reaction mixture which instantly changed colour from pale yellow to black and was stirred at 20 °C for 30 mins (monitored by HPLC). The reaction mixture was evaporated under nitrogen to 1 mL before purifying by preparative HPLC (C_{18}, 20 mL/min) isocratically at MeCN:H_2O (15%) to yield 8-decarbonyl[4.3.0]austdiol (**4**) as a yellow solid. (t_R = 8.4 min, 11.1 mg, 12.8%). $[\alpha]_D^{20}$ +20 (*c* 0.1, MeCN). UV (MeCN) λ_{max} (log ε) 364 (3.13), 295 (2.30),

247 (2.99) nm. ECD (c = 48.5 µM, l = 1 cm, T = 20 °C, MeCN) λ_{max} (Δε) 447.2 (0), 387.4 (−4.45), 362.4 (0), 330.6 (5.59), 299.8 (0), 257.6 (−2.42), 248.6 (0), 237.2 (1.97), 231 (0), 207.2 (−5.32) nm. HR-ESI(+)-MS *m/z* $[M + H]^+$ 207.0656 (calculated for $C_{24}H_{23}O_9^+$ 207.0646). ^1H and ^{13}C NMR, see **Table 10.1.3**.

*8.2.1.4. 10,10O-dihydroaustdiol (**5**)*

To a solution of austdiol (**1**; 112 mg, 0.475 mmol) in methanol/water (19:1 *v/v*; 20 mL), sodium borohydride (50 mg; 1.3 mmol) was added. The reaction mixture, remained pale yellow and was stirred 20 °C for 30 min. The reaction mixture was evaporated under nitrogen to 1 mL before being purified by preparative HPLC (C_{18}, 20 mL/min) isocratically at MeCN:H_2O (10%) to yield 10,10*O*-dihydroaustdiol (**5**) as a pale-brown solid. (t_R = 12.4 min, 6.5 mg, 6.6%). $[\alpha]_D^{20}$ +300 (*c* = 0.05, MeCN). UV (MeCN) λ_{max} (log ε) 363 (3.12), 235 (2.79) nm. ECD (*c* = 21.0 µM, l = 1 cm, T = 20 °C, MeCN) λ_{max} (Δε) 413 (0), 380 (6.08), 369 (5.93), 343.6 (1.57), 314.4 (4.75), 268 (0), 250.4 (−5.85), 238.4 (0), 228.8 (3.63), 219 (0), 211.8 (−1.85) nm. HR-ESI(+)-MS *m/z* $[M + H]^+$ 239.0908 (calculated for $C_{12}H_{15}O_5^+$ 239.0909). ^1H and ^{13}C NMR, see **Table 10.1.4**.

*8.2.1.5. Austdiol-mono-ethanolamine (**6**) and austdiol-di-ethanolamine (**7**)*

To a solution of austdiol (**1**; 102 mg, 0.432 mmol) in methanol/water (19:1 *v/v*; 20 mL), ethanolamine (200 µL, 3.31 mmol) was added. The reaction mixture, which changed colour from pale yellow to yellow, was stirred at 20 °C for 1 h (monitored by HPLC). The reaction mixture was evaporated to 1 mL under nitrogen before purification by preparative HPLC isocratically (C_{18}, 20 mL/min) at MeCN:H_2O (5%) with 0.01% TFA modifier to yield austdiol-mono-ethanolamine (**6**) as a purple solid. (t_R = 17.4 min, 6.8 mg, 5.6%). $[\alpha]_D^{20}$ +100 (*c* 0.1, MeCN). UV (MeCN) λ_{max} (log ε) 375 (3.08), 285 (2.49), 253 (2.45), 209 (2.62) nm. ECD (*c* = 35.8 µM, l = 1 cm, T = 20 °C, MeCN) λ_{max} (Δε) 396 (2.13), 370 (1.8), 358 (0), 342.6 (−4.29), 316.8 (0), 292 (9.9), 257 (−1.49), 250.6 (−0.68), 248 (0), 243.8 (−1.04), 231 (0), 227.6 (0.13), 217.6 (−1.23), 212 (0) nm. HR-ESI(+)-MS *m/z* $[M + H]^+$ 280.1185 (calculated for $C_{14}H_{18}NO_5^+$ 280.1174). ^1H and ^{13}C NMR, see **Table 10.1.5**.

Austdiol-di-ethanolamine (**7**) was obtained as a yellow oil. (t_R = 6.4 min, 5.3 mg, 3.8%). $[\alpha]_D^{20}$ +70 (*c* 0.1, MeCN). UV (MeCN) λ_{max} (log ε) 361 (3.37), 252 (2.67) nm. ECD (*c* = 31.0 µM, l = 1 cm, T = 20 °C, MeCN) λ_{max} (Δε) 394 (2.13), 376(2.13), 353.6 (3.85), 328 (0), 303.8 (−4.27), 288.8 (−0.18), 283 (2.32), 262.2 (1.28), 249.6 (6.05), 233.6 (0), 224.6 (−1.69), 215 (0), 207 (2.15), 200 (0) nm. HR-ESI(+)-MS *m/z* $[M + H]^+$ 323.1645 (calculated for $C_{16}H_{23}N_2O_5^+$ 323.1596). ^1H and ^{13}C NMR, see **Table 10.1.6**.

*8.2.1.6. Austdiol-mono-L-Val-OMe (**8**) and Austdiol-mono-D-Val-OMe (**9**)*

To a solution of austdiol (**1**; 104 mg, 0.441 mmol) in methanol/water (19:1 *v/v*; 20 mL), DL-valine methyl ester (251 mg; 0.529 mmol) was added. The reaction mixture, which changed colour from pale yellow to brown, was stirred at 20 °C for 4 h (monitored by HPLC). The reaction mixture was evaporated to 1 mL under nitrogen before purification by preparative HPLC (C_{18}, 20 mL/min) isocratically at MeCN:H_2O (20%) to yield austdiol-mono-L-Val-OMe (**8**) as a purple solid. (t_R = 9.9 min, 6.8 mg, 4.4%). $[\alpha]_D^{20}$ +100 (*c* 0.1, MeCN). UV (MeCN) λ_{max} (log ε) 255 (3.19), 284 (3.03), 382.6 (3.54) nm. ECD (c = 28.6 µM, l = 1 cm, T = 20 °C, MeCN) λ_{max} (Δε) 445 (−1.55), 441 (0), 431 (+2.47), 413 (0), 341 (−3.95), 331 (0), 311 (+26.96), 289 (0), 265 (−24.23), 240 (0), 222 (+55.59), 201 (0) nm. HR-ESI(+)-MS *m/z* $[M + H]^+$ 350.1607 (calculated for $C_{18}H_{24}NO_6^+$ 350.1596). ^1H and ^{13}C NMR, see **Table 10.1.7**.

Austdiol-mono-D-Val-OMe (**9**) was obtained as a purple solid. (t_R = 9.9 min, 5.4 mg, 3.5%). $[\alpha]_D^{20}$ +100 (*c* 0.1, MeCN). UV (MeCN) λ_{max} (log ε) 254.8 (3.28), 283.6 (3.11), 383 (3.63) nm. ECD (*c* = 28.6 µM, l = 1 cm, T = 20 °C, MeCN) λ_{max} (Δε) 392 (0), 368 (+3.90), 341 (0), 315 (+10.26), 298 (0), 273 (−11.48), 254 (−0.96), 248 (−1.41), 245 (0), 241 (+1.81), 237 (0), 220 (−33.60), 205 (0) nm. HR-ESI(+)-MS *m/z* $[M + H]^+$ 350.1607 (calculated for $C_{18}H_{24}NO_6^+$ 350.1593). ^1H and ^{13}C NMR, see **Table 10.1.8**.

*8.2.1.7. Austdiol-2'-4'-dinitrophenylhydrazone (**10**)*

To a solution of austdiol (**1**; 997 mg, 4.22 mmol) in methanol/water (19:1 *v/v*, 200 mL), a solution of 2,4-dinitrophenylhydrazine (867 mg, 4.38 mmol) with concentrated sulfuric acid (1.8 mL, 33 mmol) was added. The reaction mixture, which formed a red precipitate, was stirred for another 5 min. The precipitate was filtered off and washed with minimal acetonitrile to yield austdiol-2'-4'-dinitrophenylhydrazone (**10**) as a red solid (1514 mg, 84%). UV (MeCN) λ_{max} (log ε) 260.2 (3.19), 297.8 (3.07), 374.8 (3.19), 462.4 (3.29) nm. ECD (*c* = 12.0 µM, l = 1 cm, T = 20 °C, MeCN) λ_{max} (Δε) 450 (−23.39), 419 (−54.10), 373 (0), 351 (+14.35), 336 (0), 327 (−6.57), 323 (0), 295 (+93.34), 276 (0), 268 (−18.35), 253 (0), 233 (+33.97), 222 (0), 210 (−61.56) nm. HR-ESI(+)-MS *m/z* $[M + H]^+$ 417.1044 (calculated for $C_{24}H_{23}O_9^+$ 417.1035). ^1H and ^{13}C NMR, see **Table 10.1.9**.

*8.2.1.8. Austdiol-semicarbazone (**11**)*

To a solution of austdiol (**1**; 99.8 mg, 0.423 mmol) in methanol/water (1:1 *v/v,* 20 mL) , a solution of semicarbazide hydrochloride and sodium acetate trihydrate in methanol/water (1:1 *v/v*) was added. The reaction mixture, which changed colour from pale yellow to bright yellow, was stirred at 20 °C for 3 d. The reaction mixture was evaporated to dryness by rotary evaporator then freeze-dried. The solid was then diluted with MeOH (1 mL) before purification by preparative HPLC (C_{18}, 20 mL/min)

isocratically at MeCN:H_2O (20%) to yield austdiol-semicarbazone (**11**) as a yellow solid. (17.8 mg, 15.1%). $[\alpha]_D^{20}$ +200 (*c* 0.1, H_2O). UV (MeCN) λ_{max} (log ε) 263 (3.21), 295 (3.04), 403.8 (3.25) nm. ECD (c = 34.1 µM, l = 1 cm, T = 20 °C, MeCN) λ_{max} (Δε) 450 (0.87), 390 (6.62), 345 (0), 317 (−9.42), 296 (0), 270 (31.88), 250 (0), 241 (−10.23), 229 (0), 219 (15.42), 209 (0), 200 (−22.71) nm. HR-ESI(+)-MS *m/z* $[M + H]^+$ 294.1082 (calculated for $C_{13}H_{16}N_3O_5^+$ 294.1079). ^1H and ^{13}C NMR, see **Table 10.1.10**.

8.2.2. Semi-synthetic Analogues of Austdiol-DNP

*8.2.2.1. Austdiol-DNP-ethanolamine (**12**)*

To a solution of austdiol-DNP (52.0 mg, 0.125 mmol) in acetonitrile/water (19:1 *v/v*, 20 mL), ethanolamine (60 uL, 1.0 mmol) and triethylamine (50 µL, 360 mmol) was added. The reaction mixture, which changed colour from red to dark brown, was stirred at 40 °C for 4 h (monitored by HPLC). The reaction mixture was evaporated to dryness by rotary evaporator and the solid was washed with acetonitrile to yield austdiol-DNP-ethanolamine (**12**) as a brown solid. (33.9 mg, 59.1%). UV (MeCN) λ_{max} (log ε) 364 (3.64) nm. ECD (c = 21.8 µM, l = 1 cm, T = 20 °C, MeCN) λ_{max} (Δε) 392.2 (2.13), 325.6 (39.81), 308 (0.15), 294 (−30.81), 268.6 (−0.07), 248.8 (45.76), 236.2 (−0.49), 210 (0.02). HR-ESI(+)-MS *m/z* $[M + H]^+$ 460.1472 (calculated for $C_{20}H_{22}N_5O_8^+$ 460.1457). ^1H and ^{13}C NMR, see **Table 10.1.11**.

General procedure for the reaction of austdiol-DNP with amino acids

To a solution of austdiol-DNP (50 mg, 0.12 mmol) in DMSO/water (19:1 *v/v*, 5 mL), amino acid (0.36 mmol) and triethylamine (50 µL, 0.36 mmol) was added. The reaction mixture, which changed colour from red to dark brown, was stirred at 60 °C for 16 h (monitored by HPLC). The reaction mixture was recovered from DMSO on C_{18} silica in acetonitrile and evaporated to dryness by rotary evaporator. The solid was then washed with 0.1 M HCl, water, then acetonitrile to yield austdiol-DNP-amino acids. Optical rotations were not recorded for austdiol-DNP amino acid derivatives as λ_{max} were close to 589 nm causing inaccurate readings.

*8.2.2.2. Austdiol-DNP-L-Val (**13**)*

Brown solid (19.7 mg, 31.6%). UV (MeCN) λ_{max} (log ε) 370 (1.9) nm. ECD (c = 19.4 µM, l = 1 cm, T = 20 °C, MeCN) λ_{max} (Δε) 392.2 (2.13), 325.6 (39.81), 308 (0), 294 (−30.81), 268.6 (0), 248.8 (45.76), 236.2 (−0.49), 210 (0) nm. HR-ESI(+)-MS *m/z* $[M + H]^+$ 516.1730 (calculated for $C_{23}H_{26}N_5O_9^+$ 516.1720). ^1H and ^{13}C NMR, see **Table 10.1.12**.

*8.2.2.3. Austdiol-DNP-D-Val (**14**)*

Brown solid (26.2 mg, 42%). UV (MeCN) λ_{max} (log ε) 478 (3.3), 407 (3.27), 310 (3.12), 261 (1.56). ECD (see **Figure 10.2**). HR-ESI(+)-MS *m/z* $[M + H]^+$ 516.1730 (calculated for $C_{23}H_{26}N_5O_9^+$ 516.17251). ^1H and ^{13}C NMR, see **Table 10.1.13**.

*8.2.2.4. Austdiol-DNP-L-Gln (**15**)*

Brown solid (35.1 mg, 54%). UV (MeCN) λ_{max} (log ε) 478 (3.3), 407 (3.3), 310 (3.15), 261 (3.23). ECD (see **Figure 10.2**). HR-ESI(+)-MS *m/z* $[M + H]^+$ 545.1629 (calculated for $C_{23}H_{25}N_6O_{10}^+$ 545.1627). ^1H and ^{13}C NMR, see **Table 10.1.14**.

*8.2.2.5. Austdiol-DNP-L-Glu (**16**)*

Brown solid (22.5 mg, 35%). UV (MeCN) λ_{max} (log ε) 478 (3.3), 402 (3.27), 310 (3.10), 261 (3.21). ECD (see **Figure 10.2**). HR-ESI(+)-MS *m/z* $[M + H]^+$ 546.1469 (calculated for $C_{23}H_{25}N_6O_{10}^+$ 546.1461). ^1H and ^{13}C NMR, see **Table 10.1.15**.

8.3. Biological screening

The following methods for the preparation of test compounds and development of antibacterial, antifungal and cytotoxic assays are described by Morshed *et al*.[86] All preparations and assays were performed with the help of Daniel Vuong.

The absorbance of each well was measured using a Spectromax plate reader at 605 nm and MIC values determined visually.

8.3.1. Antibacterial assay

The antibacterial activity of the compounds used in this study were evaluated against the Gram-positive bacterium *Bacillus subtilis* (ATCC 6633) and *Staphylococcus aureus* (ATCC 25923).

8.3.2. Antifungal assay

The antifungal activity of the compounds used in this study were evaluated against *Candida albicans* (ATCC 10231) and *Saccharomyces cerevisiae* (ATCC 9763).

8.3.3. Cytotoxicity assay

For the selected analogues of austdiol, cytotoxicity in myeloma cells was evaluated using NS-1 (ATCC TIB-18) mouse myeloma cells, and cytotoxicity in mammalian cells was evaluated using Neonatal Foreskin Fibroblast (NFF) cells.

9. References

1 Nikaido, H., Multidrug Resistance in Bacteria, *Annual Review of Biochemistry*, **2009**, 78, 119-146, doi:10.1146/annurev.biochem.78.082907.145923

2 Centers for Disease Control and Prevention. Antibiotic Resistance Threats in the United States, 2019. (Atlanta, United States, 2019).

3 Organisation for Economic Co-Operation and Development. Stemming the Superbug Tide: Just A Few Dollars More. (OECD Publishing, 2018).

4 Organisation for Economic Co-Operation and Development. Antimicrobial Resistance: Tackling the Burden in the European Union. (Paris, France, 2019).

5 Hm Government. Antimicrobial Resistance: Tackling a Crisis for the Health and Wealth of Nations. (The Review on Antimicrobial Resistance, chaired by Jim O'Neill, London, England, 2014).

6 Pulia, M. *et al.*, COVID-19: An Emerging Threat to Antibiotic Stewardship in the Emergency Department, *Western Journal of Emergency Medicine*, **2020**, 21, 1283–1286, doi:10.5811/westjem.2020.7.48848

7 Topp, E., Larsson, D. G. J., Miller, D. N., Van Den Eede, C. & Virta, M. P. J., Antimicrobial resistance and the environment: assessment of advances, gaps and recommendations for agriculture, aquaculture and pharmaceutical manufacturing, *FEMS Microbiology Ecology*, **2018**, 94, doi:10.1093/femsec/fix185

8 Tenover, F. C., Mechanisms of antimicrobial resistance in bacteria, *American Journal of Infection Control*, **2006**, 34, S3-10; discussion S64-73, doi:10.1016/j.ajic.2006.05.219

9 Rice, L. B., Federal funding for the study of antimicrobial resistance in nosocomial pathogens: no ESKAPE, *The Journal of Infectious Diseases*, **2008**, 197, 1079-1081, doi:10.1086/533452

10 World Health Organization. Global Prority List of Antibiotic Resistant Bacteria. (2017).

11 Camphor, H. S., Viney, K., Polkinghorne, B. & Pennington, K., Retrospective analysis of multidrug-resistant tuberculosis case notifications in Australia (1999-2018), *Communicable Diseases Intelligence (2018)*, **2020**, 44, doi:10.33321/cdi.2020.44.68

12 Longley, D. B. & Johnston, P. G., Molecular mechanisms of drug resistance, *The Journal of Pathology*, **2005**, 205, 275-292, doi:10.1002/path.1706

13 Mansoori, B., Mohammadi, A., Davudian, S., Shirjang, S. & Baradaran, B., The Different Mechanisms of Cancer Drug Resistance: A Brief Review, *Advanced Pharmaceutical Bulletin*, **2017**, 7, 339-348, doi:10.15171/apb.2017.041

14 Newman, D. J. & Cragg, G. M., Natural Products as Sources of New Drugs over the Nearly Four Decades from 01/1981 to 09/2019, *Journal of Natural Products*, **2020**, 83, 770-803, doi:10.1021/acs.jnatprod.9b01285

15 Katz, L. & Baltz, R. H., Natural product discovery: past, present, and future, *Journal of Industrial Microbiology and Biotechnology*, **2016**, 43, 155-176, doi:10.1007/s10295-015-1723-5

16 Calixto, J. B., The role of natural products in modern drug discovery, *Anais da Academia Brasileira de Ciências*, **2019**, 91, doi:10.1590/0001-3765201920190105

17 Schatz, A., Bugie, E. & Waksman, S. A., Streptomycin, a substance exhibiting antibiotic activity against gram-positive and gram-negative bacteria. 1944, *Clinical Orthopaedics and Related Research*, **2005**, 3-6, doi:10.1097/01.blo.0000175887.98112.fe

18 Valiquette, L. & Laupland, K. B., Digging for new solutions, *Canadian Journal of Infectious Diseaes and Medical Microbiology*, **2015**, 26, 289-290, doi:10.1155/2015/971858

19 Lombardino, J. G. & Lowe, J. A., The role of the medicinal chemist in drug discovery — then and now, *Nature Reviews Drug Discovery*, **2004**, 3, 853-862, doi:10.1038/nrd1523

20 Ortholand, J.-Y. & Ganesan, A., Natural products and combinatorial chemistry: back to the future, *Current Opinion in Chemical Biology*, **2004**, 8, 271-280, doi:10.1016/j.cbpa.2004.04.011
21 Wouters, O. J., Mckee, M. & Luyten, J., Estimated Research and Development Investment Needed to Bring a New Medicine to Market, 2009-2018, *Journal of the American Medical Association*, **2020**, 323, 844, doi:10.1001/jama.2020.1166
22 Demain, A. L. & Elander, R. P., The beta-lactam antibiotics: past, present, and future, *Antonie Van Leeuwenhoek*, **1999**, 75, 5-19, doi:10.1023/a:1001738823146
23 Alberts, A. W., Lovastatin and simvastatin--inhibitors of HMG CoA reductase and cholesterol biosynthesis, *Cardiology*, **1990**, 77 Suppl 4, 14-21, doi:10.1159/000174688
24 Mauro, V. F. & Macdonald, J. L., Simvastatin: a review of its pharmacology and clinical use, *Dalian Institute of Chemical Physics*, **1991**, 25, 257-264, doi:10.1177/106002809102500309
25 Ghantous, A., Gali-Muhtasib, H., Vuorela, H., Saliba, N. A. & Darwiche, N., What made sesquiterpene lactones reach cancer clinical trials?, *Drug Discovery Today*, **2010**, 15, 668-678, doi:10.1016/j.drudis.2010.06.002
26 Schall, A. & Reiser, O., Synthesis of Biologically Active Guaianolides with a trans-Annulated Lactone Moiety, *European Journal of Organic Chemistry*, **2008**, 2008, 2353-2364, doi:10.1002/ejoc.200700880
27 Shaikenov, T. E. *et al.*, Arglabin-DMA, a plant derived sesquiterpene, inhibits farnesyltransferase, *Oncology Reports*, **2001**, 8, 173-179, doi:10.3892/or.8.1.173
28 Zhai, J.-D. *et al.*, Biomimetic Semisynthesis of Arglabin from Parthenolide, *The Journal of Organic Chemistry*, **2012**, 77, 7103-7107, doi:10.1021/jo300888s
29 Lone, S. H., Bhat, K. A. & Khuroo, M. A., Arglabin: From isolation to antitumor evaluation, *Chemico-Biological Interactions*, **2015**, 240, 180-198, doi:10.1016/j.cbi.2015.08.015
30 Grandclaudon, C. *et al.*, Semisynthesis and biological evaluation of amidochelocardin derivatives as broad-spectrum antibiotics, *European Journal of Medicinal Chemistry*, **2020**, 188, 112005, doi:10.1016/j.ejmech.2019.112005
31 Lešnik, U. *et al.*, Construction of a new class of tetracycline lead structures with potent antibacterial activity through biosynthetic engineering, *Angewandte Chemie International Edition*, **2015**, 54, 3937-3940, doi:10.1002/anie.201411028
32 Nicolaou, K. C., Vourloumis, D., Winssinger, N. & Baran, P. S., The Art and Science of Total Synthesis at the Dawn of the Twenty-First Century, *Angewandte Chemie International Edition*, **2000**, 39, 44-122, doi:10.1002/(SICI)1521-3773(20000103)39:1<44::AID-ANIE44>3.0.CO;2-L
33 Kinne-Saffran, E. & Kinne, R. K., Vitalism and synthesis of urea. From Friedrich Wöhler to Hans A. Krebs, *American Journal of Nephrology*, **1999**, 19, 290-294, doi:10.1159/000013463
34 Woodward, R. B. & Doering, W. E., The total synthesis of quinine, *Journal of the American Chemical Society*, **1944**, 66, 849-849, doi:10.1021/ja01233a516
35 Woodward, R. B. *et al.*, The Total Synthesis of Cephalosporin C, *Journal of the American Chemical Society*, **1966**, 88, 852-853, doi:10.1021/ja00956a051
36 Woodward, R. B. *et al.*, Asymmetric total synthesis of erythromycin. 3. Total synthesis of erythromycin, *Journal of the American Chemical Society*, **1981**, 103, 3215-3217, doi:10.1021/ja00401a051
37 Corey, E. J., Ohno, M., Vatakencherry, P. A. & Mitra, R. B., Total synthesis of D,L-longifolene, *Journal of the American Chemical Society*, **1961**, 83, 1251-1253, doi:10.1021/ja01466a056
38 Dhanjee, H. H. *et al.*, Total Syntheses of (+)- and (−)-Tetrapetalones A and C, *Journal of the American Chemical Society*, **2017**, 139, 14901-14904, doi:10.1021/jacs.7b09358

39 Komoda, T. *et al.*, Tetrapetalone A, a novel lipoxygenase inhibitor from *Streptomyces* sp., *Tetrahedron Letters*, **2003**, 44, 1659-1661, doi:10.1016/S0040-4039(03)00007-8
40 Komoda, T., Kishi, M., Abe, N., Sugiyama, Y. & Hirota, A., Novel Lipoxygenase Inhibitors, Tetrapetalone B, C, and D from *Streptomyces* sp., *Bioscience, Biotechnology, and Biochemistry*, **2004**, 68, 903-908, doi:10.1271/bbb.68.903
41 Agger, S., Lopez-Gallego, F. & Schmidt-Dannert, C., Diversity of sesquiterpene synthases in the basidiomycete *Coprinus cinereus*, *Molecular microbiology*, **2009**, 72, 1181-1195, doi:10.1111/j.1365-2958.2009.06717.x
42 Colmenares, A. J., Aleu, J., Durán-Patrón, R., Collado, I. G. & Hernández-Galán, R., The putative role of botrydial and related metabolites in the infection mechanism of *Botrytis cinerea*, *Journal of Chemical Ecology*, **2002**, 28, 997-1005, doi:10.1023/a:1015209817830
43 Qiao, C., Zhang, W., Han, J.-C., Dai, W.-M. & Li, C.-C., Collective total synthesis of botryanes, *Tetrahedron*, **2019**, 75, 1739-1745, doi: 10.1016/j.tet.2018.11.019
44 Osmanova, N., Schultze, W. & Ayoub, N., Azaphilones: a class of fungal metabolites with diverse biological activities, *Phytochemistry Reviews*, **2010**, 9, 315-342, doi:10.1007/s11101-010-9171-3
45 Chen, C. *et al.*, Recent advances in the chemistry and biology of azaphilones, *RSC Advances*, **2020**, 10, 10197-10220, doi:10.1039/d0ra00894j
46 Gao, J. M., Yang, S. X. & Qin, J. C., Azaphilones: chemistry and biology, *Chemical Reviews*, **2013**, 113, 4755-4811, doi:10.1021/cr300402y
47 Mapari, S. a. S., Thrane, U. & Meyer, A. S., Fungal polyketide azaphilone pigments as future natural food colorants?, *Trends in Biotechnology*, **2010**, 28, 300-307, doi:10.1016/j.tibtech.2010.03.004
48 Lin, Y. L., Wang, T. H., Lee, M. H. & Su, N. W., Biologically active components and nutraceuticals in the *Monascus*-fermented rice: a review, *Applied Microbiology and Biotechnology*, **2008**, 77, 965-973, doi:10.1007/s00253-007-1256-6
49 Silva, L. J. G., Pereira, A. M. P. T., Pena, A. & Lino, C. M., Citrinin in Foods and Supplements: A Review of Occurrence and Analytical Methodologies, *Foods*, **2020**, 10, 14, doi:10.3390/foods10010014
50 Chen, F. & Hu, X., Study on red fermented rice with high concentration of monacolin K and low concentration of citrinin, *International Journal of Food Microbiology*, **2005**, 103, 331-337, doi:10.1016/j.ijfoodmicro.2005.03.002
51 European Food Safety Authority (Efsa). Scientific Opinion on the risks for public and animal health related to the presence of citrinin in food and feed, *European Food Safety Association Journal.*, **2012**, 10, 1-82.
52 Chen, D. *et al.*, Sclerotiorin inhibits protein kinase G from *Mycobacterium* tuberculosis and impairs mycobacterial growth in macrophages, *Tuberculosis (Edinb)*, **2017**, 103, 37-43, doi:10.1016/j.tube.2017.01.001
53 Luo, J.-G., Xu, Y.-M., Sandberg, D. C., Arnold, A. E. & Gunatilaka, A. a. L., Montagnuphilones A–G, Azaphilones from *Montagnulaceae* sp. DM0194, a Fungal Endophyte of Submerged Roots of *Persicaria amphibia*, *Journal of Natural Products*, **2017**, 80, 76-81, doi:10.1021/acs.jnatprod.6b00714
54 Yu, H. *et al.*, Azaphilone Derivatives from the Fungus *Coniella fragariae* Inhibit NF-κB Activation and Reduce Tumor Cell Migration, *Journal of Natural Products*, **2018**, 81, 2493-2500, doi:10.1021/acs.jnatprod.8b00540
55 Li, W. *et al.*, Isochromans and Related Constituents from the Endophytic Fungus *Annulohypoxylon truncatum* of *Zizania caduciflora* and Their Anti-Inflammatory Effects, *Journal of Natural Products*, **2017**, 80, 205-209, doi:10.1021/acs.jnatprod.6b00698

56 Chen, M., Shen, N. X., Chen, Z. Q., Zhang, F. M. & Chen, Y., Penicilones A-D, Anti-MRSA Azaphilones from the Marine-Derived Fungus *Penicillium janthinellum* HK1-6, *Journal of Natural Products*, **2017**, 80, 1081-1086, doi:10.1021/acs.jnatprod.6b01179

57 Zhou, S.-L. *et al.*, Penicilazaphilone C, a new antineoplastic and antibacterial azaphilone from the Marine Fungus *Penicillium sclerotiorum*, *Archives of Pharmacal Research*, **2016**, 39, 1621-1627, doi:10.1007/s12272-016-0828-3

58 Wang, M. *et al.*, Penicilazaphilone C, a New Azaphilone, Induces Apoptosis in Gastric Cancer by Blocking the Notch Signaling Pathway, *Frontiers in Oncology*, **2020**, 10, 116, doi:10.3389/fonc.2020.00116

59 Vleggaar, R., Steyn, P. S. & Nagel, D. W., Constitution and absolute configuration of austdiol, the main toxic metabolite from *Aspergillus ustus*, *Journal of Chemical Society, Perkin Transcations 1*, **1974**, 1, 45-49, doi:10.1039/p19740000045

60 Steyn, P. S. & Vleggaar, R., The structure of dihydrodeoxy-8-epi-austdiol and the absolute configuration of the azaphilones, *Journal of the Chemical Society, Perkin Transactions 1*, **1976**, doi:10.1039/p19760000204

61 Engel, D. W. & Kruger, G. J., The crystal structure of 5-bromoaustdiol, C11H11O4Br, *Acta Crystallographica Section B Structural Crystallography and Crystal Chemistry*, **1976**, 32, 2545-2548, doi:10.1107/s0567740876008212

62 Wehner, F. C., Thiel, P. G., Van Rensburg, S. J. & Demasius, I. P. C., Mutagenicity to *Salmonella typhimurium* of some *Aspergillus* and *Penicillium* mycotoxins, *Mutation Research/Genetic Toxicology*, **1978**, 58, 193-203, doi:10.1016/0165-1218(78)90009-5

63 Franchi, L. P. *et al.*, The effects of the mycotoxin austdiol on cell cycle progression, cytotoxicity and genotoxicity in Chinese hamster ovary (CHO-K1) cells, *World Mycotoxin Journal*, **2016**, 9, 237-246, doi:10.3920/wmj2015.1907

64 Senadeera, S. P. D., Wiyakrutta, S., Mahidol, C., Ruchirawat, S. & Kittakoop, P., A novel tricyclic polyketide and its biosynthetic precursor azaphilone derivatives from the endophytic fungus *Dothideomycete* sp, *Organic & Biomolecular Chemistry*, **2012**, 10, 7220-7226, doi:10.1039/C2OB25959A

65 Andrioli, W. J. *et al.*, Mycoleptones A–C and Polyketides from the Endophyte *Mycoleptodiscus indicus*, *Journal of Natural Products*, **2014**, 77, 70-78, doi:10.1021/np4006822

66 Hewage, R. T., Aree, T., Mahidol, C., Ruchirawat, S. & Kittakoop, P., One strain-many compounds (OSMAC) method for production of polyketides, azaphilones, and an isochromanone using the endophytic fungus *Dothideomycete* sp, *Phytochemistry*, **2014**, 108, 87-94, doi:https://doi.org/10.1016/j.phytochem.2014.09.013

67 Wijesekera, K., Mahidol, C., Ruchirawat, S. & Kittakoop, P., Metabolite diversification by cultivation of the endophytic fungus *Dothideomycete* sp. in halogen containing media: Cultivation of terrestrial fungus in seawater, *Bioorganic & Medicinal Chemistry*, **2017**, 25, 2868-2877, doi:https://doi.org/10.1016/j.bmc.2017.03.040

68 De Oliveira, L. C. *et al.*, Antibacterial activity of austdiol isolated from *Mycoleptodiscus indicus* Against *Xanthomonas axonopodis pv*. *passiflorae*, *Rev. Virtual de Quimica*, **2019**, doi:10.21577/1984-6835.20190045

69 Yuan, C. *et al.*, A Novel Azaphilone Muyophilone A From the Endophytic Fungus *Muyocopron laterale* 0307-2, *Frontiers in Chemistry*, **2021**, 9, 734822, doi:10.3389/fchem.2021.734822

70 Colombo, L., Gennari, C., Ricca, G. S., Scolastico, C. & Aragozzini, F., Detection of one symmetrical precursor during the biosynthesis of the fungal metabolite austdiol using [1,2-$^{13}C_2$]acetate and [Me-^{13}C]methionine, *Journal of the Chemical Society, Chemical Communications*, **1981**, 575, doi:10.1039/c39810000575

71 Colombo, L. *et al.*, Evidence for a mono-oxygenase mechanism in the biosynthesis of austdiol, *Journal of the Chemical Society, Chemical Communications*, **1983**, 1436, doi:10.1039/c39830001436
72 Musso, L. *et al.*, Natural and semisynthetic azaphilones as a new scaffold for Hsp90 inhibitors, *Bioorganic & Medicinal Chemistry*, **2010**, 18, 6031-6043, doi:10.1016/j.bmc.2010.06.068
73 Matsuzaki, K. *et al.*, New brominated and halogen-less derivatives and structure-activity relationship of azaphilones inhibiting gp120-CD4 binding, *The Journal of Antibiotics (Tokyo)*, **1998**, 51, 1004-1011, doi:10.7164/antibiotics.51.1004
74 Tomoda, H. *et al.*, Structure-specific inhibition of cholesteryl ester transfer protein by azaphilones, *The Journal of Antibiotics (Tokyo)*, **1999**, 52, 160-170, doi:10.7164/antibiotics.52.160
75 Lin, L. *et al.*, Design, Synthesis and Fungicidal Activity of Novel Sclerotiorin Derivatives, *Chemical Biology & Drug Design*, **2012**, 80, 682-692, doi:10.1111/cbdd.12005
76 Abdel-Magid, A. F., Carson, K. G., Harris, B. D., Maryanoff, C. A. & Shah, R. D., Reductive Amination of Aldehydes and Ketones with Sodium Triacetoxyborohydride. Studies on Direct and Indirect Reductive Amination Procedures (1), *The Journal of Organic Chemistry*, **1996**, 61, 3849-3862, doi:10.1021/jo960057x
77 Brady, O. L. & Elsmie, G. V., The use of 2,4-dinitrophenylhydrazine as a reagent for aldehydes and ketones, *Analyst*, **1926**, 51, 77-78, doi:10.1039/AN9265100077
78 Nijampatnam, B., Dutta, S. & Velu, S. E., Recent advances in isolation, synthesis, and evaluation of bioactivities of bispyrroloquinone alkaloids of marine origin, *Chinese Journal of Natural Medicines*, **2015**, 13, 561-577, doi:10.1016/S1875-5364(15)30052-2
79 Daley, S. K. & Cordell, G. A., Alkaloids in Contemporary Drug Discovery to Meet Global Disease Needs, *Molecules (Basel, Switzerland)*, **2021**, 26, doi:10.3390/molecules26133800
80 Antipova, T. V. *et al.*, Formation of Azaphilone Pigments and Monasnicotinic Acid by the Fungus *Aspergillus cavernicola*, *Journal of Agricultural and Food Chemistry*, **2022**, 70, 7122-7129, doi:10.1021/acs.jafc.2c01952
81 B'hymer, C., Montes-Bayon, M. & Caruso, J. A., Marfey's reagent: Past, present, and future uses of 1-fluoro-2,4-dinitrophenyl-5-L-alanine amide, **2003**, 26, 7-19, doi:doi.org/10.1002/jssc.200390019
82 Bhushan, R. & Brückner, H., Marfey's reagent for chiral amino acid analysis: A review, *Amino Acids*, **2004**, 27, 231-247, doi:10.1007/s00726-004-0118-0
83 Brückner, H. & Keller-Hoehl, C., HPLC separation of DL-amino acids derivatized with N^2-(5-fluoro-2,4-dinitrophenyl)-L-amino acid amides, *Chromatographia*, **1990**, 30, 621-629, doi:10.1007/bf02269735
84 Griffin, C., Ammous, Z., Vance, G. H., Graham, B. H. & Miller, M. J., Rapid quantification of underivatized alloisoleucine and argininosuccinate using mixed-mode chromatography with tandem mass spectrometry, *Journal of Chromatography B*, **2019**, 1128, 121-786, doi:10.1016/j.jchromb.2019.121786
85 Hess, S. *et al.*, Chirality determination of unusual amino acids using precolumn derivatization and liquid chromatography–electrospray ionization mass spectrometry, *Journal of Chromatography A*, **2004**, 1035, 211-219, doi:10.1016/j.chroma.2004.02.068
86 Morshed, M.T. *et al.*, Expanding antibiotic chemical space around the nidulin chromophore, *Organic & Biomolecular Chemistry*, **2018**, 16, 3038-3051, doi:10.1039/C8OB00545A

10. Supplementary Data

10.1. Tabulated NMR data

Table 10.1.1. ^{1}H (400 MHz) and ^{13}C (100 MHz) NMR data for austdiol-dimer (**2**) in DMSO-d_6

Pos.	δ_H, mult. (*J* in Hz)	δ_C,type	HMBC	COSY	ROESY
1	8.32, d (1.1)	151.4, CH	3, 4a	8	
3		165.7, C			
4	8.66, s	106.3, CH	3, 4a, 5		1′, 9′
4a		121.90, C			
5		107.9, C			
6		198.0, C			
7		74.4, C			
7-OH	5.20, s		6, 7, 8		8-OH, 11
8	4.46, dd (4.5, 1.1)	70.7, CH	7, 11	1, 8-OH	8-OH
8-OH	5.91, d (4.5)		4a	8	7-OH, 8, 11
8a		148.7, C			
10	10.05, s	189.1, CH			
11	1.14, s	18.9, CH_3	6, 7, 8		7-OH, 8-OH
1′	7.67, s	124.3, CH	3, 3′, 4a′, 8′		4
2′		121.88, C			
3′		134.5, C			
4′	8.50, s	124.6, C	2′, 5′, 8a′, 9′		4
4a′		139.9, C			
5′		102.3, C			
6′		194.4, C			
6′-OH	Not observed				
7′		73.8, C			
7′-OH	4.77, s				
8′	4.34, d (5.0)	73.5, CH	7′, 8a′, 11′	8′-OH	8′-OH
8′-OH	5.37, d (5.0)		8a′	8′	8′, 11′
8a′		131.3, C			
9′	2.43, s	21.5, CH_3	1′, 2′, 3′		4, 4′,
10′	9.78, s	182.2, CH	4a′		
11′	0.83, s	18.6, CH_3	6′, 7′		8′-OH

Table 10.1.2. ^{1}H (400 MHz) and ^{13}C (100 MHz) NMR data for 5-deformylaustdiol (**3**) in DMSO-d_6

Pos.	δ_H, mult. (*J* in Hz)	δ_C, type	HMBC	COSY	ROESY
1	7.40, dd (1.4, 1.4)	145.0, CH	3, 4a, 8, 8a	5, 8	8
3		158.8, C			
4	6.19, s	106.1, CH	3, 4a, 5, 8a, 9		5, 9
4a		144.9, C			
5	5.18, d (1.4)	104.1, CH	3, 4, 7	1	4
6		198.4, C			
7		75.8, C			
7-OH	4.86, s		8		8-OH, 11
8	4.31, dd (4.1, 1.4)	71.5, CH		1, 8-OH	1, 8-OH
8-OH	5.68, d (4.1)			8	7-OH, 8, 11
8a		121.2, C			
9	2.12, s	18.95, CH_3	3, 4	4	4
10					
11	0.99, s	19.02, CH_3	6, 7, 8		7-OH, 8-OH

Table 10.1.3. ^{1}H (600 MHz) and ^{13}C (150 MHz) NMR data for 8-deformyl[4.3.0]austdiol (**4**) in DMSO-d_6

Pos.	δ_H, mult. (*J* in Hz)	δ_C, type	HMBC	COSY	ROESY
1	7.54, s	106.1, CH	3, 4a, 7, 8a		11
3		169.2, C			
4	8.32, d (0.6)	147.5, CH	3, 5, 8a, 9	9	9
4a		159.5, C			
5		110.9, C			
6		201.7, C			
7		72.9, C			
7-OH	5.87, s		6, 7, 8a, 11		11
8					
8-OH					
8a		131.1, C			
9	2.48, d (0.6)	20.2, CH_3	3, 4	4	4
10	9.72, s	185.5, CHO	4a, 5		
11	1.31	23.2, CH_3	6, 7, 8a		1, 7-OH

Table 10.1.4. ^{1}H (600 MHz) and ^{13}C (150 MHz) NMR data for 10,10*O*-dihydroaustdiol (**5**) in DMSO-d_6

Pos.	δ_H, mult. (*J* in Hz)	δ_C, type	HMBC	COSY	ROESY
1	7.31, d (1.9)	143.7, CH	3, 4a, 8, 8a	8	8
3		157.9, C			
4	6.26, s	104.8, CH	3, 4a, 5, 8, 8a, 9		9, 10, 11
4a		141.1, C			
5		112.8, C			
6		198.0, C			
7		75.8, C			
7-OH	4.91, s				10
8	4.23, d (1.9)	71.3, CH	1, 6, 7, 8a, 11	1, 8-OH	10, 11
8-OH	5.65, s			8	10
8a		120.9, C			
9	2.08, s	19.4, CH_3	3, 4		
10	3.27, s	18.7, CH_2	4a, 5, 6		4
10-OH	3.33, s				7-OH, 8-OH, 8, 11
11	0.92, s	19.0, CH_3	6, 7, 8		

Table 10.1.5. ^{1}H (600 MHz) and ^{13}C (150 MHz) NMR data for austdiol-mono-ethanolamine (**6**) in DMSO-d_6

Pos.	δ_H, mult. (*J* in Hz)	δ_C, type	HMBC	COSY	ROESY
1	8.07, s	138.2, CH	1′, 3, 4a, 5, 8, 8a, 9		1′, 2′, 8
3		149.8, C			
4	8.57, s	115.0, C	4a, 5, 8, 8a, 9		9
4a		102.9, C			
5		148.9, C			
6		196.2, C			
7		74.0, C			
7-OH	4.78, s		6, 7, 8, 11		
8	4.42, d (4.7)	71.7, CH	1, 6, 7, 8a, 11	8-OH	1, 7-OH, 8-OH
8-OH	5.96, d (4.7)		8, 8a	8	8, 11
8a		126.8, C			
9	2.55, s	19.7, CH_3	4		1′, 2′, 4
10	9.88, s	185.3, CH	3, 4a, 8a		
11	0.92, s	18.6, CH_3	6, 7, 8		7-OH, 8
1′	4.30, m	56.4, CH_2	1, 2′, 3	2′	1, 2′, 9
2′	3.75, m	59.9., CH_2	1′	2′-OH	1′, 1′, 2′-OH, 9
2′-OH	5.12, t (5.4)		1′, 2′	1′, 2′	2′

Table 10.1.6. ^{1}H (600 MHz) and ^{13}C (150 MHz) NMR data for austdiol-di-ethanolamine (**7**) in DMSO-d_6

Pos.	δ_H, mult. (*J* in Hz)	δ_C, type	HMBC	COSY	ROESY
1	8.32, s	141.0, CH	1′, 4a, 8, 8a		1′, 8, 8-OH
3		151.3, C			
4	7.73, s	115.4, CH	5, 4a, 8a, 9	9	9, 10
4a		150.5, C			
5		97.1, C			
6		196.8, C			
7		74.0, C			
7-OH	5.36, s		6, 7, 8, 11		8, 11
8	4.52, d (3.9)	71.2, CH	1, 4a, 6, 7, 8a, 11	8-OH	1, 7-OH, 8-OH
8-OH	6.10, d (3.9)		8	8	1, 8, 11
8a		128.9, C			
9	2.66, s	19.6, CH_3	3, 4	4	1′, 2′, 4
10	8.38, d (13.8)	157.7, C	1″, 4a, 5, 6		4
11	1.06, s	18.5, CH_3	6, 7, 8		7-OH, 8-OH
1′	4.42, m	57.0, CH_2		2′	1, 2′, 9
2′	3.80, m	59.8, CH_2		1′, 2′-OH	1′, 2′-OH, 9
2′-OH	5.21, s		1′, 2′	2′	2′
1″	3.57, m	52.2, CH_2			
2″	3.61, m	59.8, CH_2	1″	2″-OH	2″-OH
2″-OH	5.04, s			2″	2″

Table 10.1.7. ^{1}H (600 MHz) and ^{13}C (150 MHz) NMR data for austdiol-mono-L-Val-OMe (**8**) in DMSO-d_6

Pos.	δ_H, mult. (*J* in Hz)	δ_C, type	HMBC	COSY	ROESY
1	8.06, d (1.2)	134.7, CH	4a, 8, 8a, 1′	8	1′, 5′, 6′, 8
3		149.8, C			
4	8.54, s	114.7, CH	3, 5, 8a, 9		9
4a		149.0, C			
5		103.7, C			
6		196.6, C			
7		74.0, C			
8	4.46, d (1.2)	71.6, C	1, 4a, 6, 7, 8a	1	1, 11
8a		127.3, C			
9	2.55, s	20.3, CH_3	3, 4		1′, 4
10	9.90, s	186.0, CHO	4a, 5, 8a		
11	0.93, s	18.5, CH_3	6, 7, 8		8
1′	5.01, d (10.1)	68.0, CH	1, 3, 9, 5′, 6′/7′	5′	1, 6′, 7′, 9
2′		168.8, CH_3			
4′	3.75, s	53.1, CH_3	2′		7′
5′	2.52, m	30.9, CH	6, 11, 1′, 2′	1′, 6′, 7′	1, 6′, 7′
6′	0.77, d (6.5)	18.0, CH_3	1′, 5′, 7′	5′	1, 1′, 5′
7′	1.10, d (6.5)	18.9, CH_3	1′, 5′, 6′	5′	1′, 4′, 5′

Table 10.1.8. ^{1}H (600 MHz) and ^{13}C (150 MHz) NMR data for Austdiol-mono-D-Val-OMe (**9**) in DMSO-d_6

Pos.	δ_H, mult. (*J* in Hz)	δ_C, type	HMBC	COSY	ROESY
1	8.04, d (1.3)	134.4, CH	1′, 3, 5, 8, 8a, 9	8	1′, 5′, 6′, 8
3		150.0, C			
4	8.56, s	114.1, CH	1′, 4a, 5, 6, 8, 8a, 9		9
4a		103.7, C			
5		148.9, C			
6		196.6, C			
7		74.1, C			
7-OH					
8	4.42, d (1.3)	71.6, CH	1, 5, 6, 7, 8a, 11	1	1, 11
8-OH	6.02, s				
8a		127.2, C			
9	2.57, s	20.3, CH_3	3, 4		4
10	9.91, s	186.0, CH	4a, 5, 8a		
11	0.93, s	18.3, CH_3	6, 7, 8		8
1′	5.01, d (10.1)	67.7, CH	1, 2′, 3, 5′	5′	1, 6′, 7′, 9
2′		168.8, C			
4′	3.76, s	53.1, CH_3	3′		7′
5′	2.50, m	31.2, CH	1′, 2′	1′, 6′, 7′	1, 6′, 7′
6′	0.77, d (6.6)	17.8, CH_3	7′	5′	1, 1′, 5′
7′	1.09, d (6.6)	18.8, CH_3	6′	5′	1′, 4′, 5′

Table 10.1.9. ^{1}H (600 MHz) and ^{13}C (150 MHz) NMR data for austdiol 2,4-dinitrophenylhydrazone (**10**) in DMSO-d_6

Pos.	δ_H, mult. (*J* in Hz)	δ_C, type	HMBC	COSY	ROESY
1	7.90, d (1.6)	148.3, CH	3, 4a, 8	1	8, 8-OH
3		163.4, C			
4	7.81, s	106.5, CH	5, 8a, 9		9
4a		143.3, C			
5		105.7, C			
6		197.1, C			
7		74.9, C			
7-OH	5.22, s		6, 7, 8, 11		8, 8-OH, 11
8	4.40, dd (4.5, 1.6)	70.6, CH	1, 4a, 6, 7, 8a, 11	8-OH	1, 7-OH, 8-OH, 11
8-OH	5.87, d (4.6)		7, 8, 8a	8	1, 7-OH, 8, 11
8a		122.1, C			
9	2.42, d (0.5)	20.2, CH_3	3, 4		4
10	8.73, s	148.1, CH	4a, 5, 6		1′-NH
11	1.09, s	18.9, CH_3	6, 7, 8		7-OH, 8, 8-OH
1′		143.8, C			
1′-NH	11.53, s		1′, 6′, 10		5′
2′		136.2, C			
3′	8.85, d (2.6)	123.2, CH	1′, 2′/4′, 5′	5′	
4′		136.2, C			
5′	8.42, dd (9.6, 2.6)	130.0, CH	1′, 3′, 2′/4′	3′, 6′	1′-NH, 6′
6′	7.77, d (9.6)	116.2, CH	2′/4′	5′	5′

Table 10.1.10. ^{1}H (600 MHz) and ^{13}C (150 MHz) NMR data for austdiol-semicarbazone (**11**) in DMSO-d_6

Pos.	δ_H, mult. (*J* in Hz)	δ_C, type	HMBC	COSY	ROESY
1	7.70, d (1.3)	146.8, CH	3, 4a, 8, 8a	8	8, 8-OH
3		161.9, C			
4	7.61, s	106.1, CH	3, 4a, 5, 8, 8a, 9	9	9
4a		141.3, C			
5		106. 4, C			
6		197.4, C			
7		75.0, C			
7-OH	5.06, s		6, 7, 8, 11		8, 8-OH, 11
8	4.31, dd (4.6, 1.3)	70.7, CH	1, 4a, 6, 7, 8a, 11	1, 8-OH	1, 7-OH 11
8-OH	5.78, d (4.6)			8	1, 7-OH, 8, 11
8a		121.6, C			
9	2.28, s	19.7, CH_3	3, 4	4	4
10	8.02, s	138.6, CH	4a, 5, 6, 8a		1′-NH
11	1.03, s	18.9, CH_3	6, 7, 8		7-OH, 8, 8-OH
1′		156.6, C			
1′-NH	9.91, s		10, 1′		10
1′-NH_2	6.15, s				

Table 10.1.11. ^{1}H (600 MHz) and ^{13}C (150 MHz) NMR data for austdiol-DNP-ethanolamine (**12**) in DMSO-d_6

Pos.	δ_H, mult. (*J* in Hz)	δ_C, type	HMBC	COSY	ROESY
1	7.95, d (0.9)	136.7, CH	1'', 3, 4a, 8	8	1'', 2''
3		149.3, C			
4	8.30, s	115.1, CH			9
4a		147.1, C			
5		96.8, C			
6		193.4, C			
7		74.4, C			
7-OH	4.82, s		6, 7, 8		11
8	4.44, d (4.7, 0.9)	71.8, CH	7, 8a, 11	1, 8-OH	8-OH
8-OH	5.94, d (4.7)		8a	8	8
8a		126.9, C			
9	2.64, s	20.1, CH_3	3, 4		4
10	8.80, s	150.4, CH	4a, 5		1'-NH
11	0.95, s	18.8, CH_3	6, 7, 8		7-OH
1'		143.3, C			
1'-NH	11.41, s				2''-OH, 10
2'		135.0, C			
3'	8.85, s	123.6, CH			
4'		135.0, C			
5'	8.38, d (8.6)	129.8, CH		6'	
6'	7.76, d (8.6)	116.0, C		5'	
1''	4.29, m	56.0, CH_2		2''	1, 2''
2''	3.77, m	60.1, CH_2		1'', 2''-OH	1, 1'', 2''-OH
2''-OH	5.13, t (5.3)		2''	2''	1'-NH, 2''

Table 10.1.12. ^{1}H (500 MHz) and ^{13}C (125 MHz) NMR data for austdiol-DNP-L-Val (**13**) in DMSO-d_6

Pos.	δ_H, mult. (*J* in Hz)	δ_C, type	HMBC	COSY	ROESY
1	7.90, s	132.5, CH	1'', 3, 4a, 8		1'', 3'', 5'', 8
3		149.0, C			
4	8.26, s	114.6, CH			9
4a		146.7, C			
5		97.9, C			
6		194.4, C			
7		74.4, C			
7-OH	4.85, s				
8	4.47, d (4.4)	71.7, CH	7, 8a, 11	8-OH	1, 8-OH
8-OH	5.98, d (4.4)		8a	8	8
8a		127.3, C			
9	2.64, s	20.8, CH_3	3, 4		1'', 4
10	8.78, s	149.9, CH	4a, 5, 6		1'-NH
11	0.94, s	18.7, CH_3	6, 7, 8	8	
1'		143.3, C			
1'-NH	11.42, s		1', 6', 10		10
2'		135.2[a], C	3', 6'		
3'	8.85, s	123.5, CH	2'		
4'		135.2[a], C	3', 6'		
5'	8.37, d (9.2)	129.8, CH	1', 3'	6'	
6'	7.77, d (9.2)	116.0, CH		5'	
1''	4.83, d (10.2)	68.4, CH	2'', 3, 3''	3''	1, 4'', 5'', 9
2''		169.6, C			
2''-OH	13.83, b				
3''	2.49, m	30.2, CH		1'', 4'', 5''	1, 4'', 5''
4''	1.15, d (6.7)	19.1, CH_3	1'', 3'', 5''	3''	1'', 3'', 5''
5''	0.81, d (6.7)	18.1, CH_3	1'', 3'', 4''	3''	1, 1'', 3'', 4''

[a] – Overlapping

Table 10.1.13. ^{1}H (500 MHz) and ^{13}C (125 MHz) NMR data for austdiol-DNP-D-Val (**14**) in DMSO-d_6

Pos.	δ_H, mult. (*J* in Hz)	δ_C, type	HMBC	COSY	ROESY
1	7.93, s	132.7, CH	1'', 3, 4a, 8		1'', 3'', 5'', 8
3		149.3, C			
4	8.23, s	114.5, CH	8a		10
4a		146.8, C			
5		98.1, C			
6		194.5, C			
7		74.5, C			
7-OH					
8	4.45, s	71.6, C	6, 7, 8a, 11		11
8-OH					
8a		127.4, C			
9	2.65, s	20.7, CH_3	3, 4		5''
10	8.77, s	150.3, CH	4a, 5, 6		1'-NH, 4
11	0.96, s	18.5, CH_3	6, 7, 8		8
1'		143.6, C			
1'-NH	11.40, s		1', 6', 10		10
2'		128.0, C			
3'	8.85, d (2.1)	123.4, CH	1', 4', 5'	5'	
4'		135.3, C			
5'	8.38, dd (9.2, 2.1)	129.8, CH	1', 3'	3', 6'	
6'	7.73, s	116.0, CH	2', 4'	5'	
1''	4.88, d (9.2)	68.1, CH	1, 3, 3'', 2''	3''	3'', 4'', 5'', 9
2''		169.7, C			
2''-OH	13.88, b				
3''	2.49, m	30.7, CH		1'', 4'', 5''	1'', 4'', 5''
4''	1.13, d (6.5)	19.0, CH_3	1'', 3'', 5''	3''	1'', 3''. 5''
5''	0.81, d (6.5)	18.0, CH_3	1'', 3'', 4''	3''	1'', 3'', 4'', 9

Table 10.1.14 ^{1}H (500 MHz) and ^{13}C (125 MHz) NMR data for austdiol-DNP-L-Gln (**15**) in DMSO-d_6

Pos.	δ_H, mult. (*J* in Hz)	δ_C, type	HMBC	COSY	ROESY
1	7.76[a], s	132.8, CH	3, 4a, 8		1'', 3'', 8
3		149.2, C			
4	8.26, s	114.7, CH			9
4a		146.9, C			
5		97.8, C			
6		194.3, C			
7		74.4, C			
7-OH					
8	4.45, s	71.8, CH	7, 8a, 11		1, 11
8-OH	5.98, s				
8a		127.4, C			
9	2.60, s	20.3, CH_3	3, 4		1'', 4
10	8.80, s	150.0, CH	4a, 5, 6		1'-NH
11	0.95, s	18.8, CH_3	6, 7, 8		8
1'		143.5, C			
1'-NH	11.43, s		1', 6', 10		10
2'		127.9, C			
3'	8.85, s	123.5, CH			
4'		135.2, C			
5'	8.39, d (9.4)	129.9, CH		6'	
6'	7.76[a], s	116.0, CH		5'	
1''	5.37, dd (9.4, 5.9)		1, 2''	$3''_a$, $3''_b$	1, 4'', 9
2''		170.0, COOH			
2''-OH	13.75, b				
$3''_a$	2.49, m	26.7, CH_2		1'', $3''_b$, 4''	1
$3''_b$	2.25, m	26.7, CH_2		1'', 3''a, 4''	1
4''	2.12, m	30.3, CH_2	3'', 5''	$3''_a$, $3''_b$	1'', 5''-NH_a, 5''-NH_b
5''		172.7, C			
5''-NH_a	7.35, s				4''
5''-NH_b	6.89, s				4''

[a] – Overlapping

Table 10.1.15. ^{1}H (500 MHz) and ^{13}C (125 MHz) NMR data for austdiol-DNP-L-Glu (**16**) in DMSO-d_6

Pos.	δH, mult. (*J* in Hz)	δC, type	HMBC	COSY	ROESY
1	7.78, s	116.0, CH	3, 4a		1'', 3''a, 3''b, 8
3		149.1, C			
4	8.26, s	114.9, CH	8a		9
4a		146.8, C			
5		97.2, C			
6		194.5, C			
7		74.4, C			
7-OH	4.81, s				
8	4.44, s	71.8, CH	7, 8a, 11		1, 8-OH, 11
8-OH	5.94, s				8
8a		127.9, C			
9	2.57, s	20.4, CH_3	3, 4		4
10	8.80, s	149.9, CH	4a, 5, 6		1'-NH
11	0.94, s	18.9, CH_3	6, 7, 8		8
1'		143.2, C			
1'-NH	11.43, s		1', 6', 10		10
2'		127.4, C			
3'	8.85, d (2.0)	123.5, CH		5'	
4'		135.2, C			
5'	8.38, dd (9.1, 2.0)	129.7, CH	1'	3', 6'	
6'	7.75, d (9.1)	133.2, CH		5'	
1''	5.37, t (7.4)	64.2, CH		3''a, 3''b	1, 3''a, 3''b
2''		170.0, C			
2''-OH	13.82, b				
3''a	2.40, m	26.3, CH		1'', 3''a, 4''	1, 1''
3''b	2.40, m	26.3, CH		1'', 3''b, 4''	1, 1''
4''	2.28, m	29.8, CH_2	5''	3''a, 3''b	
5''		173.4, C			
5''-OH	12.38, b				

10.2. ECD spectra of austdiol and semi-synthetic austdiol derivatives

Austdiol (**1**) in MeOH

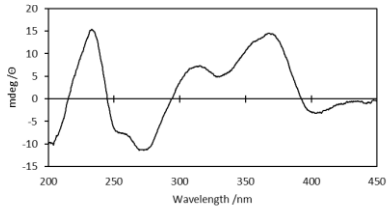

Austdiol-dimer (**2**) in MeCN

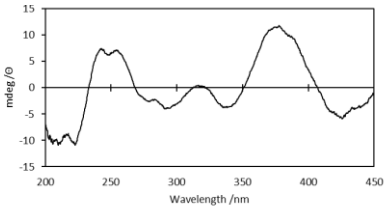

5-deformylaustdiol (**3**) in MeCN

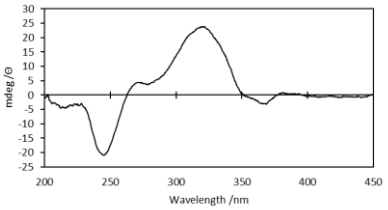

8-decarbonyl[4.3.0]austdiol(**4**) in MeCN

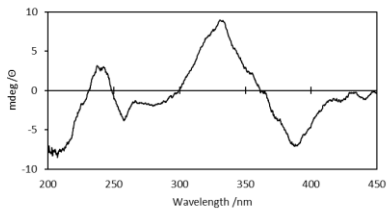

Austdiol-mono-L-Val-OMe (**8**) in MeCN

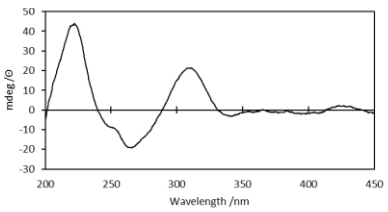

Austdiol-mono-D-Val-OMe (**9**) in MeCN

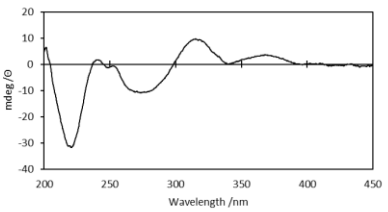

Austdiol-DNP (**10**) in MeCN

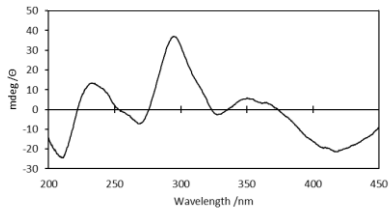

Austdiol-semicarbazone (**11**) in H_2O

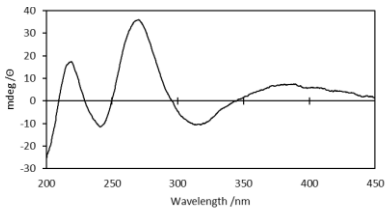

Austdiol-DNP-ethanolamine (**12**) in MeCN

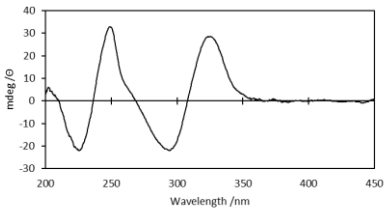

Austdiol-DNP-L-Val (**13**) in MeCN

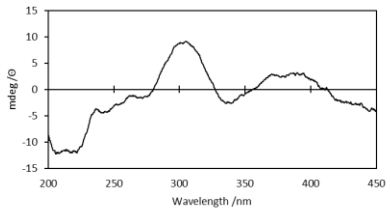

Austdiol-DNP-D-Val (**14**) in MeCN

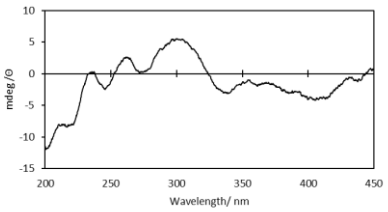

Austdiol-DNP-L-Gln (**15**) in MeCN

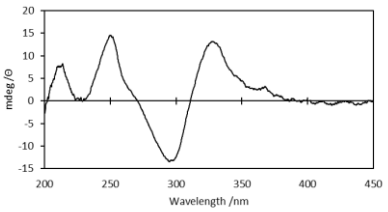

Austdiol-DNP-L-Glu (**16**) in MeCN

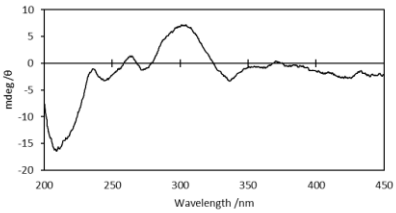

10.3. Cytotoxicity of austdiol and derivatives against mouse NS-1 myeloma

austdiol (**1**)

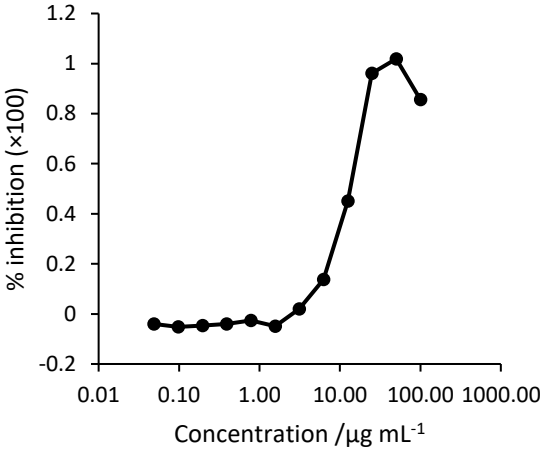

8-decarbonyl[4.3.0]austdiol (**4**)

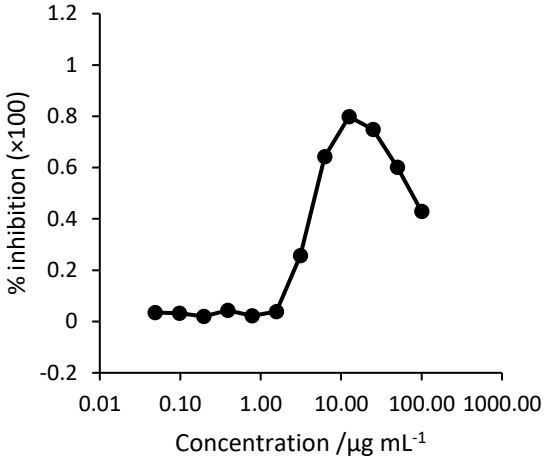

10,10*O*-dihydroaustdiol (**5**)

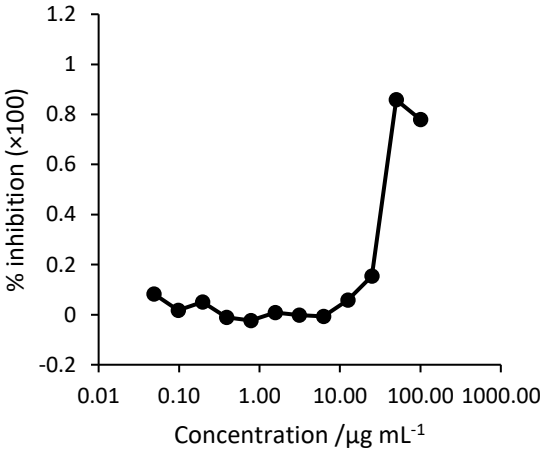

austdiol-mono-ethanolamine (**6**)

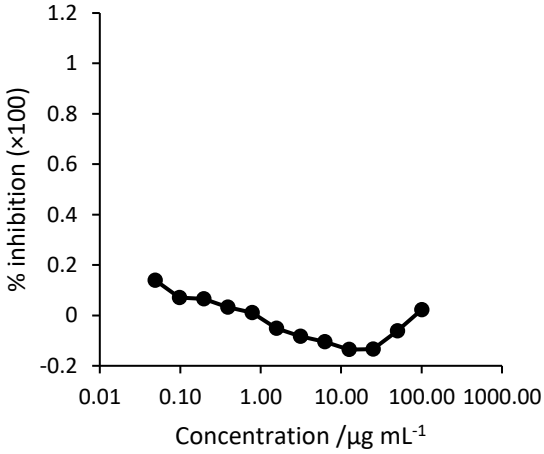

austdiol-mono-L-Val-OMe (**8**)

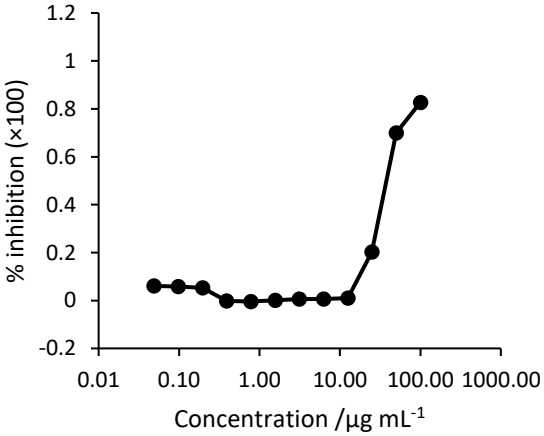

austdiol-DNP (**10**)

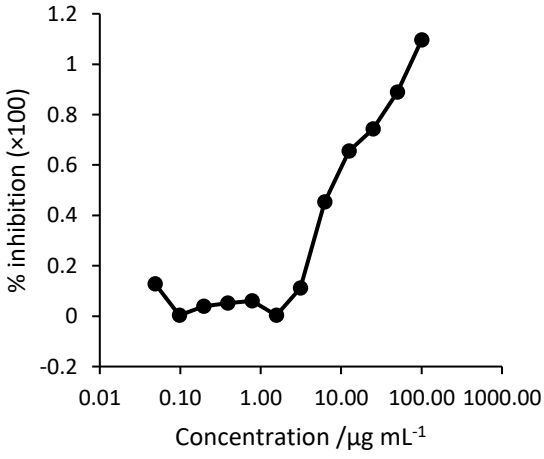

10.4. Retention times of austdiol-DNP L- and D- amino acid derivatives

Amino acid	t_R of L (min)	t_R of D (min)	$\lvert\Delta t_R\rvert$ (min)	t_R of L in LD mix (min)	t_R of D in LD mix (min)	$\lvert\Delta t_R\rvert$ mix (min)
Alanine	29.451	28.186	1.265	31.016	29.788	1.228
Arginine	24.014	24.441	0.427	24.490	25.078	0.588
Asparagine	23.299	23.174	0.125	23.670	23.67	0.000
Aspartic acid	25.546	25.788	0.242	25.922	26.168	0.246
Cysteine	-	-	-	-	-	-
Glutamic acid	27.882	28.255	0.473	28.273	28.650	0.377
Glutamine	24.648	24.244	0.404	24.655	24.655	0.000
Histidine	22.354	22.251	0.103	22.824	22.824	0.000
Isoleucine	45.283	48.157	2.874	45.665	48.492	2.827
Alloisoleucine	45.577	48.487	2.910	46.020	48.845	2.825
Leucine	45.377	47.936	2.559	45.833	48.330	2.497
Lysine	22.656	22.103	0.553	23.300	23.300	0.000
	25.259	24.721	0.538	25.821	25.821	0.000
Methionine	40.487	42.564	2.077	41.035	43.115	2.080
Phenylalanine	45.622	47.98	2.358	46.211	48.554	2.343
Proline	-	-	-	-	-	-
Serine	24.043	21.608	2.435	25.206	24.728	0.522
Threonine	28.390	30.249	1.859	29.054	30.914	1.860
Tryptophan	44.483	45.847	1.364	44.535	45.857	1.322
Tyrosine	34.754	34.42	0.334	35.305	35.107	0.198
Valine	40.563	41.615	1.052	40.985	43.619	2.634

[1]

[1]5-50% MeCN/H_2O in 0.01% TFA modifier achieved by 95-50% channel A (H_2O), 0-45% channel B (MeCN), and 5% isocratic channel D (MeCN - 0.2% TFA) over 60 min with 1 mL/min flow rate on a Zorbax SB-C_{18} (4.6 × 150 mm, 5 µm)